

Westinghouse  
Astronuclear  
Laboratory

MASTER



NOTICE

PORTIONS OF THIS REPORT ARE ILLEGIBLE. It has been reproduced from the available copy to permit the broadest possible availability.



WANL-TME-1915  
AUGUST 1970

DATA ITEM T-119

RADIATION ENVIRONMENT  
ON CHESH COMPONENTS (U)

FINAL REPORT

DISTRIBUTION OF THIS DOCUMENT IS UNLIMITED

## **DISCLAIMER**

**This report was prepared as an account of work sponsored by an agency of the United States Government. Neither the United States Government nor any agency Thereof, nor any of their employees, makes any warranty, express or implied, or assumes any legal liability or responsibility for the accuracy, completeness, or usefulness of any information, apparatus, product, or process disclosed, or represents that its use would not infringe privately owned rights. Reference herein to any specific commercial product, process, or service by trade name, trademark, manufacturer, or otherwise does not necessarily constitute or imply its endorsement, recommendation, or favoring by the United States Government or any agency thereof. The views and opinions of authors expressed herein do not necessarily state or reflect those of the United States Government or any agency thereof.**

## **DISCLAIMER**

**Portions of this document may be illegible in electronic image products. Images are produced from the best available original document.**

123



~~CONFIDENTIAL~~

Westinghouse  
Astronuclear  
Laboratory

MASTER



123

**NOTICE**  
This report was prepared as an account of work sponsored by the United States Government. Neither the United States nor the United States Energy Research and Development Administration, nor any of their employees, nor any of their contractors, subcontractors, or their employees, makes any warranty, express or implied, or assumes any legal liability or responsibility for the accuracy, completeness or usefulness of any information, apparatus, product or process disclosed, or represents that its use would not infringe privately owned rights.

Subcontract NP-1  
CODE IDENT NO. 14683

WANL-TME-1915  
AUGUST 1970

~~NOTICE~~

PORTIONS OF THIS REPORT ARE REFUGIBLE. It has been made available to the public in a limited copy to permit the use of available availability.

Classification cancelled (or changed to \_\_\_\_\_)

by authority of \_\_\_\_\_  
by H.F.C. TIC, date SEP 12 1973

DATA ITEM T-119

RADIATION ENVIRONMENT  
ON CHESH COMPONENTS (U)

FINAL REPORT

DISTRIBUTION OF THIS DOCUMENT IS UNLIMITED

APPROVED BY:

J. G. Gallagher, Manager  
NERVA Design Engineering

SPECIAL REREVIEW FINAL DETERMINATION Class: <u>U</u>	Reviewed	Class.	Date
	<u>JRP U</u>	<u>U</u>	<u>4-29-82</u>

~~GROUP - 1  
EXCLUDED FROM AUTOMATIC DOWNGRADING  
AND DECLASSIFICATION~~

~~INFORMATION CATEGORY  
Confidential - RD  
F. J. Frank 7-24-70  
AUTHORIZED CLASSIFIER DATE~~

~~CONFIDENTIAL  
RESTRICTED DATA~~

~~Atomic Energy Commission~~ DISTRIBUTION OF THIS DOCUMENT UNLIMITED

BLANK

## ABSTRACT

The PAX/R-1 reactor was utilized for measurements of the radiation environment at the mockups of the R-1 Cluster Hot End Support Hardware (CHESH). The results obtained include neutron flux densities obtained with sulfur ( $E > 2.9$  Mev), U-238 ( $E > 1.5$  Mev), bare and cadmium-covered Dy ( $E < 0.4$  ev). Fast neutron dose rates from Phylatrons and gamma dose rates from  $\text{CaF}_2$  thermoluminescent dosimeters and Bragg-Gray chambers were also determined.

Experimental data are compared with analytical calculations obtained with the two-dimensional discrete ordinates transport code, DOT. An  $S_{124}$  angular quadrature was employed in the DOT code. The analytical model is based on the actual PAX-G1A reactor, operating at ambient conditions. Reasonable agreement between the calculations and experimental data was generally observed.

BLANK

## TABLE OF CONTENTS

<u>Section</u>		<u>Page</u>
1.0	INTRODUCTION	1-1
	1.1 TEST IDENTIFICATION	1-1
	1.1.1 Type of Report	1-1
	1.1.2 Scope of Test Document	1-1
	1.1.3 Functional Category of Test	1-1
	1.1.4 Contractor	1-1
	1.1.5 Test Facility	1-1
	1.2 PURPOSE	1-1
2.0	REFERENCES AND ASSUMPTIONS	2-1
	2.1 REFERENCES	2-1
	2.1.1 Specification	2-1
	2.1.2 Data Item Description	2-1
	2.1.3 Scope of Test Document	2-1
	2.1.4 Drawing	2-1
	2.1.5 External Document	2-1
	2.1.6 Data Release Memorandum	2-2
	2.2 ASSUMPTIONS	2-2
3.0	TEST ARTICLE CONFIGURATION	3-1
	3.1 PAX-G1A REACTOR	3-1
	3.2 CHESH ASSEMBLY	3-2
	3.3 REFERENCE ASSEMBLY	3-2
	3.4 BORAL ENCLOSURE	3-3



## TABLE OF CONTENTS (Continued)

<u>Section</u>		<u>Page</u>
4.0	SUMMARY OF TESTS	4-1
4.1	NARRATIVE	4-1
4.1.1	Test Description	4-1
4.1.2	Passive Dosimetry	4-3
4.1.3	Active Dosimetry	4-20
4.2	TEST RESULTS	4-24
4.2.1	General	4-24
4.2.2	Dysprosium-Aluminum Wires	4-24
4.2.3	Sulfur Pellets	4-37
4.2.4	Uranium-238 Foils	4-37
4.2.5	Thorium Foils	4-37
4.2.6	Comparison of Fast Fluxes	4-37
4.2.7	TLD Chips	4-37
4.2.8	Phylatrons	4-45
4.2.9	Bragg-Gray Chambers	4-45
5.0	ANALYSIS OF TESTS	5-1
5.1	INTRODUCTION	5-1
5.2	ANALYTICAL MODEL	5-1
5.3	METHOD OF ANALYSIS	5-6

**TABLE OF CONTENTS (Continued)**

<u>Section</u>		<u>Page</u>
5.4	<b>COMPARISON OF EXPERIMENTAL AND ANALYTICAL RESULTS</b>	5-9
5.4.1	Sulfur ( $E > 2.9$ MeV) Fast Neutron Flux Data	5-10
5.4.2	U-238 ( $E > 1.5$ MeV) Fast Neutron Flux Data	5-12
5.4.3	Dysprosium ( $E < 0.4$ eV) Thermal Neutron Flux Data	5-14
5.4.4	Fast Neutron Absorbed Dose Rate Data	5-14
5.4.5	Photon Absorbed Dose Rate Data	5-17
5.4.6	Bragg-Gray Ion Chamber Heating Rate Data	5-19
5.5	<b>STATISTICAL ANALYSIS OF THE DATA</b>	5-21
5.5.1	Introduction	5-21
5.5.2	Statistical Results	5-21
5.6	<b>APPLICABILITY OF COMPARISONS TO DESIGN CALCULATIONS</b>	5-23
5.7	<b>REFERENCES</b>	5-26
6.0	<b>CONCLUSIONS</b>	6-1
	<b>APPENDIXES</b>	
A	Passive Dosimeters	A-1
B	Reactor Power Levels	B-1

## LIST OF ILLUSTRATIONS

<u>Figure</u>		<u>Page</u>
3-1	PAX-G1A Reflector Assembly	3-4
3-2	Top View of Cluster Region of CHESH Location	3-5
3-3	Close-Up of the CHESH Measurement Region	3-6
3-4	CHESH Cluster Assembly	3-7
3-5	Close-Up of CHESH Hardware	3-8
3-6	CHESH Assembly - Aft End	3-9
3-7	CHESH Assembly - Forward End	3-10
3-8	Reference Assembly - Aft End	3-11
3-9	Boral Enclosure for CHESH Experiment	3-12
4-1	Dy-Al and Phylatron Dosimetry Assemblage	4-4
4-2	Cd-Covered Dy-Al Dosimetry Assemblage	4-5
4-3	Sulfur Dosimetry Assemblage	4-6
4-4	Cd-Covered U-238 and Th-232 Dosimetry Assemblage	4-7
4-5	TLD Dosimetry Assemblage	4-8
4-6	Dy-Al and Phylatron Dosimetry in Place	4-9
4-7	Cd-Covered Dy-Al Dosimetry in Place	4-10
4-8	Sulfur Dosimetry in Place	4-11
4-9	Cd-Covered U-238 and Th-232 Dosimetry in Place	4-12
4-10	TLD Dosimetry in Place	4-13
4-11	Location of Bragg-Gray Ion Chamber on Reference Assembly	4-22
4-12	Bragg-Gray Chambers in Place	4-23
4-13	CHESH Experiment - Bare Dy Activity	4-25'

## LIST OF ILLUSTRATIONS (Continued)

<u>Figure</u>		<u>Page</u>
4-14	CHESH Experiment - Cd-Covered Dy Activity	4-26
4-15	CHESH Experiment - Thermal Flux From Dy-Al	4-27
4-16	CHESH Experiment - Dy-Al Cadmium Ratios	4-28
4-17	CHESH Experiment - Fast Flux From Sulfur	4-38
4-18	CHESH Experiment - Fast Flux From U-238	4-39
4-19	CHESH Experiment - Fast Flux Exterior to CHESH	4-40
4-20	CHESH Experiment - Fast Flux Interior to CHESH	4-41
4-21	CHESH Experiment - Fast Flux Exterior W/O CHESH	4-42
4-22	CHESH Experiment - Fast Flux Interior W/O CHESH	4-43
4-23	CHESH Experiment - Gamma Dose Rate From CaF <sub>2</sub>	4-44
4-24	Fast Neutron Dose Rate From Phylatrons (Outside)	4-47
4-25	Fast Neutron Dose Rate From Phylatrons (Inside)	4-48
5-1	CHESH Experiment DOT Geometry Mockup	5-2
5-2	CHESH Experiment Calculational Flow Chart	5-7
5-3	Comparison of the Calculated and Experimental Sulfur Fast Neutron Flux ( $E > 2.9$ MeV) As a Function of Axial Position Above the Top of the Fuel	5-11
5-4	Comparison of the Calculated and Experimental U-238 Fast Neutron Flux ( $E > 1.5$ MeV) As A Function of Axial Position Above the Top of the Fuel	5-13
5-5	Comparison of the Calculated and Experimental Dy Thermal Neutron Flux ( $E < 0.4$ eV) As A Function of Axial Position Above the Top of the Fuel	5-15
5-6	Comparison of the Calculated and Experimental Phylatron Fast Neutron Absorbed Dose Rate As a Function of Axial Position Above the Top of the Fuel	5-16
5-7	Comparison of the Calculated and Experimental CaF <sub>2</sub> TLD Gamma Ray Absorbed Dose Rate As a Function of Axial Position Above the Top of the Fuel	5-18
5-8	Comparison of the Gamma Ray Dose Rate Obtained by an Explicit and a Smeared Representation of the CHESH as a Function of Axial Position Above the Fuel	5-24

## LIST OF ILLUSTRATIONS (Continued)

<u>Figure</u>		<u>Page</u>
A-1	Dy-Al Alloy Content Report	A-2
A-2	Thermoluminescent Dosimeters with Tygon Covers	A-5
A-3	View of Silicon Diode Phylatron Dosimeters	A-7
A-4	Dy-Al Wire Activity Calibration Report	A-8
A-5	U-238, Th, and S Calibration Report	A-10
B-1	Sectioned Fuel Element	B-4
B-2	Fission Analysis of Fuel Wafers	B-5

## LIST OF TABLES

<u>Table</u>		<u>Page</u>
3-1	Weights of Cluster Hot End Support Hardware	3-13
4-1	Passive Dosimeters	4-2
4-2	Constants Used in Data Reduction	4-15
4-3	Sources of Random and Biasing Uncertainties	4-17
4-4	Sources of Systematic Uncertainties in Absolute Activity and Flux	4-18
4-5	TLD and Phylatron Measurement Uncertainties	4-19
4-6	CHESH Experiment - Dy-Al Foils - Thermal Flux and Cadmium Ratio	4-29
4-7	CHESH Experiment - Dy-Al Foils - Bare, Cd-Covered and Thermal	4-31
4-8	CHESH Experiment - Sulfur Pellets	4-34
4-9	CHESH Experiment - U-238 Foils	4-35
4-10	CHESH Experiment - Calcium Fluoride TLD Chips	4-36
4-11	Fast Neutron Dose Rates From Phylatrons	4-46
4-12	Dose Rates and Heating Rates From Bragg-Gray Detectors	4-49
5-1	Radial (R) and Axial (Z) DOT Mesh	5-3
5-2	CHESH Experiment Atom Densities (Atoms/BN-CM)	5-5
5-3	Comparison of Calculated and Experimental Photon Heating Rates from Bragg-Gray Detectors	5-20
5-4	Statistical Analysis of the Difference Between Calculated and Experimental Data	5-22

## 1.0 INTRODUCTION

### 1.1 TEST IDENTIFICATION

#### 1.1.1 Type of Report

This report is a complete Final Report.

#### 1.1.2 Scope of Test Document

The applicable Scope of Test Document Number is M57DW-271-1.

#### 1.1.3 Functional Category of Test

This is a Development test.

#### 1.1.4 Contractor

The Westinghouse Astronuclear Laboratory (WANL/14683) under Subcontract NP-1, CY' 69 is the contractor.

#### 1.1.5 Test Facility

These tests were performed at the Westinghouse Astronuclear Experimental Facility located at the Westinghouse Waltz Mill Site June 17 to June 23, 1969.

### 1.2 PURPOSE

The purpose of this experiment was to:

1. Experimentally determine the radiation environment on the following NERVA reactor components.

A. Cluster hot end support, EC 677557.

B. Cluster miscellaneous hardware, EC 677558.

2. Provide experimental data for comparison with analytical predictions.

These experiments are being performed to satisfy, in part, the requirements of Paragraphs 3.1 and 4.1 of the applicable specification for the preceding engineering components.

## 2.0 REFERENCES AND ASSUMPTIONS

### 2.1 REFERENCES

#### 2.1.1 Specifications

EC 677557 - Part I. Performance/Design and Qualification Requirements  
Cluster Hot End Support for 677555A NERVA Nuclear Subsystem, 1/23/69

EC 677558 - Part I. Performance/Design and Qualification Requirements  
Support Stem & Cluster Miscellaneous Hardware for 677555A NERVA Nuclear Subsystem, 1/23/69

#### 2.1.2 Data Item Description

Form 9, Data Item Description, T-119, dated 4/2/69

#### 2.1.3 Scope of Test Document

M57DW-271-1 - Scope of Test for Experimentally Determining the Radiation  
Environment on the Cluster Hot End Support Components

#### 2.1.4 Drawing

577F515 - Support Stem Assembly Fuel Cluster Assembly

711J496 - Reactor/Vessel Assembly, R-1 PAX

711J489 - Cluster Assembly, Fuel R-1 PAX

711J498B - Segment, Reflector Assembly, R-1 PAX

711J567 - Cluster Assembly, Fuel R-1 PAX

939J685E - NERVA R-1 Conceptual Reference Design

#### 2.1.5 External Document

WANL-TME-1852, Volume 1 - R-1 Parametric Shield Measurements Conducted  
on the NERVA Permanent Assembly Experiment (PAX) Reactor

WANL-TME-1911 - PAX-G0 Power Distribution Measurements

WANL-TME-1917 - PAX-G1 Gross Power Measurements

WANL-TME-1798, Volume 6 - NERVA Engineering Data and Design Concepts -  
Summary & Recommendations

WANL-TME-1914 - Radiation Environment in Various Reactor Components



### 2.1.6 Data Release Memorandum

51105C - Flow Charts for an Integrated Nuclear and Radiation, Thermal and Structural Analysis Procedure, and Identification and Description of Computer Code

51150 - Parts Inventory in the PAX-G0 Reactor

51150A - Parts Inventory in the PAX-G0A, B, and C Reactors

51163 - Parts Inventory in the PAX-G1 Reactor

51163A - Parts Inventory in the PAX-G1A Reactor

51166 - PAX-G1 Shim Wire Inventory

51166A - PAX-G1 Shim Wire Inventory

51171 - Parts List Containing As-Built Weights for the CHESH and Support Stem

#### Assembly Experiments

51176 - Calibration of Thermoluminescent Dosimeters (TLD s)

51176A - Calibration of Thermoluminescent Dosimeters (TLD s)

51177 - Calibration of Bragg-Gray Heating Rate Detectors for Use at WANEF

51178 - Experimental Determination of Heating Rate on CHESH Stems

51179 - Use of Bragg-Gray Ionization Chambers for Heating Rate Measurements

51927 - Radiation Heating Rates in the R-1 Reference Design (Drawing No. 939J685-E)

## 2.2 ASSUMPTIONS

1) Measurements on a similar cluster in adjacent sector where no CHESH hardware is located gives background radiation results for direct comparison with measurements in the presence of the CHESH components.

2) Boral enclosure over measurement area does not affect measurements and eliminates all extraneous thermal neutrons produced in the test cell and support blocks.

3) Removal of support blocks in a local area fully simulates desired radiation source for operating conditions. This means that adjacent support blocks and protruding wires do not significantly perturb measurement area.

4) The power perturbation caused by the introduction of R-1 type support stems is not sufficiently significant to affect power calibration and, hence, the data reduced on a per watt basis from fission flux density measurements made without R-1 support stems present can be used for the measurements with stems present.

5) It is assumed that the heating rate measurements by Bragg-Gray detectors located adjacent to the support stem assembly and liner sleeve are characteristic of those in the CHESH components.

6) Similarly, it is assumed that the heating rates measured in graphite or stainless steel detectors are characteristic of those in the CHESH components which are constructed of different material.

7) The assumptions regarding use of Bragg-Gray detectors, which are discussed in DRM 51179, are valid.

### 3.0 TEST ARTICLE CONFIGURATION

#### 3.1 PAX-G1A REACTOR

The PAX reactor, modified as shown in Figure 3-1 and designated PAX-G1A, has been used to perform standard reactor experiments during the initial phases of the R-1 design program to support the release of R-1 fuel specifications and provide information on the adequacy of the control capability of the R-1 reflector system and hydrogen in the support stems. Basically, the reactor has a large core (no inner reflector) and a 60 degree mockup of the R-1, 18 control drum configuration in the reflector.

The present R-1 reactor core design contains 1878 fueled and 349 unfueled elements. The PAX/R-1 also contains a total of 2227 elements, but the number of fueled elements is greater. This R-1 design calls for uranium loadings as high as  $630 \text{ mg/cm}^3$ . In order to mockup the overall uranium content using available fuel (loadings less than  $500 \text{ mg/cm}^3$ ), approximately one-half of the central elements in PAX/R-1 are fueled. These are made from existing fuel elements by drilling and tapping the ends. To accommodate the increase in the total number of elements, an extension to the core support plate is inserted into the support plate region of the PAX/R-1 as seen in Figure 3-1. Approximately 245 kg of highly enriched uranium are contained in the PAX-G1A core.

The PAX-G1A reflector is obtained by replacing two 30 degree KIWI sectors of the 12 drum NRX configuration with a 60 degree R-1 reflector mockup segment. This reflector mockup segment is constructed of laminated beryllium slabs. The non-beryllium fraction in this segment is the same as that of the present R-1 reflector. The lateral support hardware is mocked up in the plunger holes by the same amount of material as in R-1. This reflector segment contains three control drums whose vanes are  $\text{Al-B}^{10}$ , 100 mils thick, with a  $\text{B}^{10}$  surface concentration of 0.13 gram per square centimeter. The R-1 mockup control drums have a vane span of 120 degrees.

The PAX-G1A reactor build (including shim wire inventory, parts inventory, fuel element listing, and/or representative as-built weights) are detailed in Drawings 711J496 and 711J498B, DRM's 51166, 51166A, 51163, 51163A, 51150 and 51150A.

The special modifications required for this experiment consisted of:

- 1) The insertion of special graphite central elements in clusters 4C2 and 5C2.

2) The removal of the support blocks, Nb and "X" wires in the region defined by Figure 3-2 and replacing the wires in the core at the locations from which they were removed.

3) The removal of the R-1 support stems from cluster locations 4C2 and 5C2 and inserting the CHESH at 4C2 (Figure 3-6) and the modified support stem and sleeve liner at 5C2 (Figure 3-8).

4) The removal of all the Nb and "X" wires at locations (1,2,6) D3, (1,2,3) D1, and IE4 in order to bring the delayed critical drum bank to within  $115^{\circ} \pm 1^{\circ}$ .

Figure 3.3 shows a detailed photograph of the top of the core in the region where the measurements were performed.

### 3.2 CHESH ASSEMBLY

The Cluster Hot End Support Hardware (CHESH) is defined in EC 677557 and WANL Drawing No. 711J567. The CHES hardware assembly is placed in a special graphite central element (Part No. 388D262H02 of WANL Drawing No. 711J489) which is a regular PAX central element with a Nb coating and with a larger central hole to accommodate the R-1 support stem assembly. Figures 3-4 and 3-5 show photographs of the CHES hardware. Figures 3-6 and 3-7 show detail drawings of the assembled cluster. Table 3-1 presents typical and as-built weights of the various components of the CHESH assembly.

### 3.3 REFERENCE ASSEMBLY

The reference assembly, to which radiation measurements on the CHESH assembly were compared, consists of a complete cluster assembly with a special graphite central element and support stem. This assembly includes every item on WANL Drawing No. 711J567) except the following:

- a. Item 3, the pedestal.
- b. Item 7, the sleeve spacer.
- c. Item 9, the cup, protection.

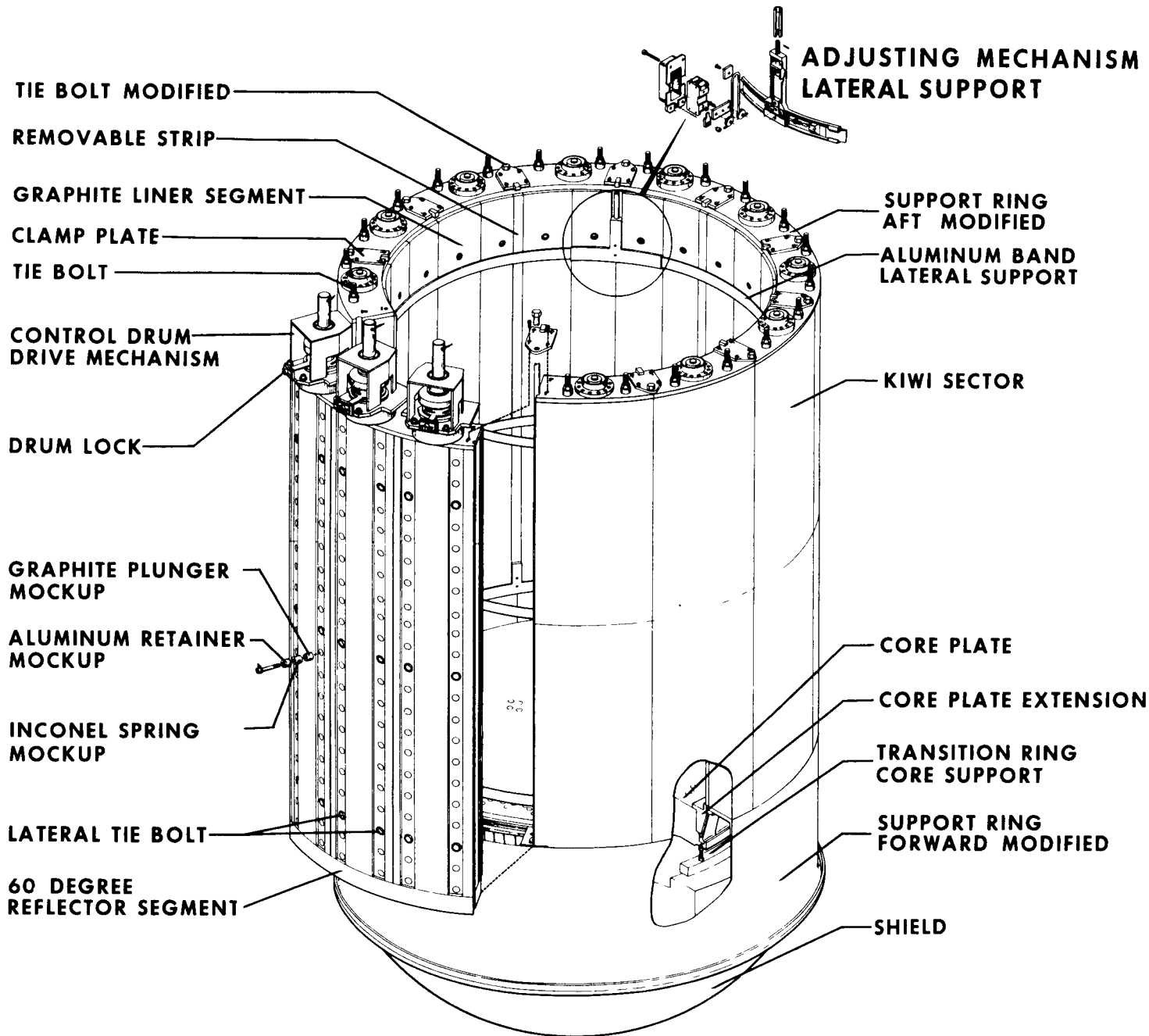
- d. Item 16, the cap, closure.
- e. Item 17, the cup, cap insulating.
- f. Item 18, the cap, insulation.
- g. Item 19, the cup, cap protection.
- h. Item 23, the screw, cap closure.
- i. Item 24, the spacer.
- j. Item 25, the washer, insulating

Figure 3-8 shows details of the cluster assembly.

#### 3.4 BORAL ENCLOSURE

A Boral enclosure was placed over the aft region of the PAX-G1 core (with support blocks removed in the local region) for all reactor runs in this experiment, as outlined in Figure 3-2 and shown in the photograph of Figure 3-9. The purpose of the enclosure was to reduce the test cell and /or support block produced thermal neutrons to the experimental region of measurement.

The Boral enclosure was fabricated from 1/8 inch thick Boral sheets that were securely fastened together with epoxy glue (the procedure used in the past for the fabrication of small boron-containing boxes used for reactor experiments). The final form is a 6-1/4" W x 11-3/4" L x 8" H five sided enclosure. The enclosure weighs 3700 gms.



612397-3

Figure 3-1. PAX-G1A Reflector Assembly

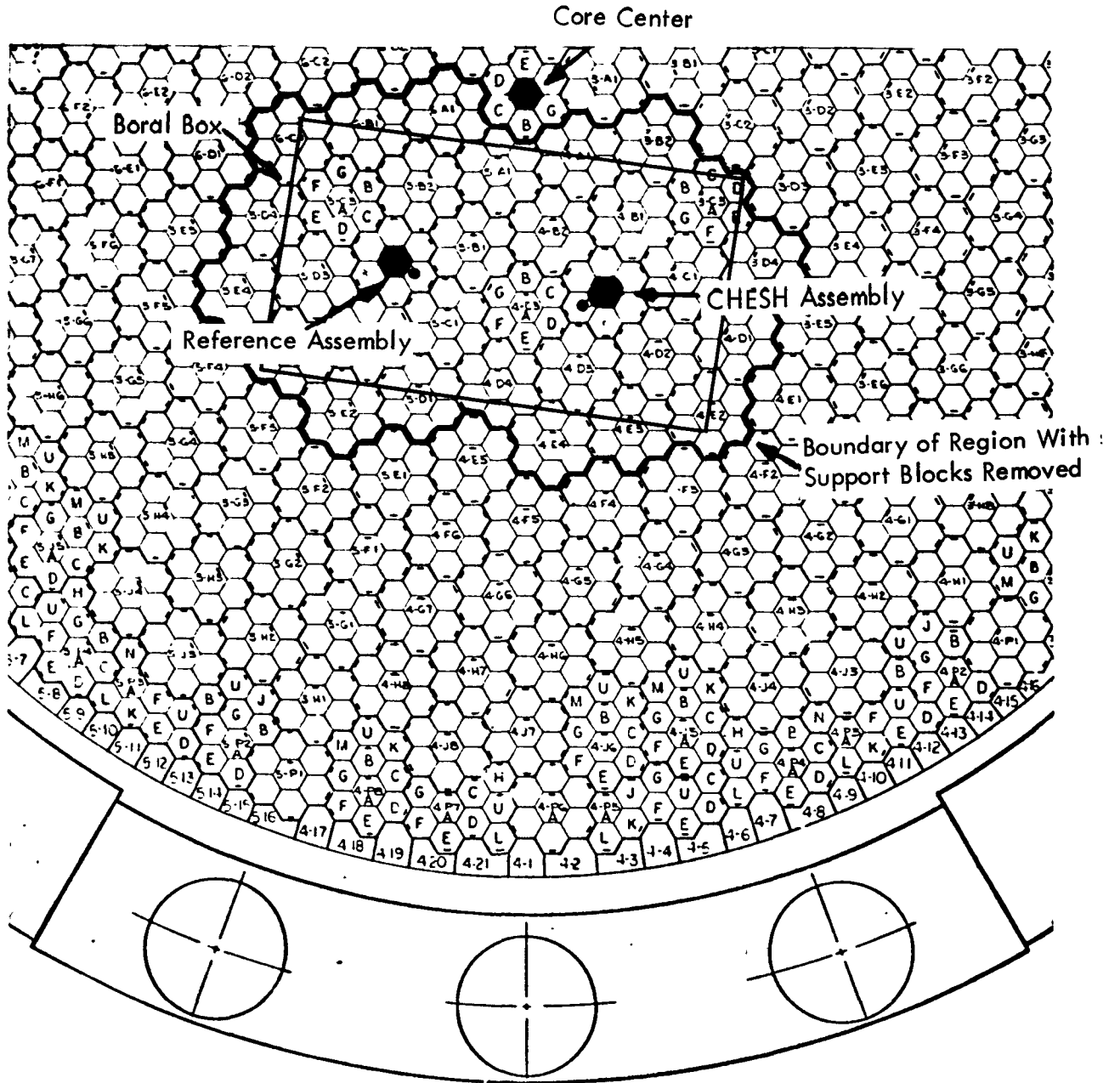


Figure 3-2. Top View of Cluster Region of CHESH Location

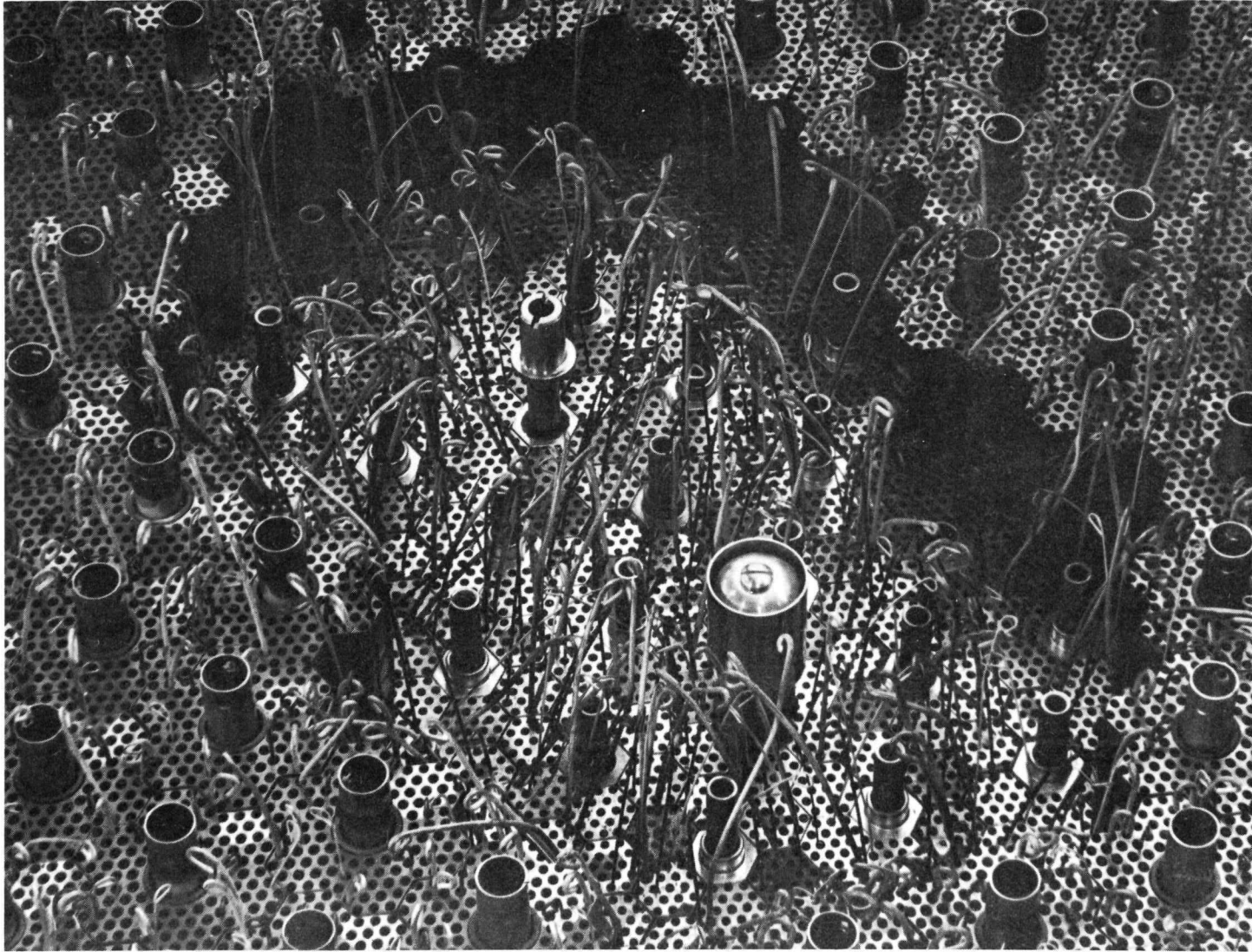


Figure 3-3. Close-Up of the CHESH Measurement Region (U)





**CONFIDENTIAL**

3-7

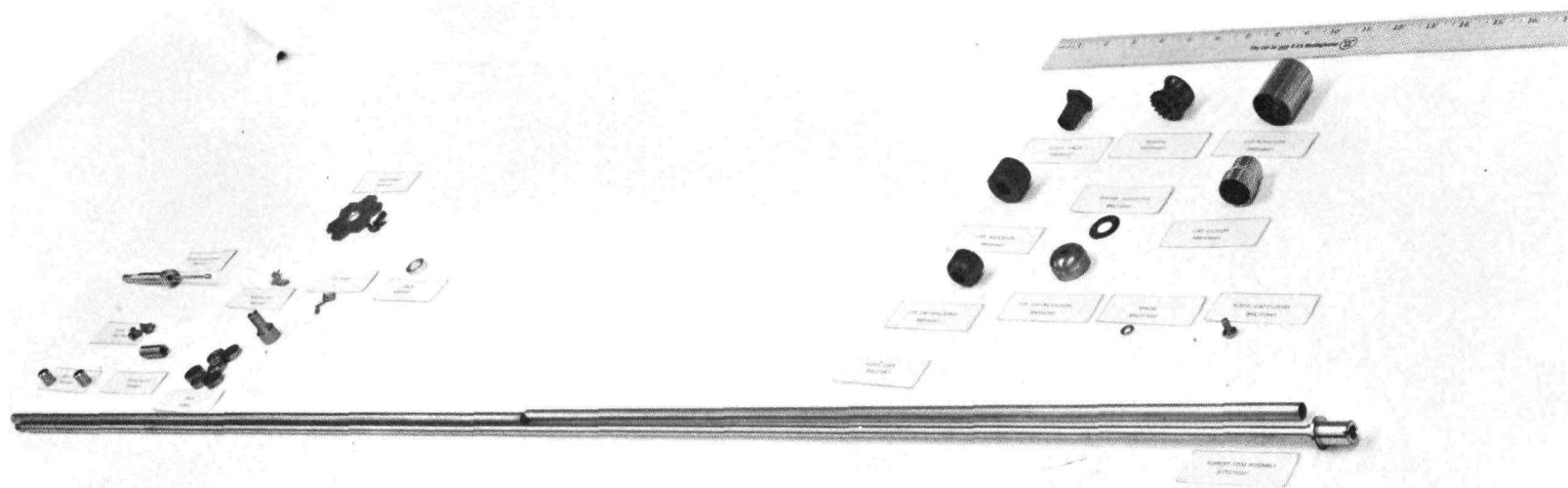
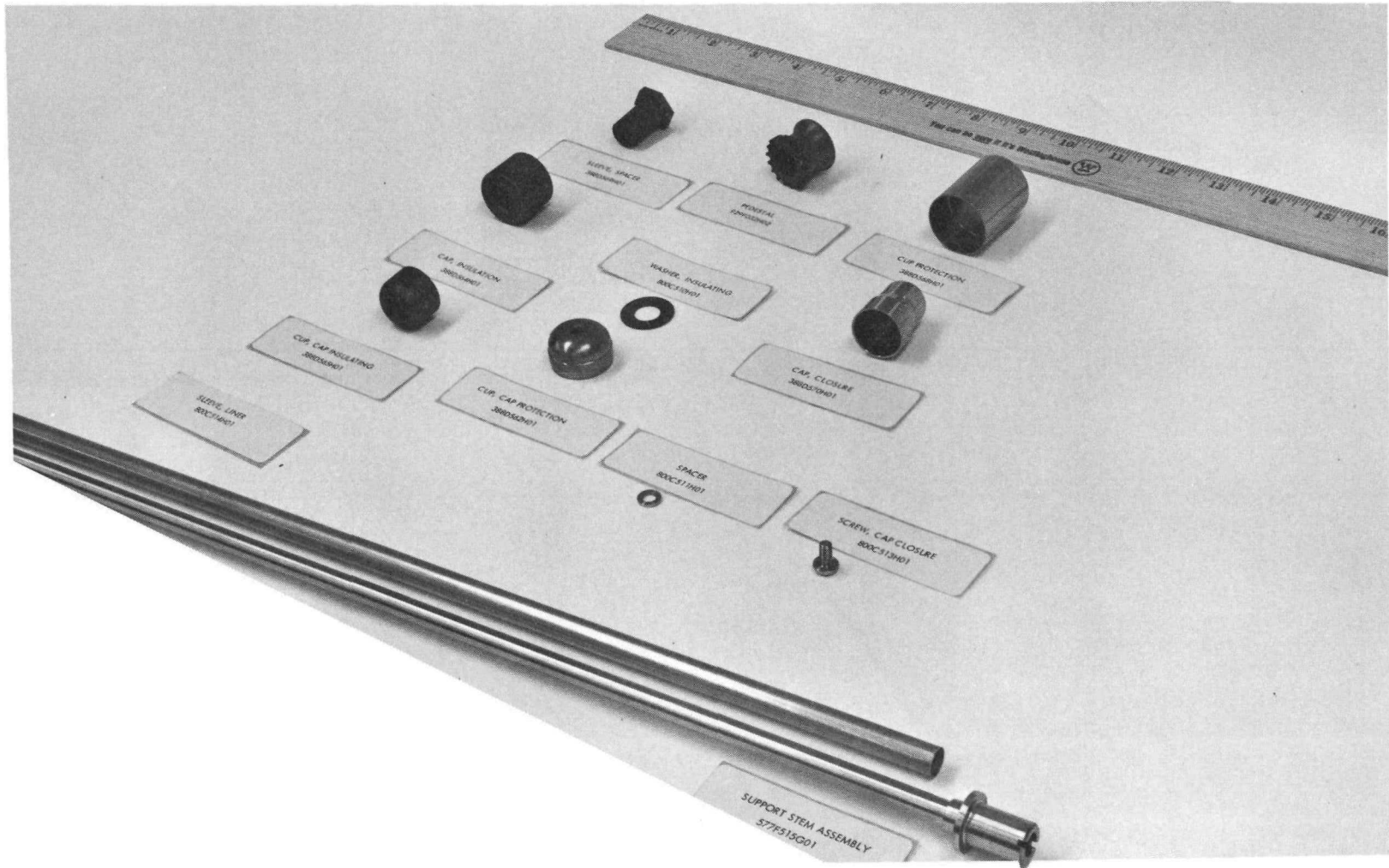


Figure 3-4. CHESH Cluster Assembly (U)

**CONFIDENTIAL**

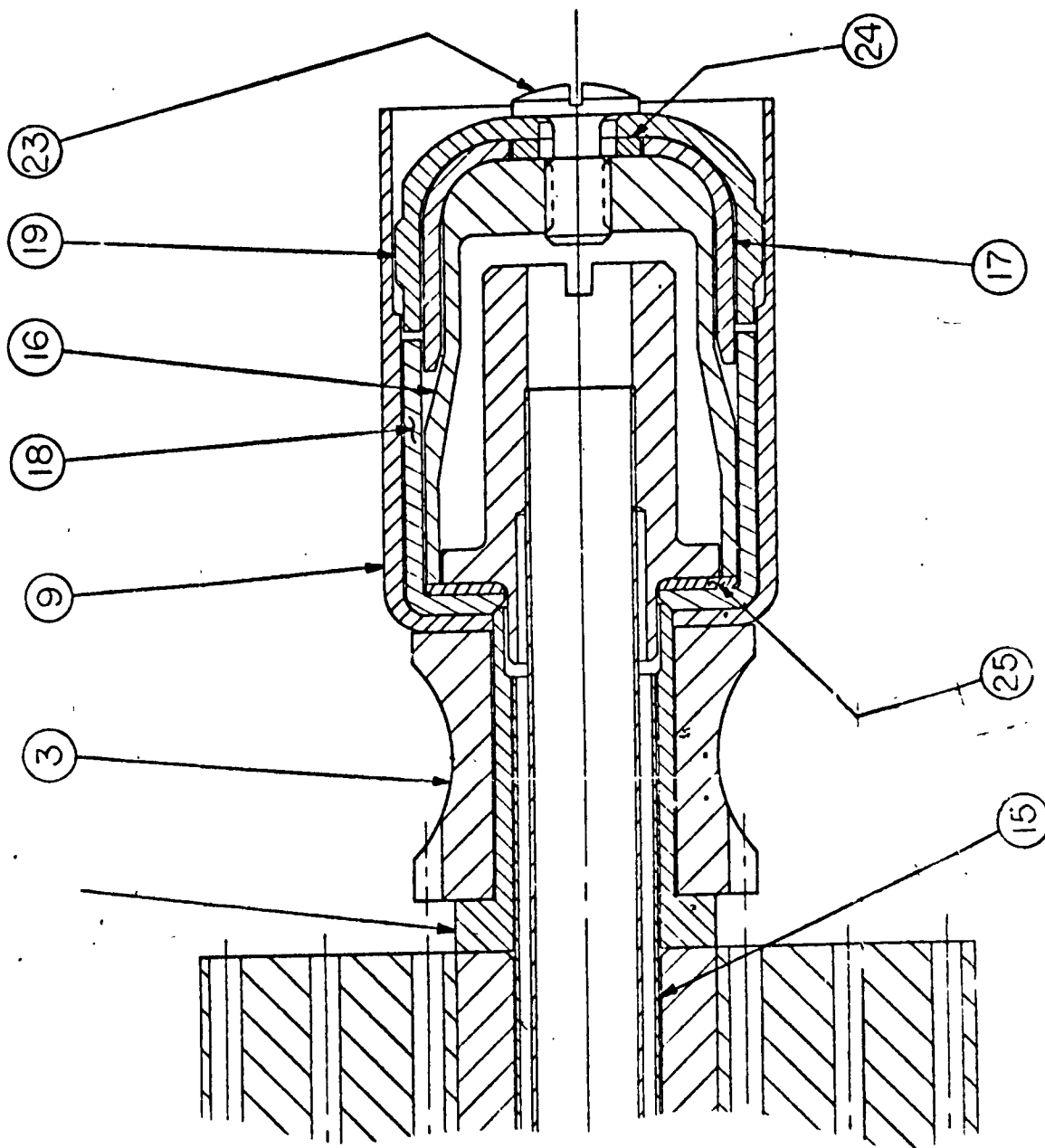
CONFIDENTIAL

3-8



CONFIDENTIAL

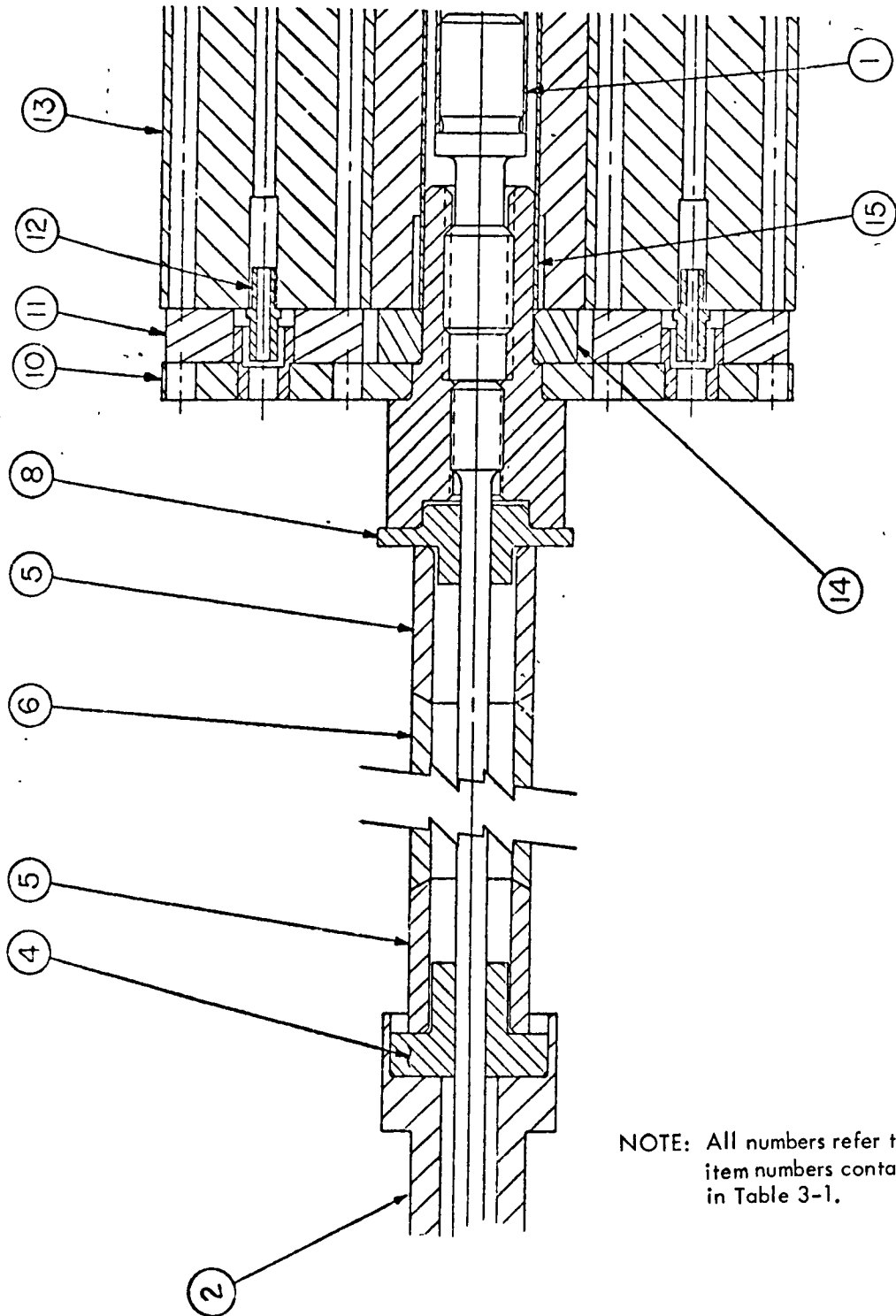
Figure 3-5. Close-Up of CHESH Hardware (U)



NOTE: All numbers refer to the item numbers contained in Table 3-1.

Figure 3-6. CHESH Assembly - Aft End (U)

~~CONFIDENTIAL~~



NOTE: All numbers refer to the item numbers contained in Table 3-1.

Figure 3-7. CHESH Assembly - Forward End (U)

~~CONFIDENTIAL~~

THIS PAGE UNCLASSIFIED

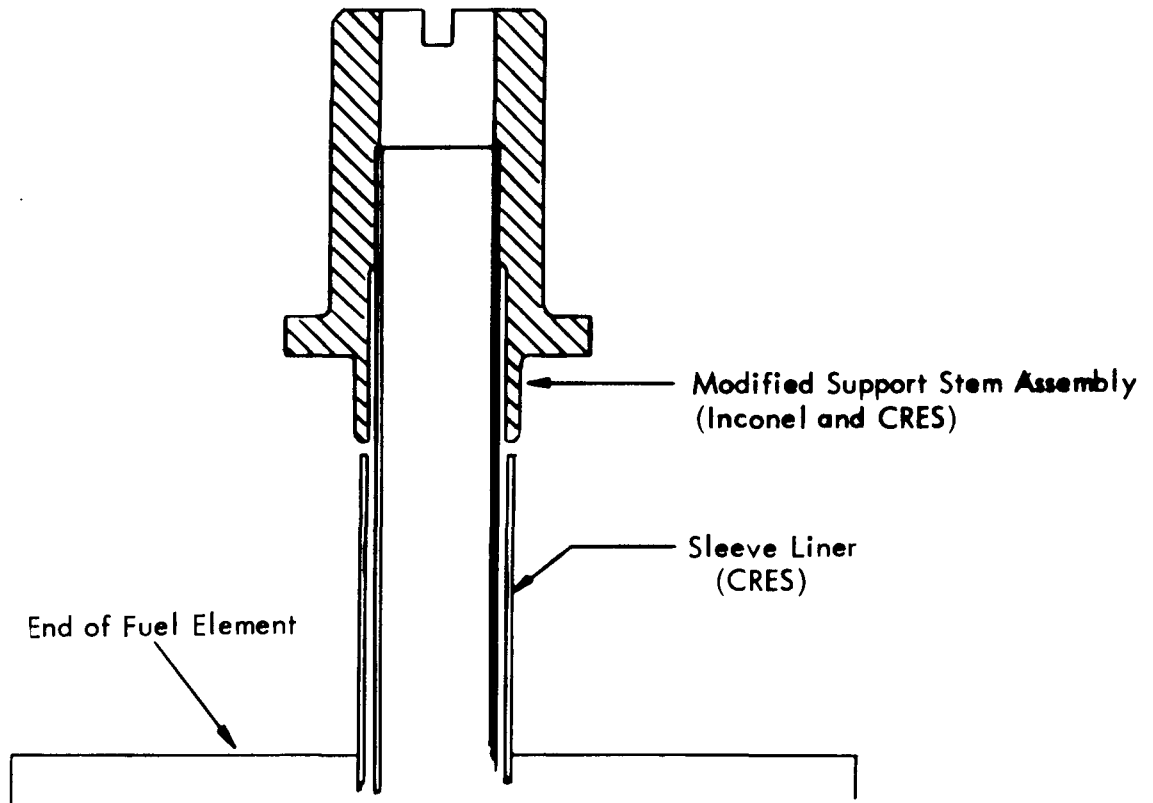
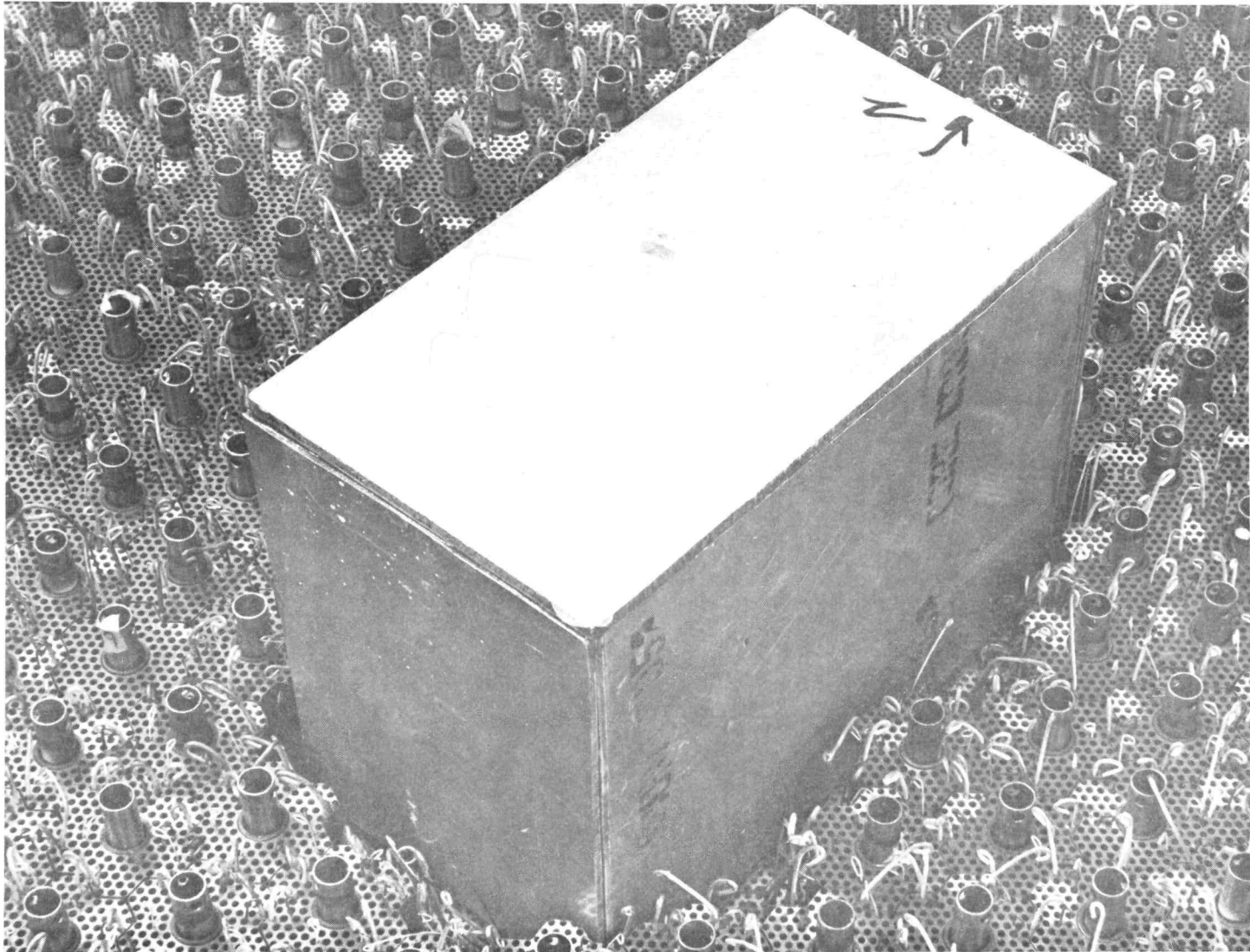


Figure 3-8. Reference Assembly - Aft End

THIS PAGE UNCLASSIFIED

~~CONFIDENTIAL~~

3-12



~~CONFIDENTIAL~~

Figure 3-9. Boral Enclosure for CHESH Experiment (U)

TABLE 3-1  
WEIGHTS OF CLUSTER HOT END SUPPORT HARDWARE (U)

<u>Description</u>	<u>Item No. *</u>	<u>Part No.</u>	<u>Quantity Weighed</u>	<u>Weight (grams)</u>	<u>Material</u>
Support Stem Assembly	1	577F515G01	1	105.8	CRES and Inconel
Tie Rod Holder	2	388D343G01	19	925.0	CRES
Pedestal	3	929F032H02	1	18.4	NbC Graphite
Split Washer	4	800C198H01	21 gps of 2	124.2	CRES
Spring Mockup	5	793C849H01	456	2426.0	CRES
Spring Mockup	6	793C848H01	30	322.5	CRES
Spacer Sleeve	7	388D569H01	1	3.45	Graphite
Split Bushing	8	946C216H01	50 gps of 2	78.2	Aluminum
Protection Cup	9	388D568H01	1	77.6	Tungsten
Plate Assembly	10	576F961H02			
Consists of:					
a. 1 cluster plate		909E529H01	19	636.0	CRES
b. 6 orifice jet bushing		946C172H01 sub for 944C959	126	19.2	Aluminum
c. 6 centering bushing		388D341H01	18	450.2	CRES
Spacer	11	609B030	30	250.0	CRES
Jet Orifice	12	--	100	28.8	
Spacer	14	800C576H01	21	46.0	Aluminum
Liner Sleeve	15	800C514H01	1	105.0	CRES
Closure Cap	16	388D570H01	1	27.6	CRES
Cap Insulating Cup	17	388D565H01	1	2.75	Graphite
Insulation Cap	18	388D564H01	1	4.55	Graphite
Cap Protection Cup	19	388D562H01	1	47.0	Tungsten
Cap Closure Screw	23	800C513H01	1	2.0	CRES
Spacer	24	800C511H01	1	0.4	CRES
Insulating Washer	25	800C510H01	1	0.5	Graphite

\* Obtained from Drawing No. 711J567, "Cluster Assembly, Fuel R-1 PAX"

3-13

CONFIDENTIAL

CONFIDENTIAL


 Astronuclear  
Laboratory

## 4.0 SUMMARY OF TESTS

### 4.1 NARRATIVE

#### 4.1.1 Test Description

The radiation environment was measured in and around a CHESH assembly placed at location 4C2 in the PAX-G1A reactor and at location 5C2 at which the cluster hardware was similar but with the CHESH assembly absent. In order to adequately mockup the reactor configuration desired, the cluster blocks in the vicinity of these locations were removed. The Nb and "X" wires were not removed from this region, however, and were left protruding from the ends of the fuel elements to the extent of the thickness of the support blocks. Figure 3-1 and 3-2 show this region of the core surface.

The measurements were performed with the core shimmed to a cold critical drum bank of  $115^{\circ} \pm 1^{\circ}$ .

The radiation environment was measured both with passive and with active types of dosimeters. The passive dosimeters consisted of Dy-Al foils to measure thermal neutron flux; sulfur, U-238, and thorium foils to measure fast neutron flux; thermoluminescent dosimeters to measure gamma dose rate; and Phylatrons to measure fast neutron dose rate.

The types and sizes of passive dosimeters used are presented in Table 4-1. A detailed description of each type appears in Appendix A.

The methods used for establishing reactor power levels are discussed in Appendix B.

The active dosimeters were Bragg-Gray chambers with stainless steel and with carbon walls.

Additional measurements with bare and cadmium-covered dysprosium dosimeters on the support stem assembly without the CHESH components are reported in WANL-TME-1914.



TABLE 4-1  
PASSIVE DOSIMETERS

Type	Length (l) Thickness (t) (Inches)	Diameter (Inches)	Average Weight (Grams)	Radiation Measured
Dy-Al Wires <sup>(1)</sup>	1/4 l	0.030	0.00834	Thermal Neutron Flux ( $E < 0.4$ eV)
S Pellets	0.266 t	1/4	0.348	Fast Neutron Flux ( $E > 2.9$ MeV)
U-238 Foils <sup>(2)</sup>	0.005 t	1/4	0.0729	Fast Neutron Flux ( $E > 1.5$ MeV)
Th-232 Foils	0.004 t	1/4	0.0437	Fast Neutron Flux ( $E > 1.35$ MeV)
CaF <sub>2</sub> TLD <sup>(3)</sup>	1/16 t	1/8 - square	0.0476	Gamma Dose Rate
LiF TLD <sup>(3)</sup>	1/16 t	1/8 - square	0.0399	Gamma Dose Rate
Phylatron	0.290 l	0.115 Max.	0.213	Fast Neutron Dose Rate

(1) 10.86 weight percent dysprosium in an aluminum matrix. (See Appendix A)

(2) 190 ppm U-235.

(3) Hot-pressed chips.

## 4.1.2 Passive Dosimetry

### 4.1.2.1 Positioning Techniques and Accuracies

In order to place the various types of dosimeters in the desired locations on the inside and outside of the CHESH and reference assemblies, extensive use was made of cardboard jigs, tape, and glue. In general, the locations selected for CHESH consisted of four axially spaced locations along the outside of the CHESH, two locations within the top of the support stem, one at the top end of the support stem, and one on top of the CHESH. For the reference assembly, effort was made to duplicate these locations as closely as practicable. For the Dy-Al measurements, the 1/4 inch lengths of wire were stacked axially on top of each other and, therefore, a greater number of measurements were made both along the outside of the CHESH and along the inside of the support stem.

Figures 4-1 through 4-5 show the dosimeters taped to the jigs prior to placement on the reactor. Figures 4-6 through 4-10 show the dosimeters in place on the reactor prior to covering with the Boral enclosure.

Figures 4-1 and 4-6 show the dosimeters for the run involving bare Dy-Al wires and Phylatrons. The Phylatron results are not reported because of incorrect exposures which caused saturation of many of the Phylatrons.

Figures 4-2 and 4-7 show the dosimetry for the reactor run involving cadmium-covered Dy-Al wires. The ends of the Cd tubes were pinched shut subsequent to these photographs. Also Phylatrons were added to the assembly in a manner similar to that shown in Figures 4-1 and 4-6.

Figures 4-3 and 4-8 show the dosimetry for the sulfur irradiation. The sulfur pellets within the support stems were inserted into tubes of rolled paper.

Figures 4-4 and 4-9 show the cadmium-covered U-238 and Th-232 foils mounted on holders and on the test assemblies, respectively.

Figures 4-5 and 4-10 show the TLD dosimetry mounting with two TLDs at each location (one  $\text{CaF}_2$  and one LiF chip). The TLDs inside the support stem were enclosed in a plastic tube as shown. The remaining TLDs were individually enclosed in packets consisting of Tygon tubing and identification tape as described in Appendix A.

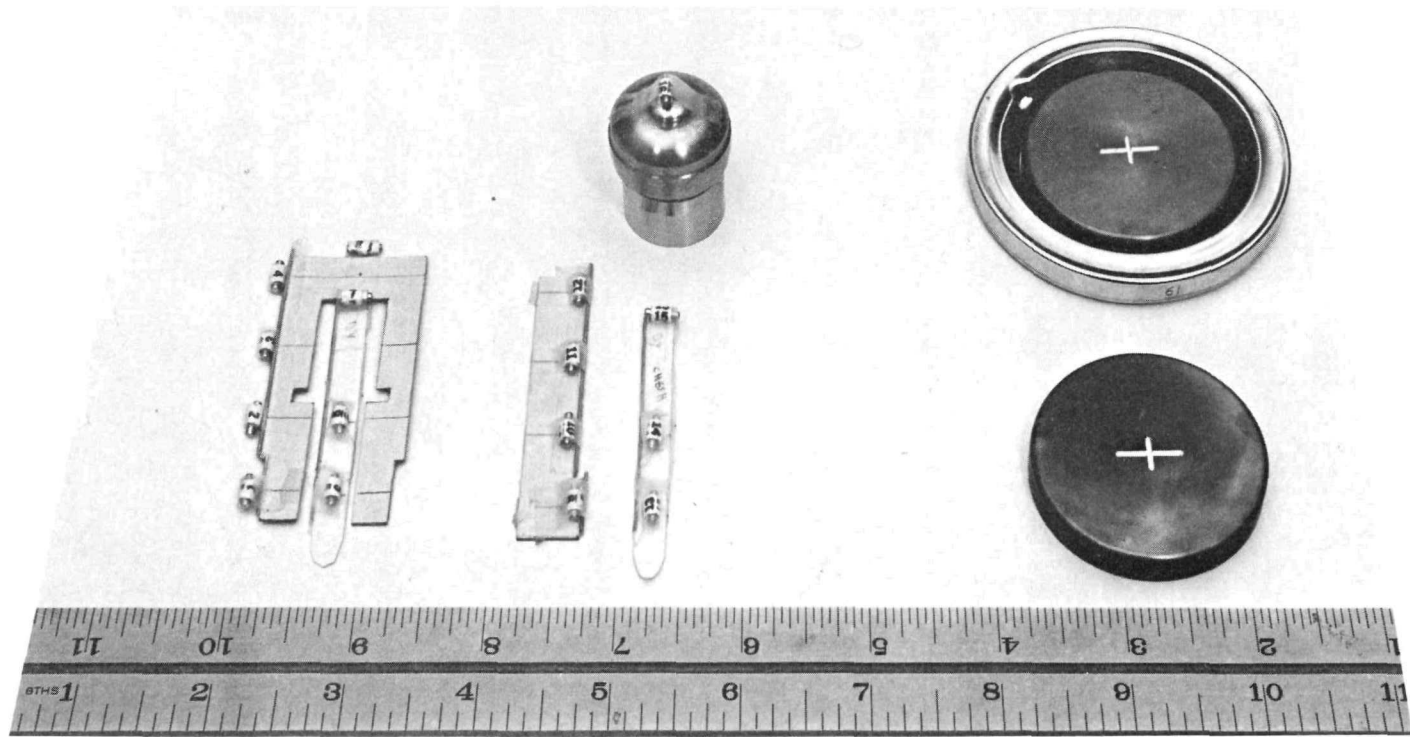


Figure 4-1. Dy-Al and Phylatron Dosimetry Assemblage

4-5

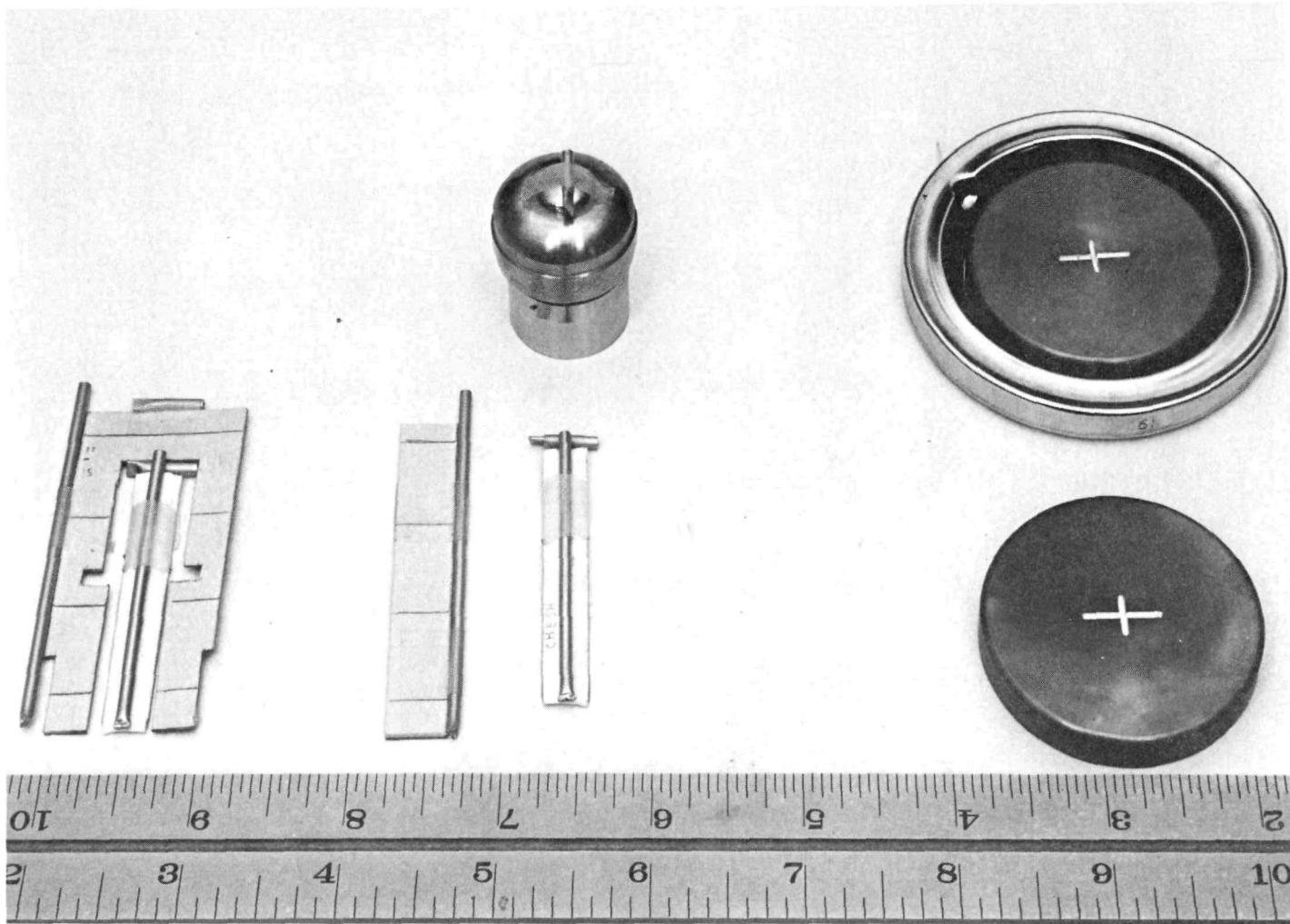


Figure 4-2. Cd-Covered Dy-Al Dosimetry Assemblage

4-6

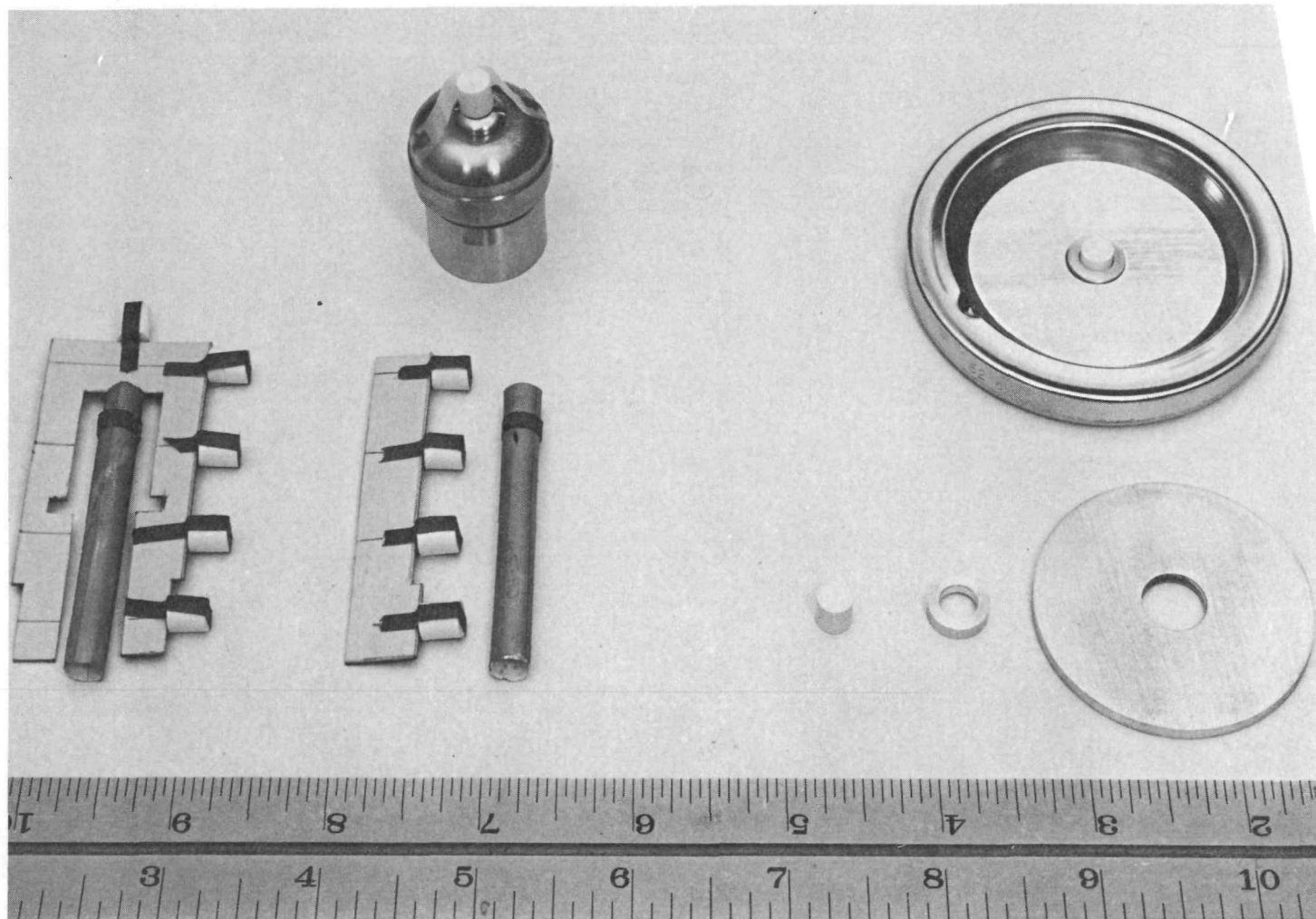


Figure 4-3. Sulfur Dosimetry Assemblage

4-7

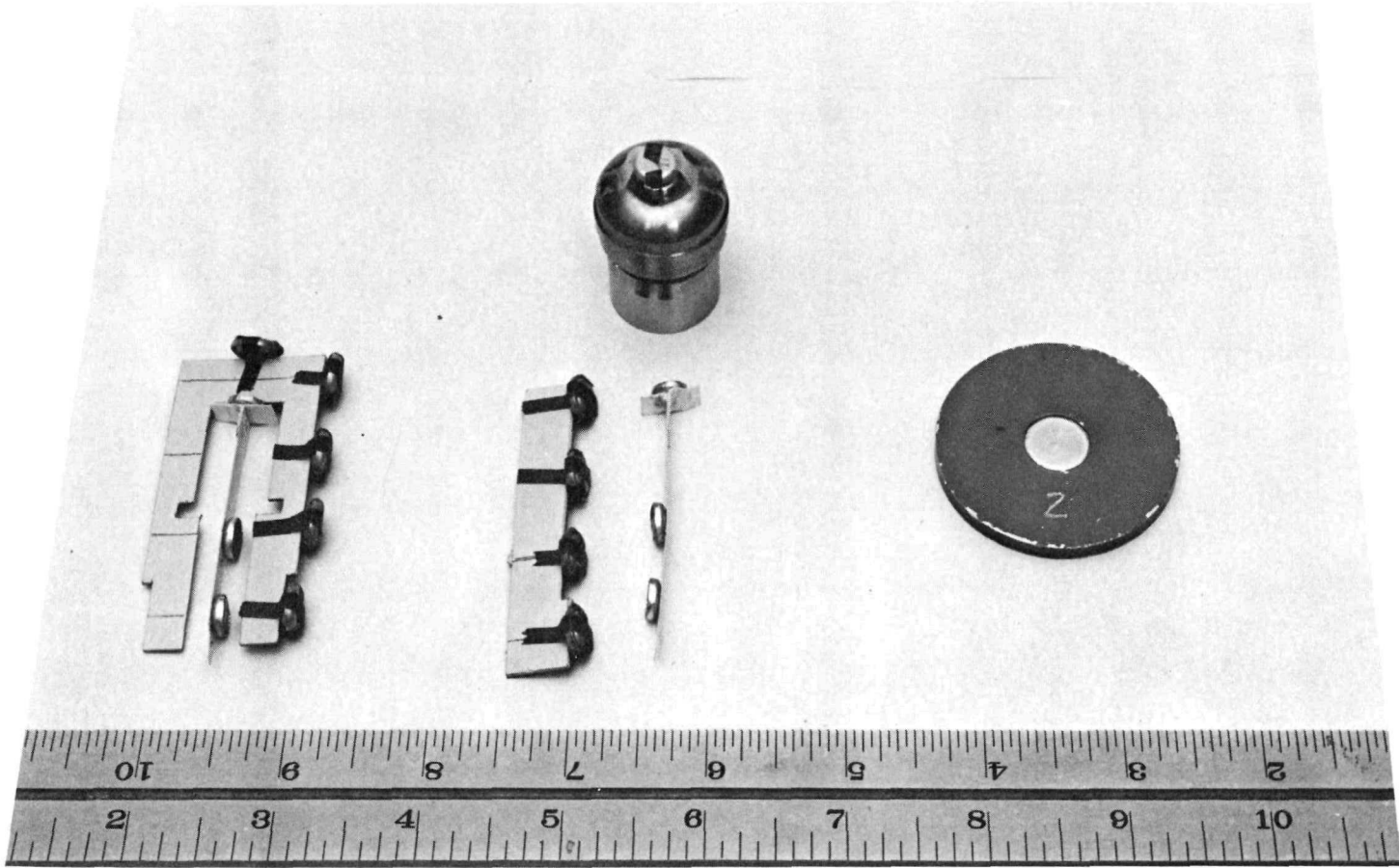


Figure 4-4. Cd-Covered U-238 and Th-232 Dosimetry Assemblage

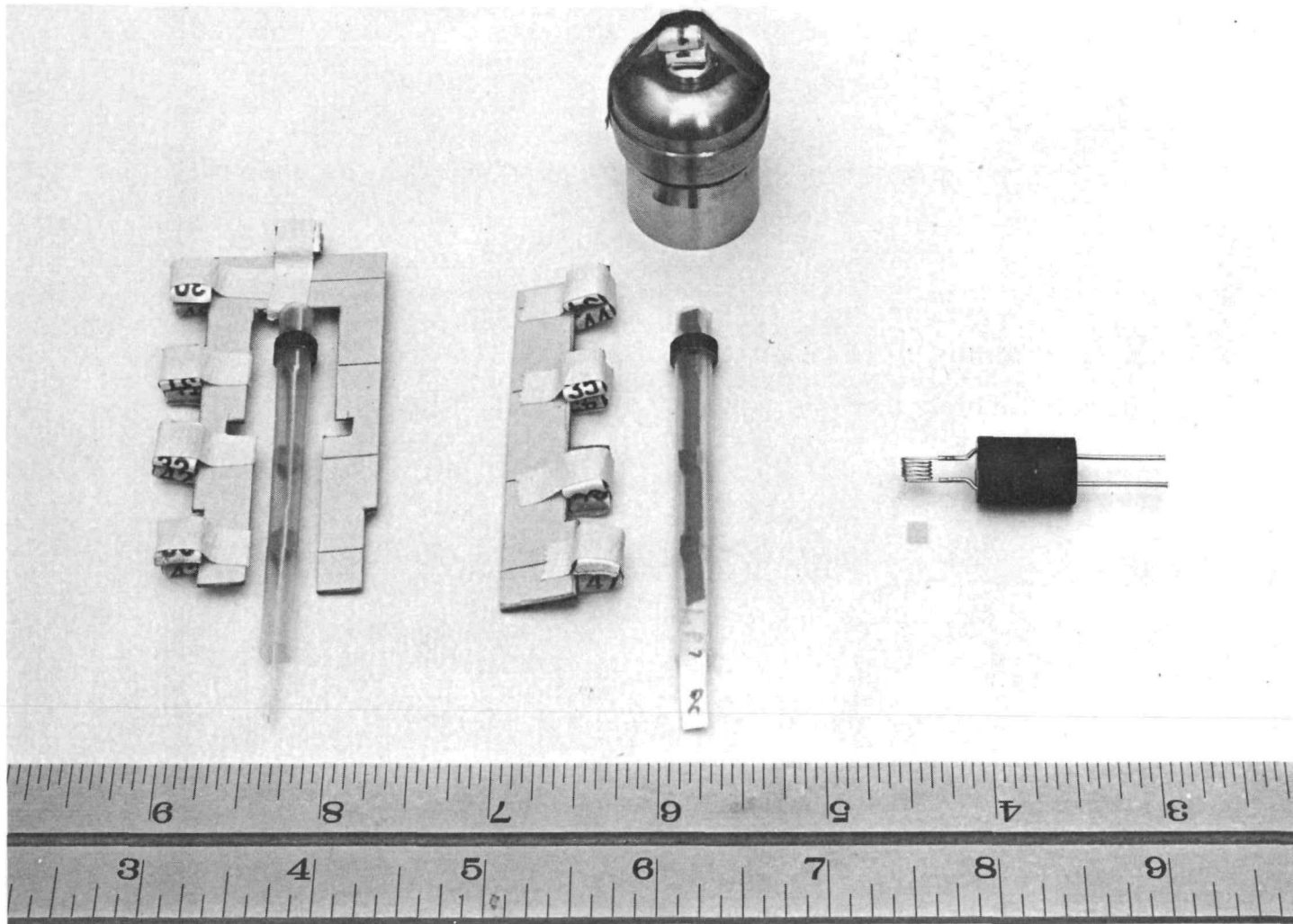


Figure 4-5. TLD Dosimetry Assemblage

**CONFIDENTIAL**

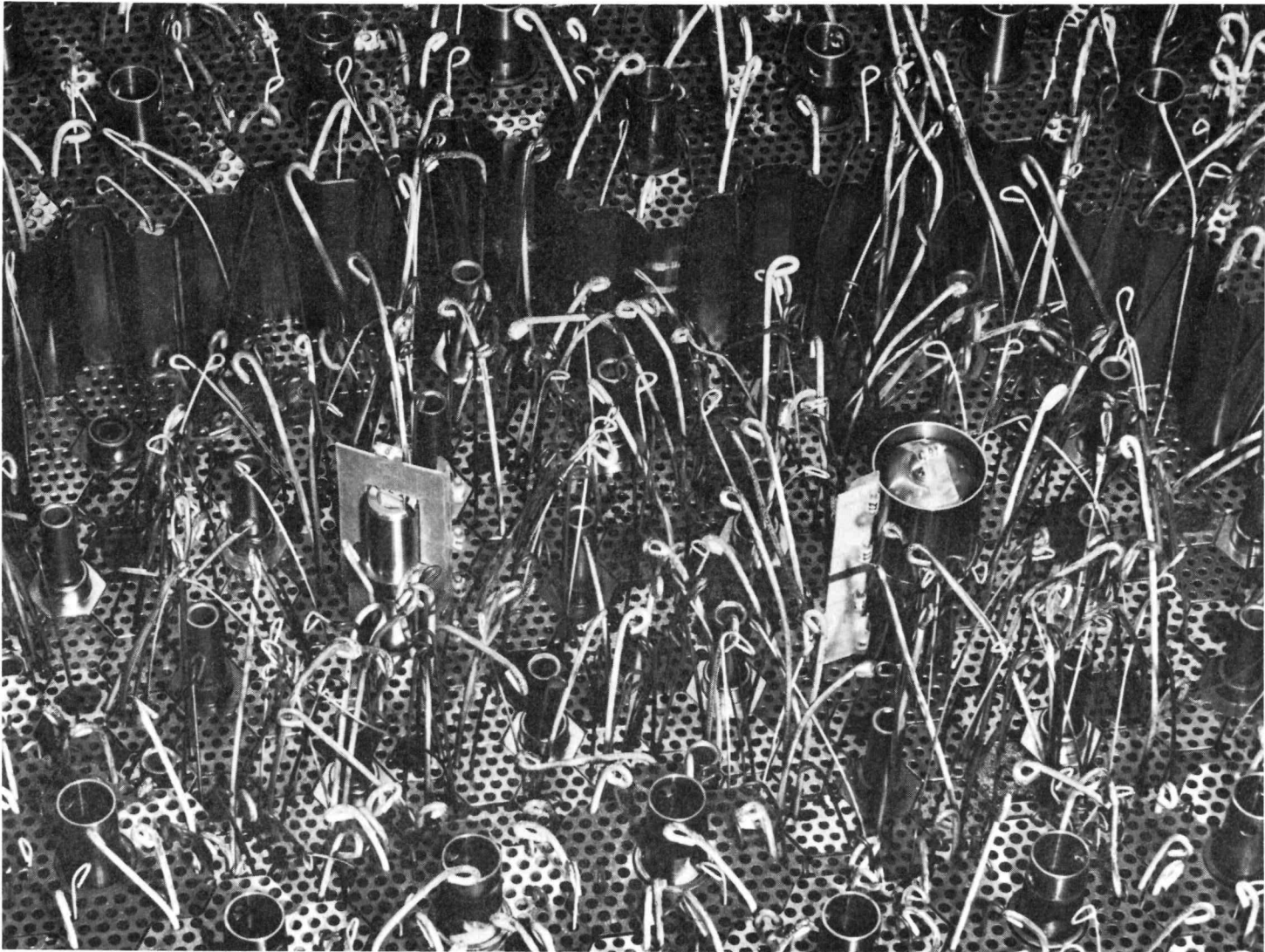
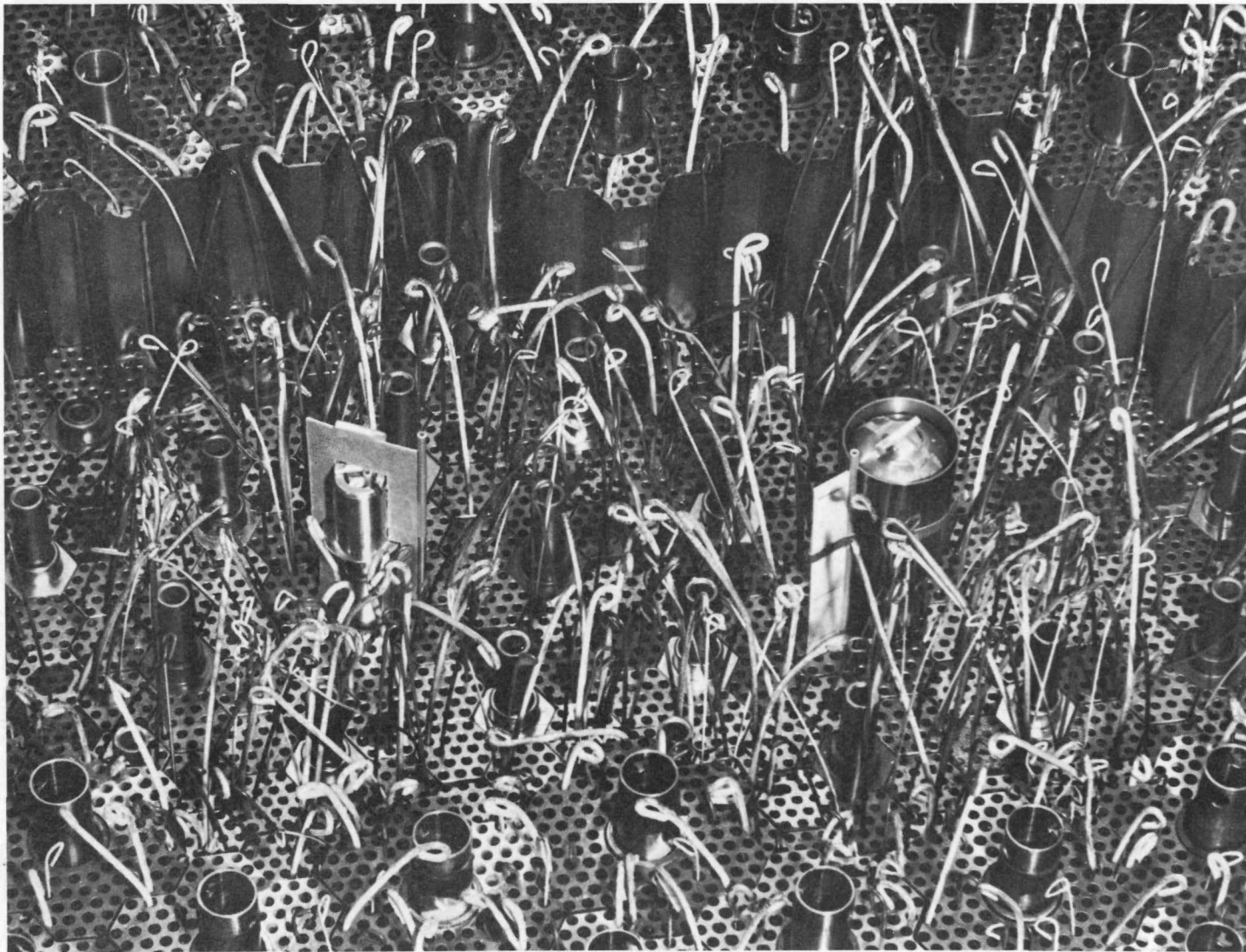


Figure 4-6. Dy-Al and Phylatron Dosimetry in Place

**CONFIDENTIAL**



**CONFIDENTIAL**



**CONFIDENTIAL**

Figure 4-7. Cd-Covered Dy-Al Dosimetry in Place

**CONFIDENTIAL**

 Astronuclear  
Laboratory

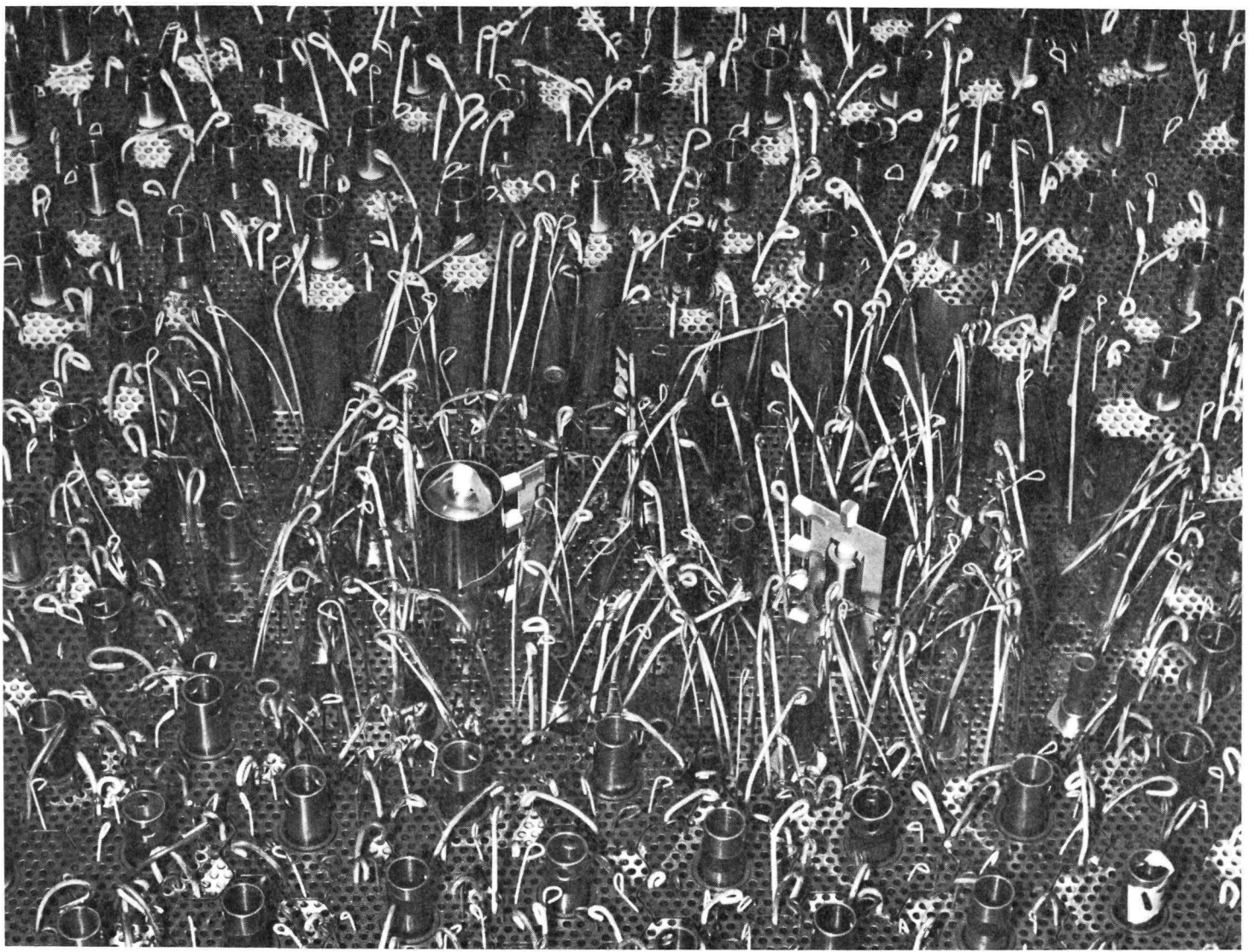
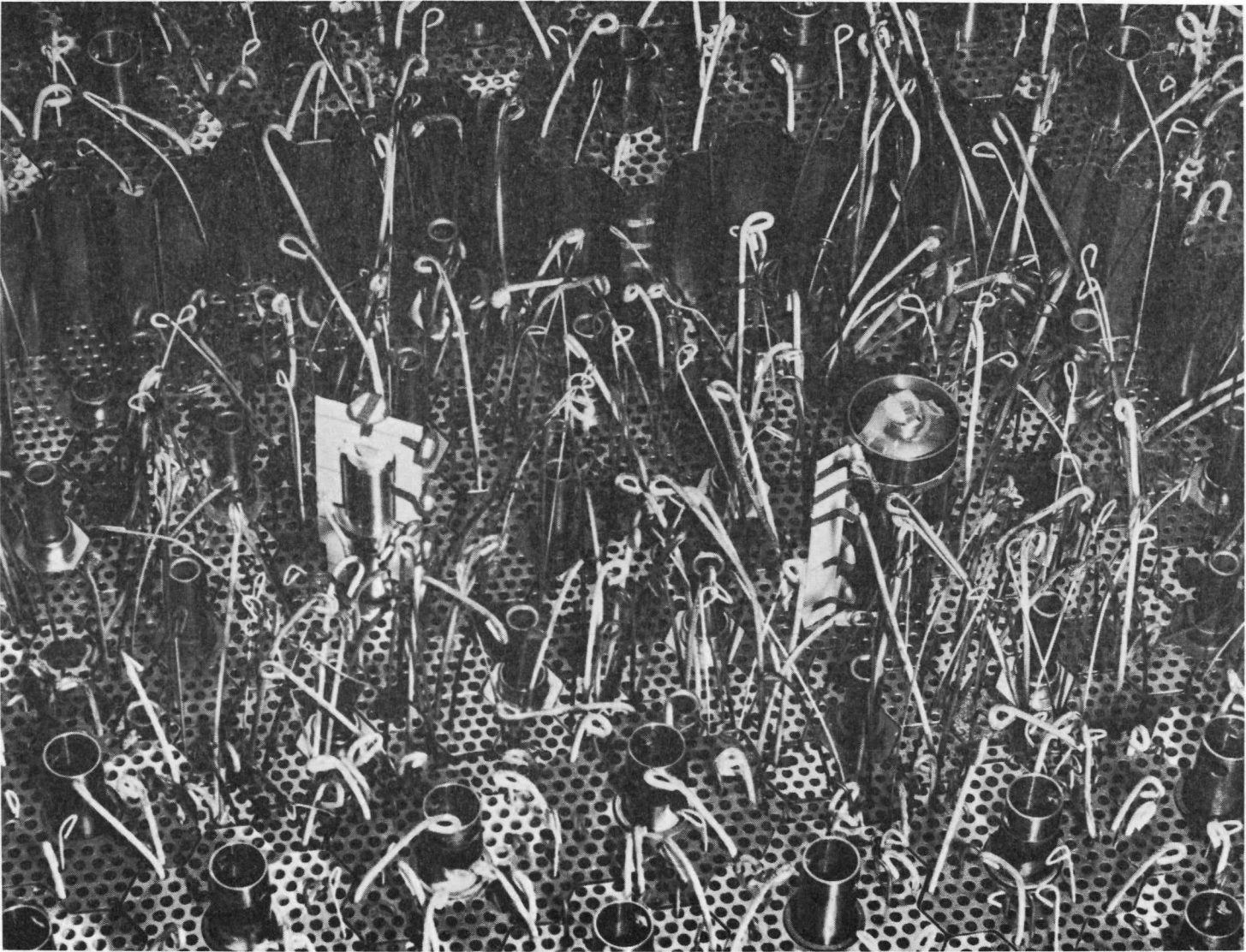


Figure 4-8. Sulfur Dosimetry In Place

**CONFIDENTIAL**

CONFIDENTIAL



CONFIDENTIAL

4-12

Figure 4-9. Cd-Covered U-238 and Th-232 Dosimetry In Place

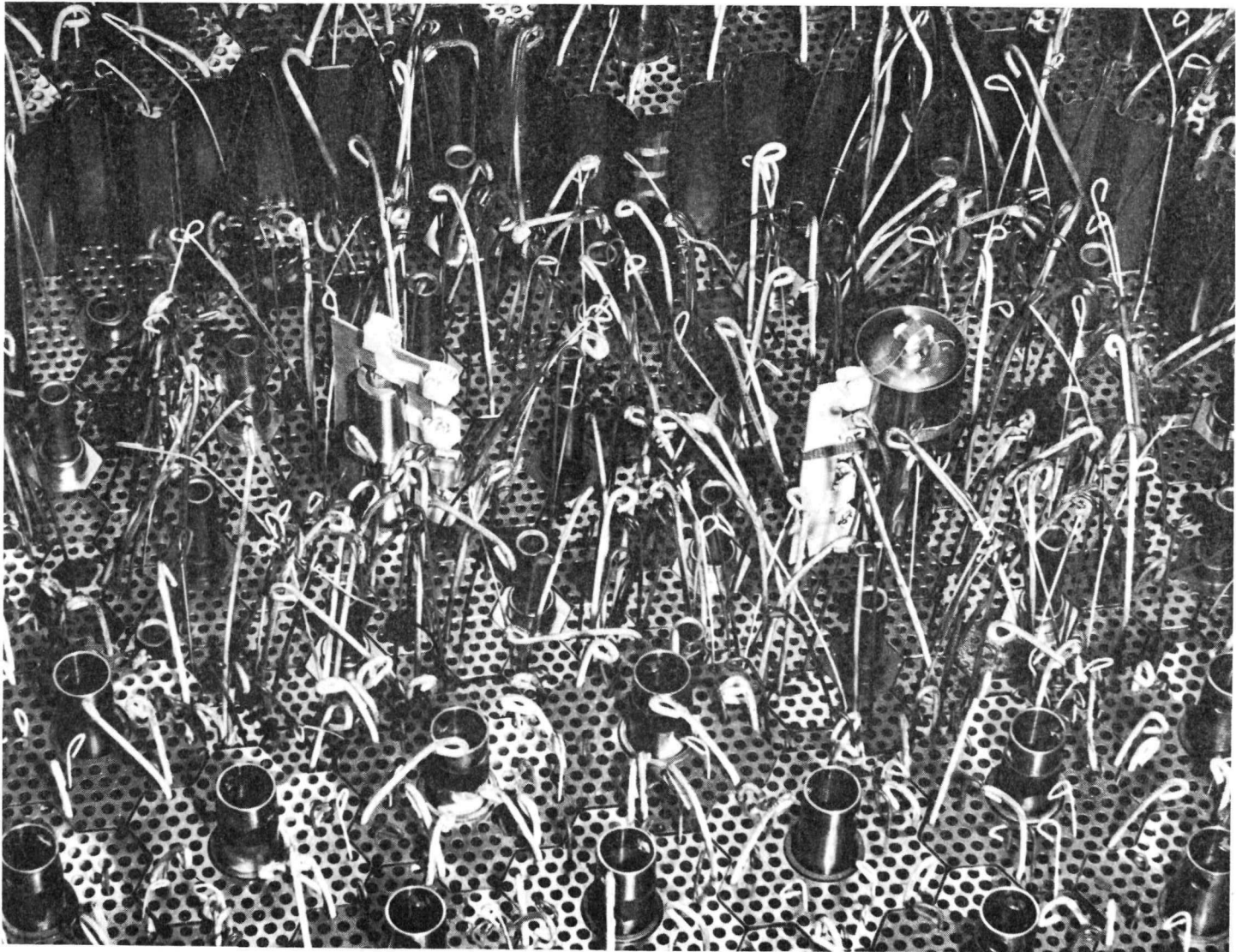


Figure 4-10. TLD Dosimetry In Place

**CONFIDENTIAL**

4-13

**CONFIDENTIAL**



Astronautical  
Laboratory

~~CONFIDENTIAL~~

This Page UNCLASSIFIED

Figures 4-1 through 4-4 also show, on the right hand side, the planchets on which the foils, pellets, and wires were counted. Figure 4-5 shows the heating coil from the reader system in which the TLD chips are placed for readout.

The accuracy of placement of any of the dosimeters is known to within  $\pm 0.1$  cm in any direction as referenced from the top (aft end of core) and from the centerline of the central fuel element in the cluster. These positions are reported in the data tables.

#### 4.1.2.2 Data Reduction Techniques

All activation type of passive dosimetry data was taken in the form of counts compared to counts on a normalizer dosimeter of the same type which has been irradiated in the same reactor run. These data were then analyzed by a set of data reduction codes\* on the CDC-6600 computer. The analysis included corrections for counter background, system resolving times, relative counter efficiencies, and dosimeter weights. The corrected counts on each dosimeter were divided by the corrected counts on the normalizer dosimeter. The results of more than one count on a given detector were also averaged. This produced intermediate results which gave the activity of each dosimeter relative to the activity of the normalizer. Computations were then made of the absolute detector activity and of the activity-to-flux correction. Application of these correction factors produced the final results which were both tabulated and plotted. For the Dy-Al foils, additional programming allowed both subtraction and ratioing of the bare and cadmium-covered activities to produce sub-cadmium or thermal activity and flux and to produce cadmium ratios. Throughout the data reduction, an error analysis was performed based on counting statistics and other estimated sources of error.

Some of the constants required for the data reduction are presented in Table 4-2.

The TLD data reduction was considerably simpler, requiring mainly a subtraction of an instrumentation background and a correction for calibration factors and integrated reactor power. This data reduction plus error computation, table preparation and graph preparation was also performed on the CDC-6600 computer.\*

The Phylatron data reduction was performed on a desk calculator. The computation included correction to absolute dose and division by integrated reactor power.

\* See DRM-51105C

~~CONFIDENTIAL~~

TABLE 4.2 CONSTANTS USED IN DATA REDUCTION

	Dy <sup>164</sup>	Dy <sup>165</sup>	S <sup>32</sup>	p <sup>32</sup>	U <sup>238</sup>
Atomic Number	66	66	16	15	92
Isotopic Weight <sup>1)</sup>	163.9392		31.97207		238.0508
Abundance <sup>1)</sup>	0.2818		0.950		
Half Life <sup>1)</sup>		141 min.		14.3 days	
Decay Constant		$4.9159 \times 10^{-3} \text{ min.}^{-1}$		$3.3661 \times 10^{-5} \text{ min.}^{-1}$	
Thermal Cross-Section <sup>2)</sup>	2700 barns				
Fast Cross-Section	$\pm 7.4\%$		0.300 barns		0.555 barns
Effective Threshold Energy			2.9 MeV		1.5 MeV

4-15

1. Chart of Nuclides, July 1966
2. BNL 325, 2nd Edition, Supp. 2

#### 4.1.2.3 Uncertainty Analysis

The analysis of the counting data included an uncertainty analysis for each dosimeter based on counting statistics and uncertainties of background rates, system resolving times, dosimeter weights and counting time. In addition to these quantities, the other possible sources of uncertainty were estimated for each type of dosimeter and were inserted into the final steps of the data reduction. Tables 4-3 and 4-4 list the significant sources of uncertainty and estimated magnitudes in terms of one-sigma standard deviations in percent.

In order to more completely describe the uncertainty calculation, consider  $E_0$  to be defined as the uncertainty calculated from the quantities listed in the first sentence of the preceding paragraph and the quantities  $E_1$ ,  $E_2$ , and  $E_3$  to be defined as shown in Tables 4-3 and 4-4. Then the uncertainty calculated for the fast flux is the vector sum of  $E_0$ ,  $E_1$ , and  $E_2$ . The uncertainty calculated for the cadmium ratios is the vector sum of  $E_{0B}$ ,  $E_{0C}$ ,  $E_{1B}$  and  $E_{1C}$ , where the subscripts, B and C, denote the bare and Cd-covered activities, respectively. Using the same subscripts, the "statistical" uncertainty calculated for the thermal flux is composed of  $E_{0B}$ ,  $E_{0C}$ ,  $E_{1B}$ ,  $E_{1C}$ , T1 and T2, where T1 and T2 are, respectively, the percent uncertainties in the  $C_1$  and  $C_2$  parameters of the thermal activity calculations:

$$A_T = C_1 \left[ A_B - (C_2) A_C \right]$$

where  $C_1$  and  $C_2$  are the first order correction factors relating to perturbations of the sub-cadmium and epi-cadmium flux by the foils and the cadmium covers, and where  $A_B$  and  $A_C$  are, respectively, the bare and Cd-covered activities. The "total" uncertainty calculated for the thermal flux is the vector sum of the "statistical" uncertainty described above plus the uncertainties  $E_{2B}$  and  $E_{3B}$ .

The accuracy of the TLD and Phylatron measurements have also been estimated. Table 4-5 summarizes the principal sources of uncertainty on the basis of one-sigma estimates given in percent. The total uncertainty is in the range of  $\pm 16$  percent to  $\pm 19$  percent for the TLD s and ( $\pm 23$  percent  $\pm 5$  rads) for the Phylatrons.

TABLE 4-3  
SOURCES OF RANDOM AND BIASING ERRORS

Source	Dy	S	U-238	Th
Spectral Dependent Variations of Cross Section	1.0	7.0	5.0	5.0
Variations in Alloy Content	2.0	-	-	-
Counter Inter-Normalization	2.0	0.5	5.0	5.0
Variations in Dosimeter Weights, if uncorrected	-	0.5	-	-
Contributions From Unwanted Reactions	-	0.5	5.0	5.0
TOTAL	E1	3.0	7.1	8.6

(Percent errors on a one-sigma basis.)



TABLE 4-4  
SOURCES OF SYSTEMATIC ERRORS IN ABSOLUTE ACTIVITY AND FLUX

Source	Dy	S	U-238	Th
Isotopic Abundance	0.1	0.1	-	-
Alloy Content	7.0	-	-	-
Normalizer Count Rate	1.0	1.0	1.0	1.0
Saturation Exposure Calculation	0.1	1.0	-	-
Reactor Power	6.0	6.0	6.0	6.0
Absolute Counting Efficiency of Normalizer	6.0	10.0	10.0	25.0
Contribution of Unwanted Activities	-	1.0	-	-
SUBTOTAL E2	11.0	11.8	11.7	25.7
Cross Section (for Flux Computation only) E3	7.4	7.0	10.0	10.0
TOTAL	13.3	13.7	15.4	27.6

TABLE 4-5  
TLD AND PHYLATRON MEASUREMENT UNCERTAINTIES

Source of Uncertainty	One-Sigma Percent	
	TLD	Phylatron
Reproducibility	5	2
Uniformity	12	10
Power	6	6
Calibration	6.4***	20
Readout Accuracy	1 to 10	5**(rads)
TOTAL	16 to 19 *	23% + 5**(rads)

\*An additional uncertainty results from use in a mixed gamma-neutron field as a direct consequence of the 3 mole percent Mn:F<sub>2</sub> contained in the CaF<sub>2</sub>:Mn TLD's. It is felt, however, that an upper limit of approximately 30 percent (due to neutron capture by the Mn) would be a reasonable assumption for these measurements.

\*\*Absolute uncertainties [rads (tissue)]

\*\*\*See Appendix A.

### 4.1.3 Active Dosimetry

#### 4.1.3.1 Bragg-Gray Chambers

The active dosimetry consisted of Bragg-Gray chambers with graphite and with stainless steel walls. A description of the chambers used and the theory and method of the measurements appear in DRM 51179.

#### 4.1.3.2 Calibration

The Bragg-Gray calibration constants  $K_m$  were obtained by exposing the chamber to a known (traceable to NBS radiation standards) gamma ray field from a Co-60 source as described in DRM 51177. The calibration constants of the detectors employed in these measurements are:

$$K_m \text{ Graphite} = 9.76 \times 10^{12} \pm 3.9\% \text{ rads/hr-amp}$$
$$K_m \text{ Stainless Steel} = 7.36 \times 10^{12} \pm 4.9\% \text{ rads/hr-amp}$$

#### 4.1.3.3 Positioning

The radiation heating rates in materials located near the CHESH components at reactor core position 5C2 and 4C2 were measured by graphite and stainless steel Bragg-Gray ionization chambers, respectively, placed adjacent to the components as shown in Figures 4-11 and 4-12.

#### 4.1.3.4 Data Reduction Techniques

The data reduction consists of converting the ionization chamber current readings to the form of the absorbed gamma ray dose rate in the detector material in  $\text{rads}_m/\text{hr-watt}$ , or  $\text{watts/gm-megawatt}$  by use of the expression:

Absorbed dose rate in Bragg-Gray chamber material

$$(\text{rads}_m/\text{hr-watt}) = \frac{K_m J}{W}$$

$$\text{Watts/gm-megawatt} = \frac{\text{rads}_m/\text{hr-watt}}{3.6 \times 10^2}$$

where

$K_m$  = Bragg-Gray calibration constant in  $\text{rads}_m/\text{hr-amps}$  in material  $m$  as determined by the chamber calibration procedures discussed above

$J$  = Ion current in amperes

$W$  = Reactor power in watts

#### 4.1.3.5 Uncertainty Analysis

The uncertainty in these measurement results from the vectorial sum of uncertainties in detector calibration (about 6%), uncertainty in current reading with the picoammeter from manufacturer's specifications (approximately 1%), and uncertainties in the reactor power (approximately 6%). Assuming that these uncertainties are independent, the vector sum of the results is ( $\pm 8.5\%$ ).

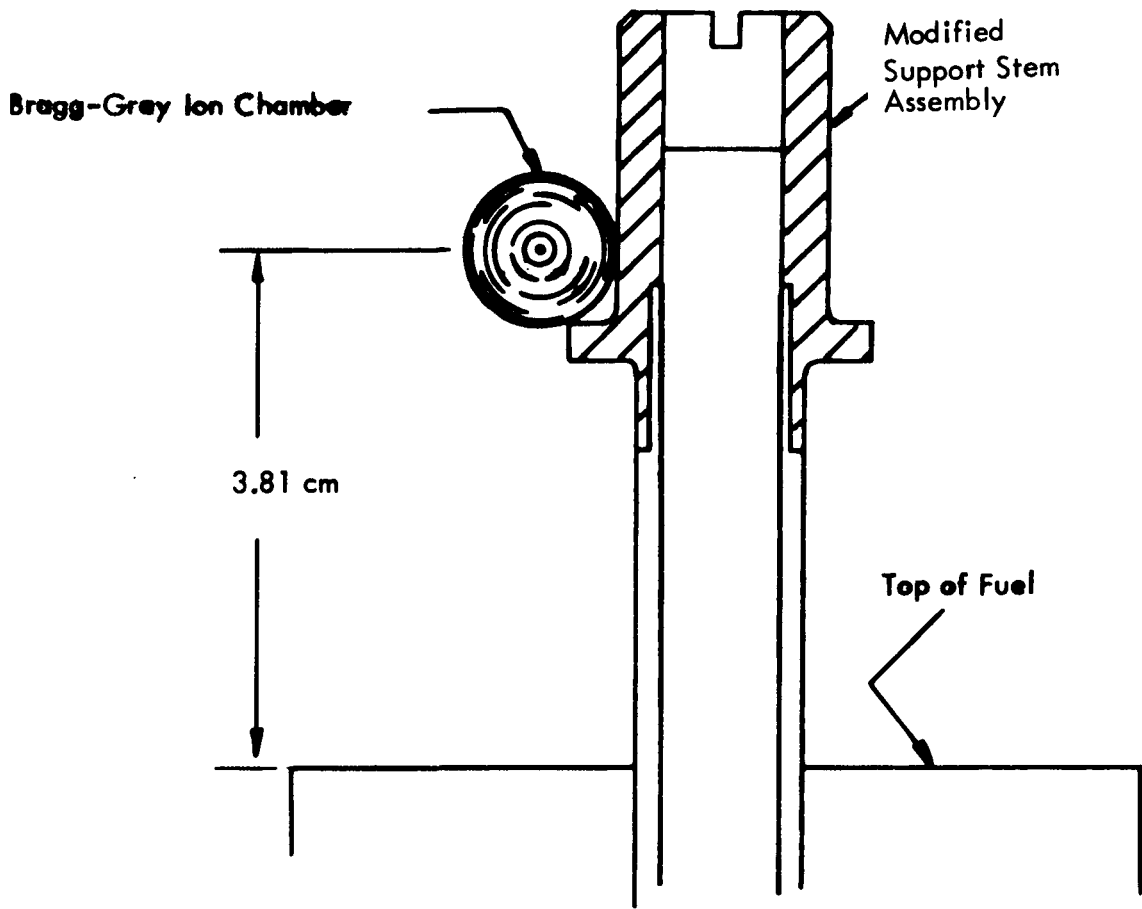


Figure 4-11. Location of Bragg-Gray Ion Chamber on Reference Assembly

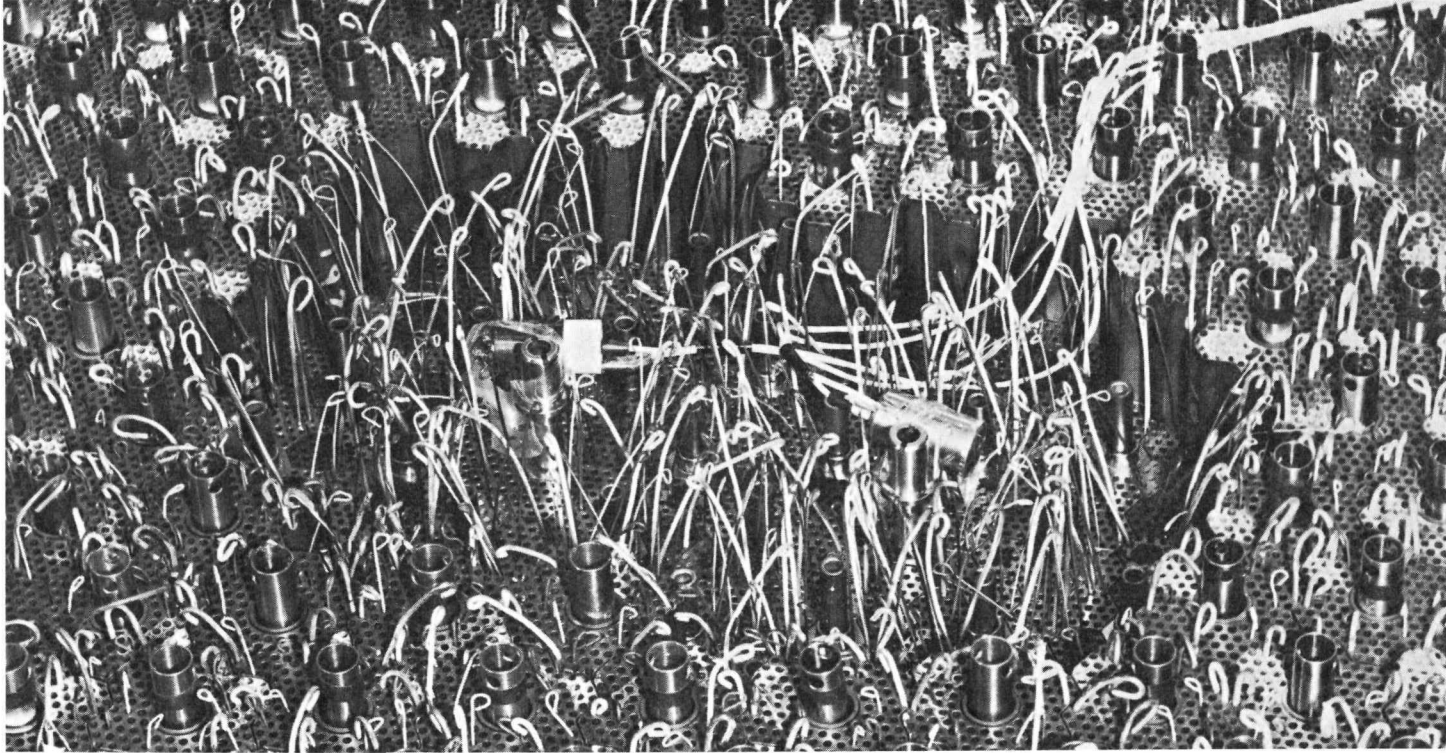


Figure 4-12. Bragg-Gray Chambers In Place

In addition to these known uncertainties, systematic errors may also exist which affect the result. However, the magnitudes of these errors cannot, at present, be experimentally defined. These include:

1. Uncertainty in heating rate measurement due to use of the detector in a reactor environment with the calibration performed with monoenergetic gamma rays.

A. Effects of fast and thermal neutrons on the Bragg-Gray ion current due to neutron capture, fast neutron inelastic scattering and charged particle production in the walls and gas of the chamber.

B. Effect of wide spectral range of gamma ray energies (from 50 keV - 9 MeV) on the detector operation.

2. Uncertainty due to the fact that the detector is placed adjacent to the support stem and will be partially shielded by it.

## 4.2 TEST RESULTS

### 4.2.1 General

The results of the measurements are reported in both tabular and graphical form. Positions are reported in terms of the radius in centimeters from the centerline of the support stem and the elevation in centimeters beyond the end of the fuel element. A location code is given denoting whether the measurement was internal (INT) or external (EXT) to the support stem and whether it was performed with (W) or without (WO) the CHESH assembly.

Estimates of error are presented for each data point in terms of percent standard deviation on a one-sigma basis.

### 4.2.2 Dysprosium-Aluminum Wires

Table 4-6 presents the thermal flux and the cadmium ratios calculated from the Dy-Al measurements. Table 4-7 presents the thermal flux in conjunction with the bare and cadmium-covered activities from which the flux was obtained. Figures 4-13 through 4-16 present axial plots of the bare activity, Cd-covered activity, thermal flux, and cadmium ratio, respectively.

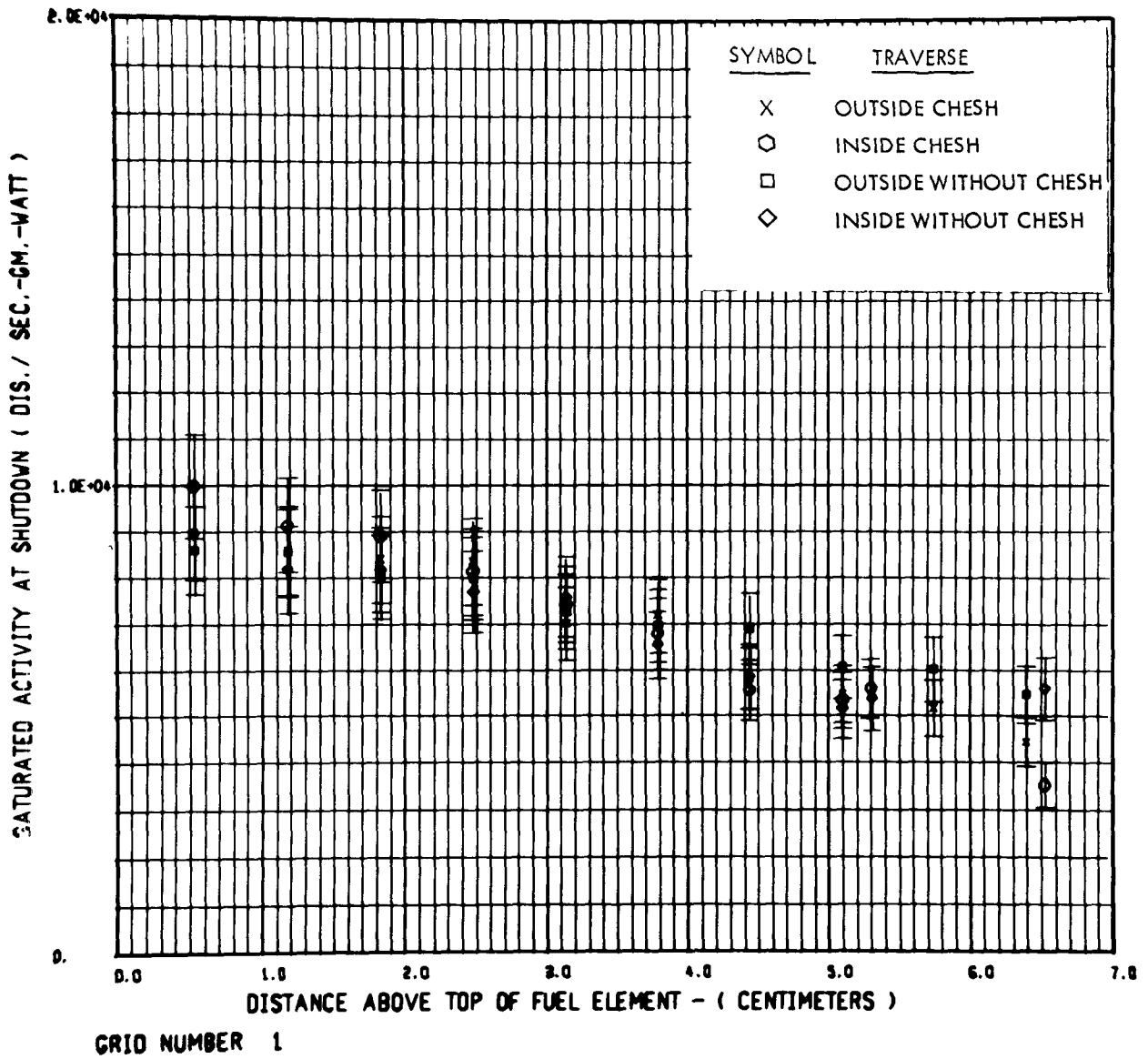


Figure 4-13. CESH Experiment - Bare Dy Activity



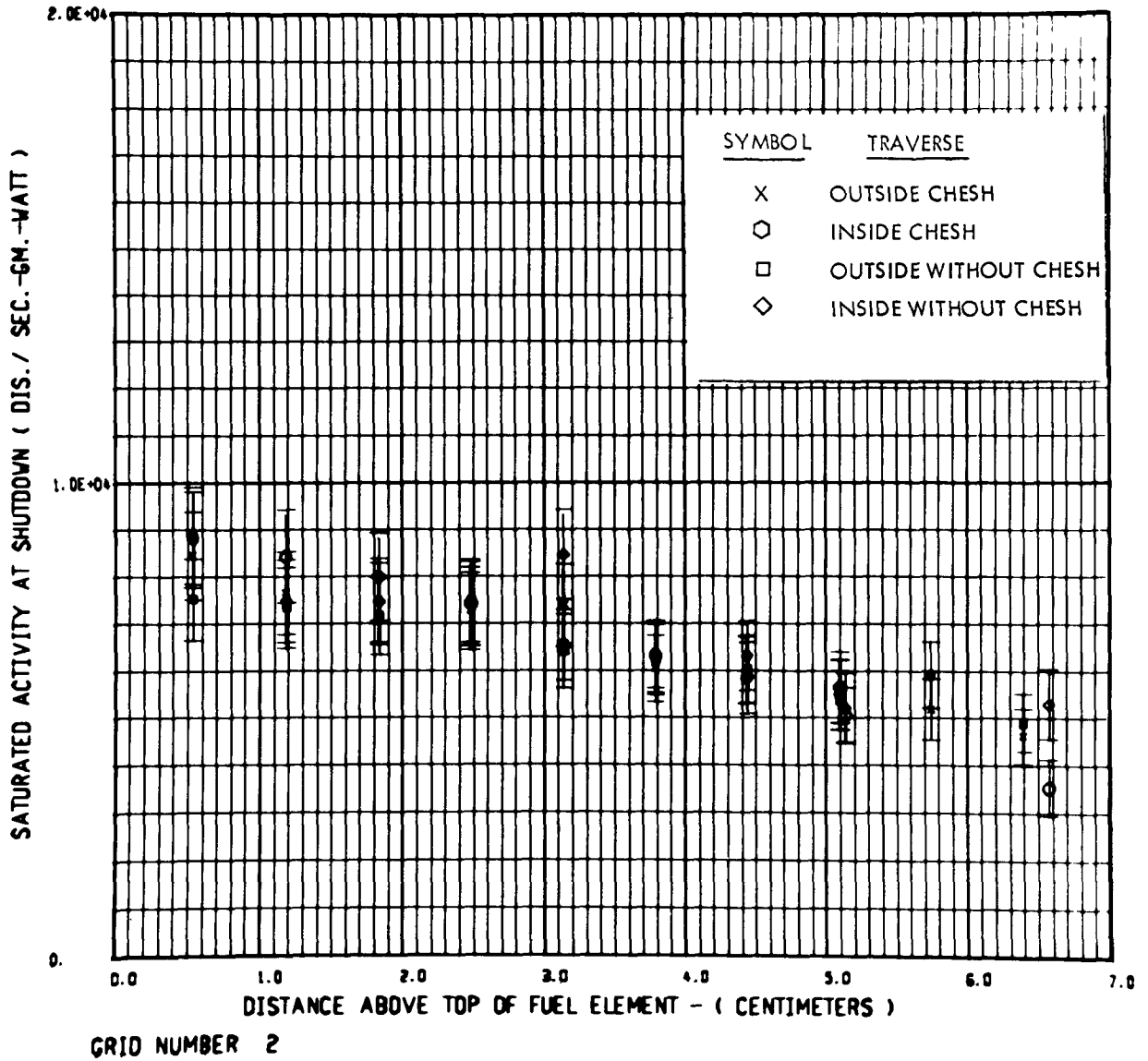


Figure 4-14. CHESH Experiment - Cd-Covered Dy Activity

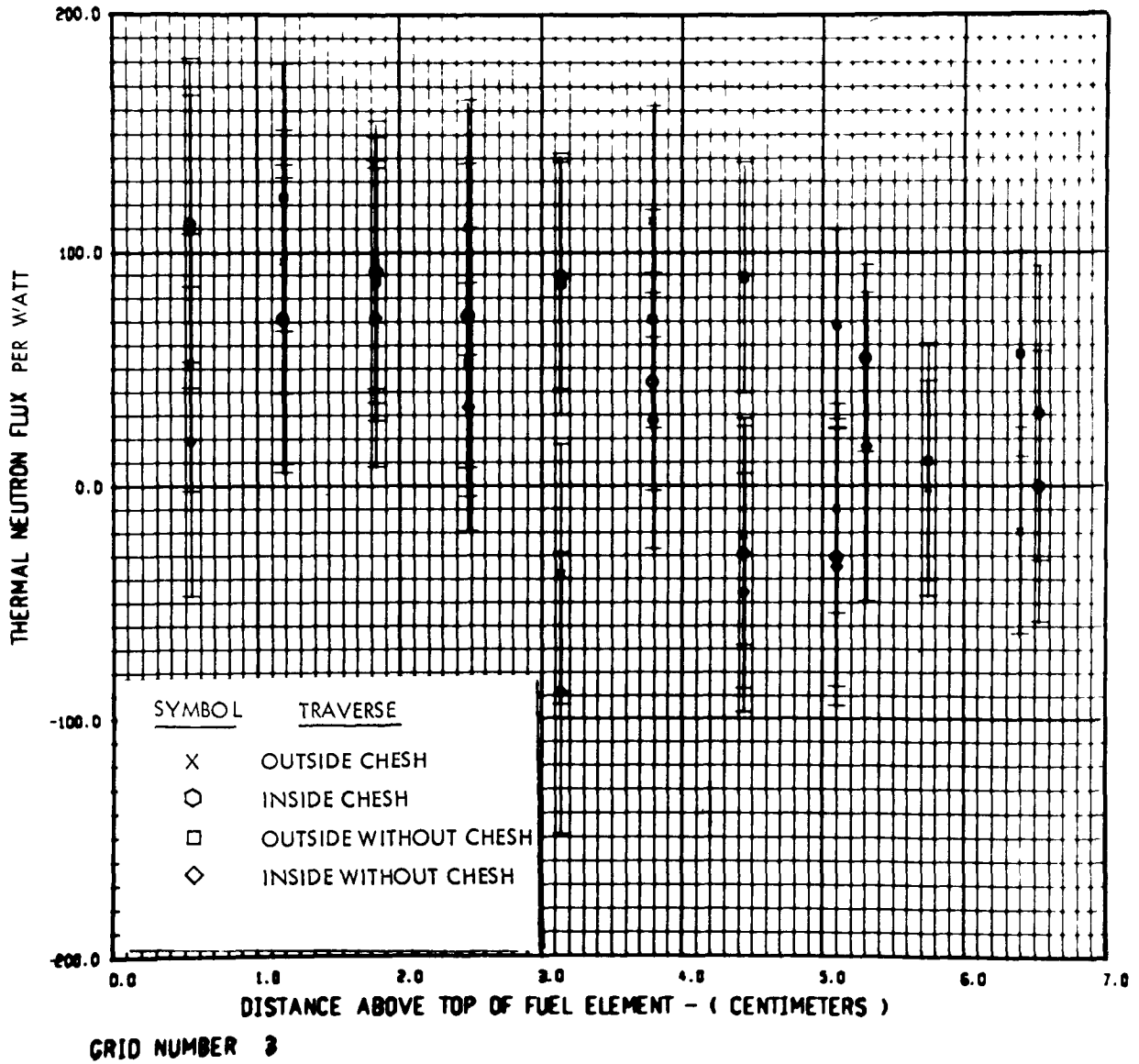


Figure 4-15. CHESH Experiment - Thermal Flux From Dy-Al

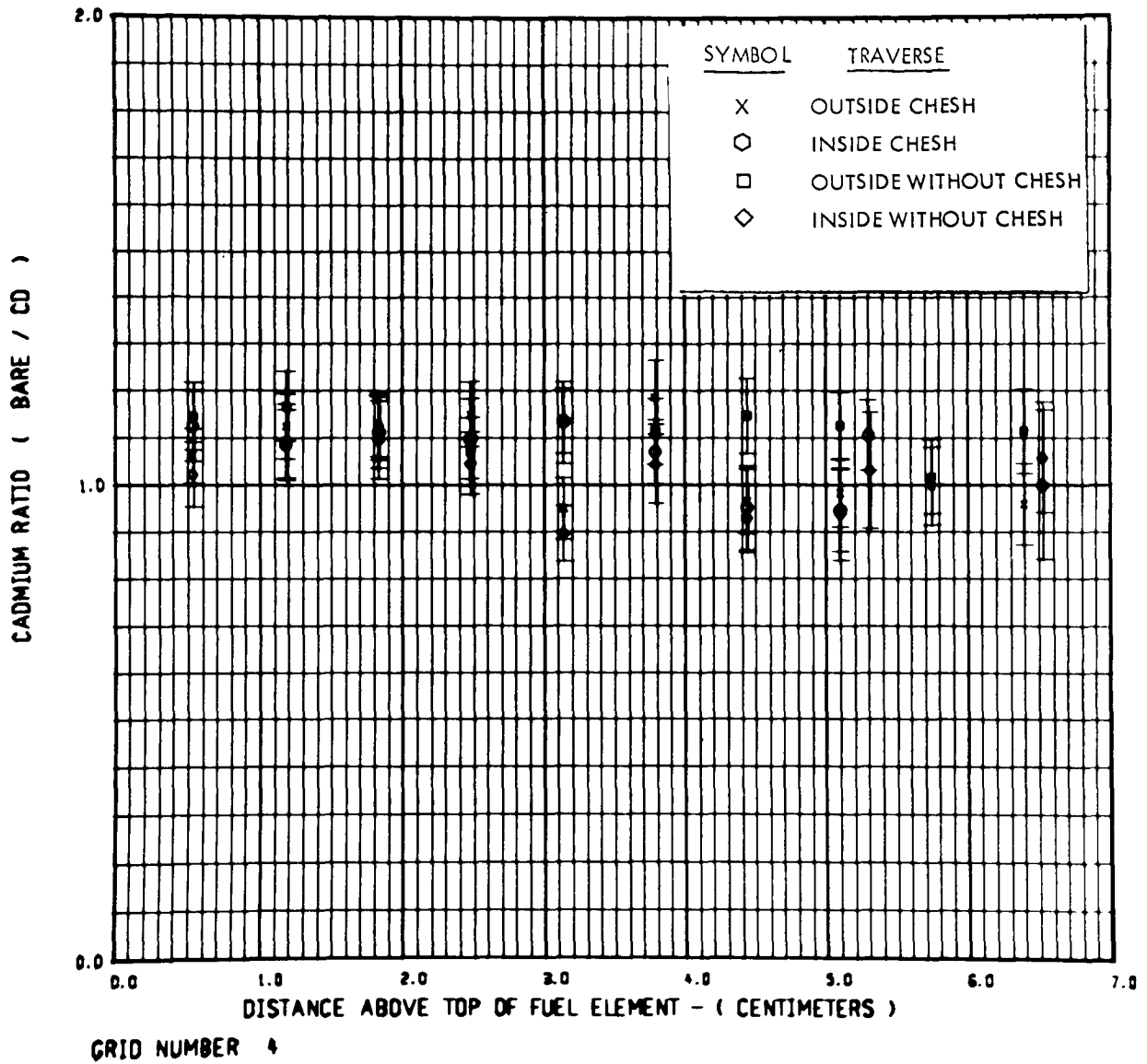


Figure 4-16. CHESH Experiment - Dy-Al Cadmium Ratios

TABLE 4-6

## CHESH EXPERIMENT - DY-AL FOILS - THERMAL FLUX AND CADMIUM RATIO

Page 1 of 2

OCTOBER 3, 1969

LOCATION	RADIUS (CM.)	AZIMUTH (DEG.)	ELEVATION (CM.)	THERMAL FLUX	TOTAL STD.DEV.	STAT. STD.DEV.	CD. RATIO	TOTAL STD.DEV.
EXT-WO	1.49	90.00	.53	1.097E+02	51.78	50.16	1.14	6.29
EXT-WO	1.49	90.00	1.14	1.231E+02	46.26	44.44	1.17	6.35
EXT-WO	1.49	90.00	1.83	4.727E+01	59.06	58.26	1.12	6.04
EXT-WO	1.49	90.00	2.44	5.274E+01	109.42	108.66	1.07	6.82
EXT-WO	1.49	90.00	3.14	8.603E+01	65.30	64.02	1.13	7.70
EXT-WO	1.49	90.00	3.79	7.130E+01	65.53	64.26	1.11	6.32
EXT-WO	1.49	90.00	4.44	8.902E+01	55.45	53.45	1.15	6.42
EXT-WO	1.49	90.00	5.10	6.884E+01	59.28	57.87	1.13	6.38
EXT-WO	1.49	90.00	5.75	1.047E+01	482.70	482.53	1.02	7.88
EXT-WO	1.49	90.00	6.40	5.635E+01	78.16	77.09	1.11	8.00
EXT-WO	0.00	90.00	6.53	-2.662E-01	21794.45	21794.45	1.00	16.02
EXT-W	1.50	90.00	.53	5.260E+01	104.71	103.92	1.06	5.51
EXT-W	1.50	90.00	1.14	9.593E+01	58.91	57.49	1.12	6.18
EXT-W	1.50	90.00	1.83	9.583E+01	56.47	54.98	1.13	5.94
EXT-W	1.50	90.00	2.44	1.102E+02	49.50	47.80	1.15	6.06
EXT-W	1.50	90.00	3.14	-3.624E+01	145.60	145.03	.95	6.94
EXT-W	1.50	90.00	3.79	1.130E+02	43.64	41.70	1.19	6.67
EXT-W	1.50	90.00	4.44	-2.159E+01	217.95	217.60	.96	7.25
EXT-W	1.50	90.00	5.10	-1.002E+01	449.69	449.50	.98	7.51
EXT-W	1.50	90.00	5.75	-1.156E+00	2992.54	3992.62	1.00	8.32
EXT-W	1.50	90.00	6.40	-1.950E+01	226.42	226.05	.96	9.11
EXT-W	0.00	90.00	6.53	3.106E+01	202.34	201.93	1.06	11.17
INT-WO	.34	90.00	.53	1.847E+01	350.15	349.92	1.02	6.82
INT-WO	.34	90.00	1.14	7.061E+01	86.75	85.79	1.09	7.16
INT-WO	.34	90.00	1.83	7.219E+01	88.78	87.84	1.10	7.65
INT-WO	.34	90.00	2.44	3.358E+01	159.77	158.25	1.05	6.34
INT-WO	.34	90.00	3.14	-6.899E+01	67.63	66.40	.90	6.61
INT-WO	.34	90.00	3.79	2.775E+01	198.18	197.76	1.04	8.08
INT-WO	.34	90.00	4.44	-4.601E+01	111.46	110.71	.93	7.76
INT-WO	.34	90.00	5.10	-3.495E+01	170.43	169.95	.94	10.52
INT-WO	0.00	90.00	5.31	1.647E+01	401.94	401.74	1.03	12.08
INT-W	.34	90.00	.53	1.119E+02	62.43	61.10	1.13	6.71
INT-W	.34	90.00	1.14	7.163E+01	92.15	91.25	1.08	6.90
INT-W	.34	90.00	1.83	9.178E+01	70.06	68.87	1.11	6.93
INT-W	.34	90.00	2.44	7.300E+01	89.32	88.39	1.10	7.78
INT-W	.34	90.00	3.14	8.956E+01	54.33	52.79	1.14	6.17

TABLE 4-6 (Continued)

CHESH EXPERIMENT - DY-AL FOILS - THERMAL FLUX AND CADMIUM RATIO

OCTOBER 3, 1969

LOCATION	RADIUS (CM.)	AZIMUTH (DEG.)	ELEVATION (CM.)	THERMAL FLUX	TOTAL STD.DEV.	STAT. STD.DEV.	CU. RATIO	TOTAL STD.DEV.
INT-W	.34	90.00	3.79	4.437E+01	105.74	104.95	1.07	6.44
INT-W	.34	90.00	4.44	-2.934E+01	197.45	197.03	.95	9.52
INT-W	.34	90.00	5.10	-3.089E+01	170.20	178.74	.95	9.35
INT-W	0.00	90.00	5.30	5.446E+01	73.50	72.37	1.11	6.80

4-30

TABLE 4-7

## CHESH EXPERIMENT - DY-AL FOILS - BARE, CD-COVERED AND THERMAL

Page 1 of 3

OCTOBER 3, 1969

LOCATION	RADIUS (CM.)	AZIMUTH (DEG.)	ELEVATION (CM.)	BARE ACTIVITY	STD. DEV.	CD. COVERED ACTIVITY	STD. DEV.	THERMAL EQUIV. FLUX 1.097F+02	STD. DEV.
EXT-WO	1.49	90.00	.53	8.598F+03	11.14				51.78
EXT-WO	1.56	90.00	.53			7.510F+03	11.66		
EXT-WO	1.49	90.00	1.18	8.542E+03	11.20			1.231E+02	46.26
EXT-WO	1.56	90.00	1.18			7.321F+03	11.64		
FXT-WO	1.49	90.00	1.83	8.013E+03	11.26			8.727E+01	59.66
FXT-WO	1.56	90.00	1.83			7.148E+03	11.41		
EXT-WO	1.49	90.00	2.48	7.984E+03	11.29			5.274F+01	109.42
FXT-WO	1.56	90.00	2.48			7.460E+03	11.81		
EXT-WO	1.49	90.00	3.14	7.248F+03	11.26			8.603E+01	65.30
EXT-WO	1.56	90.00	3.14			6.395F+03	12.36		
EXT-WO	1.49	90.00	3.79	6.946E+03	11.29			7.130E+01	65.53
FXT-WO	1.56	90.00	3.79			6.239F+03	11.53		
EXT-WO	1.49	90.00	4.44	6.883E+03	11.39			8.902E+01	55.45
FXT-WO	1.56	90.00	4.44			6.000F+03	11.77		
EXT-WO	1.49	90.00	5.10	6.048E+03	11.27			6.884E+01	59.28
EXT-WO	1.56	90.00	5.10			5.365F+03	11.59		
FXT-WO	1.49	90.00	5.75	6.008E+03	11.77			1.047E+01	482.70
FXT-WO	1.56	90.00	5.75			5.904F+03	12.01		
EXT-WO	1.49	90.00	6.40	5.459E+03	11.32			5.635F+01	78.16
EXT-WO	1.56	90.00	6.40			4.901F+03	12.50		
FXT-WO	0.00	90.00	6.53	3.529E+03	13.54			-2.662E-01	794.45
FXT-WO	0.00	90.00	6.58			3.531F+03	17.14		
*									
EXT-W	1.50	90.00	.53	8.964E+03	11.17			5.260E+01	104.71
EXT-W	1.57	90.00	.53			8.442F+03	11.23		
EXT-W	1.50	90.00	1.18	6.586E+03	11.23			9.593F+01	58.91
EXT-W	1.57	90.00	1.18			7.635F+03	11.52		
EXT-W	1.50	90.00	1.83	8.387E+03	11.32			9.563E+01	56.47
EXT-W	1.57	90.00	1.83			7.438F+03	11.30		
FXT-W	1.50	90.00	2.48	8.341E+03	11.38			1.102E+02	49.50
FXT-W	1.57	90.00	2.48			7.248F+03	11.30		
EXT-W	1.57	90.00	3.14	6.998E+03	11.23			-3.824E+01	145.60
EXT-W	1.50	90.00	3.14			7.378F+03	11.94		
FXT-W	1.57	90.00	3.14					1.130E+02	43.64
EXT-W	1.50	90.00	3.79	7.151E+03	11.24				
EXT-W	1.57	90.00	3.79			6.030F+03	11.77		

TABLE 4-7 (Continued)

CHESH EXPERIMENT - DY-AL FOILS - BARE, CD-COVERED AND THERMAL

Page 2 of 3

OCTOBER 3, 1969

LOCATION	RADIUS (CM.)	AZIMUTH (DEG.)	ELEVATION (CM.)	BARE ACTIVITY	STD. DEV.	CD. COVERED ACTIVITY	STD. DEV.	THERMAL EQUIV. FLUX	STD. DEV.
EXT-W	1.50	90.00	4.44	5.803E+03	11.51			-2.159E+01	217.98
EXT-W	1.57	90.00	4.44			6.017E+03	11.85		
EXT-W	1.50	90.00	5.10	5.462E+03	11.48			-1.002E+01	449.69
EXT-W	1.57	90.00	5.10			5.562E+03	12.04		
EXT-W	1.50	90.00	5.75	5.167E+03	11.74			-1.156E+00	3992.64
EXT-W	1.57	90.00	5.75			5.179E+03	12.33		
EXT-W	1.50	90.00	6.40	4.431E+03	11.94			-1.950E+01	226.42
EXT-W	1.57	90.00	6.40			4.625E+03	12.69		
EXT-W	0.00	90.00	6.53	5.600E+03	12.12			3.106E+01	202.34
EXT-W	0.00	90.00	6.58			5.292E+03	14.09		
*									
INT-WO	.34	90.00	.53	8.969E+03	11.31			1.897E+01	350.15
INT-WO	.26	90.00	.53			8.781E+03	11.79		
INT-WO	.34	90.00	1.18	8.179E+03	11.48			7.061E+01	86.75
INT-WO	.26	90.00	1.18			7.479E+03	11.83		
INT-WO	.34	90.00	1.83	8.170E+03	11.33			7.219E+01	88.78
INT-WO	.26	90.00	1.83			7.454E+03	12.27		
INT-WO	.34	90.00	2.48	7.694E+03	11.49			3.358E+01	158.77
INT-WO	.26	90.00	2.48			7.361E+03	11.34		
INT-WO	.34	90.00	3.14	7.576E+03	11.57			-8.899E+01	67.63
INT-WO	.26	90.00	3.14			8.458E+03	11.41		
INT-WO	.34	90.00	3.79	6.527E+03	11.27			2.775E+01	198.18
INT-WO	.26	90.00	3.79			6.251E+03	12.60		
INT-WO	.34	90.00	4.44	5.842E+03	12.05			-4.601E+01	111.46
INT-WO	.26	90.00	4.44			6.299E+03	11.64		
INT-WO	.34	90.00	5.10	5.145E+03	12.16			-3.495E+01	170.43
INT-WO	.26	90.00	5.10			5.491E+03	13.54		
INT-WO	0.00	90.00	5.31	5.375E+03	12.96			1.647E+01	401.94
INT-WO	0.00	90.00	5.14			5.212E+03	14.09		
*									
INT-W	.34	90.00	.53	9.976E+03	11.27			1.119E+02	62.43
INT-W	.26	90.00	.53			8.866E+03	11.77		
INT-W	.34	90.00	1.18	9.134E+03	11.19			7.163E+01	92.15
INT-W	.26	90.00	1.18			8.423E+03	11.96		
INT-W	.34	90.00	1.83	8.900E+03	11.36			9.178E+01	70.06
INT-W	.26	90.00	1.83			7.990E+03	11.81		

TABLE 4-7 (Continued)

CHESH EXPERIMENT - DY-AL FOILS - BARE, CD-COVERED AND THERMAL

Page 3 of 3

OCTOBER 3, 1969

LOCATION	RADIUS (CM.)	AZIMUTH (DEG.)	ELEVATION (CM.)	BARE ACTIVITY	STD. DEV.	CD. COVERED ACTIVITY	STD. DEV.	THERMAL EQUIV. FLUX	STD. DEV.
INT-W	.34	00.00	2.48	8.124E+03	11.65			7.300E+01	89.32
INT-R	.26	00.00	2.48			7.404F+03	12.06		
INT-V	.34	00.00	3.14	7.413E+03	11.22			8.958E+01	54.33
INT-W	.26	00.00	3.14			6.525F+03	11.52		
INT-V	.34	00.00	3.79	6.761E+03	11.43			4.437E+01	105.74
INT-W	.26	00.00	3.79			6.321F+03	11.46		
INT-W	.34	00.00	4.44	5.542E+03	11.90			-2.934E+01	197.45
INT-W	.26	00.00	4.44			5.833F+03	13.03		
INT-W	.34	00.00	5.10	5.331E+03	11.40			-3.089E+01	179.20
INT-W	.26	00.00	5.10			5.637F+03	13.34		
INT-W	0.00	00.00	5.30	5.585E+03	11.46			5.446E+01	73.50
INT-W	0.00	00.00	5.14			5.045F+03	11.64		

4-33



TABLE 4-8

## CHESH EXPERIMENT - SULPHUR PELLETS

Page 1 of 1

OCTOBER 3, 1969

LOCATION	RADIUS (CM.)	AZIMUTH (DEG.)	ELEVATION (CM.)	EQUIV. FLUX	TOTAL STD. DEV.	Saturated Activity	Total Std. Dev.
EXT-WO	1.62	90.00	.72	9.79940E+04	16.77	553.8	15.24
FXT-WO	1.79	90.00	2.41	1.19066E+05	16.09	672.8	14.49
EXT-WO	1.79	90.00	4.19	1.20172E+05	16.09	679.1	14.49
EXT-WO	1.79	90.00	5.97	1.06042E+05	16.09	599.3	14.49
FXT-WO	0.00	90.00	6.83	9.71832E+04	16.09	549.2	14.49
FXT-W	1.64	90.00	.72	1.27685E+05	16.09	721.6	14.49
EXT-W	1.81	90.00	2.41	1.16780E+05	16.09	660.0	14.49
FXT-W	1.81	90.00	4.19	1.06686E+05	16.09	602.9	14.49
FXT-W	1.81	90.00	5.97	9.86360E+04	16.09	557.4	14.49
EXT-W	0.00	90.00	6.83	8.29234E+04	16.10	468.6	14.50
INT-WO	0.00	90.00	.72	1.17297E+05	16.09	662.9	14.49
INT-WO	0.00	90.00	2.41	1.20074E+05	16.09	678.6	14.49
INT-WO	0.00	90.00	4.92	1.15117E+05	16.09	650.5	14.49
INT-W	0.00	90.00	.72	1.25212E+05	16.09	707.6	14.49
INT-W	0.00	90.00	2.41	1.09054E+05	16.09	616.3	14.49
INT-W	0.00	90.00	4.92	9.44890E+04	16.09	534.0	14.49

TABLE 4-9

## CHESH EXPERIMENT - URANIUM-238 FOILS

Page 1 of 1

OCTOBER 3, 1969

LOCATION	RADIUS (CM.)	AZIMUTH (DEG.)	ELEVATION (CM.)	EQUIV. FLUX	TOTAL STD. DEV.
FAT-WO	1.41	90.00	.68	2.15995E+05	17.50
FAT-WO	1.59	90.00	2.36	2.07831E+05	17.51
FAT-WO	1.59	90.00	4.14	1.90004E+05	17.53
EXT-WO	1.59	90.00	5.92	1.71270E+05	17.57
FXT-WO	0.00	90.00	6.56	1.62207E+05	17.60
EXT-W	1.43	90.00	.68	2.18461E+05	17.51
EXT-W	1.61	90.00	2.36	2.08869E+05	17.52
EXT-W	1.61	90.00	4.14	1.76874E+05	17.55
EXT-W	1.61	90.00	5.92	1.57691E+05	17.60
EXT-W	0.00	90.00	6.56	1.27807E+05	17.70
INT-WO	0.00	90.00	.73	2.21530E+05	17.52
INT-WO	0.00	90.00	2.41	2.11806E+05	17.51
INT-WO	0.00	90.00	5.25	1.62594E+05	17.61
INT-W	0.00	90.00	.73	2.20757E+05	17.52
INT-W	0.00	90.00	2.41	1.94745E+05	17.55
INT-W	0.00	90.00	5.25	1.57354E+05	17.64

TABLE 4-10

## CHESH EXPERIMENT - CALCIUM FLUORIDE TLD CHIPS

Page 1 of 1

OCTOBER 16, 1969

LOCATION	RADIUS (CM.)	AZIMUTH (DEG.)	ELEVATION (CM.)	DOSE RATE	TOTAL STD.DEV.
INT-W	0.00	90.00	5.16	1.8216F+03	19.62
INT-W	0.00	90.00	4.21	1.7071E+03	19.62
INT-W	0.00	90.00	2.38	2.1443E+03	19.62
INT-W	0.00	90.00	.71	2.1287E+03	19.62
INT-WO	0.00	90.00	5.16	1.5769E+03	19.62
INT-WO	0.00	90.00	4.21	1.7695E+03	19.62
INT-WO	0.00	90.00	2.38	2.2693E+03	19.62
INT-WO	0.00	90.00	.71	2.3786E+03	19.62
EXT-WO	0.00	90.00	6.75	1.8424E+03	19.62
EXT-WO	1.61	90.00	5.95	1.8320E+03	19.62
EXT-WO	1.61	90.00	4.21	2.1027E+03	19.62
EXT-WO	1.61	90.00	2.38	2.3005E+03	19.62
EXT-WO	1.61	90.00	.71	2.2745E+03	19.62
EXT-W	0.00	90.00	6.75	1.8268F+03	19.62
EXT-W	1.61	90.00	5.95	2.1287E+03	19.62
EXT-W	1.61	90.00	4.21	2.4307E+03	19.62
EXT-W	1.61	90.00	2.38	2.4983E+03	19.62
EXT-W	1.61	90.00	.71	1.2646E+03	19.62
ROT WHL	0.00	90.00	0.00	1.2490E+03	19.62
ROT WHL	0.00	90.00	0.00	1.4155E+03	19.62

Note that for some of the data points the experimental thermal flux, as calculated from the difference of bare and Cd-covered activity, was negative and the cadmium ratio less than one. This occurred because the counting statistics were not good enough to resolve the small differences between the bare and Cd-covered activities. For these points the statistical accuracies reported are, in general, greater than  $\pm 100$  percent on a one-sigma basis.

The activities in each case are the calculated saturated activities in units of disintegrations per second per gram of Dy-164 per watt. The cadmium ratios are defined as the ratio of bare to cadmium-covered activity.

#### 4.2.3 Sulfur Pellets

Table 4-8 and Figure 4-17 present the fast fluxes per watt, above 2.9 MeV, calculated from the sulfur measurements. Table 4-8 also gives the saturated activities in units of disintegrations per second per gram of S-32 per watt.

#### 4.2.4 Uranium-238 Foils

Table 4-9 and Figure 4-18 present the fast neutron flux per watt, above 1.5 MeV, calculated from the U-238 measurements.

#### 4.2.5 Thorium Foils

The activity obtained on the thorium foils was extremely low and, hence, the data obtained were erratic and inconsistent. Accordingly, the results are not presented.

#### 4.2.6 Comparison of Fast Fluxes

Figures 4-19 through 4-22 present a comparison of the fast fluxes obtained with sulfur ( $E > 2.9$  MeV) and with uranium-238 ( $E > 1.5$  MeV) for the four axial traverses measured.

#### 4.2.7 TLD Chips

The data obtained with lithium fluoride TLD chips are not presented because of unexplained inconsistencies which are believed to be due to a larger impurity of Li6 than was quoted by the vendor.

The calcium fluoride TLD results are presented in Table 4-10 and Figure 4-26 in units of rads (carbon) per hour per watt.

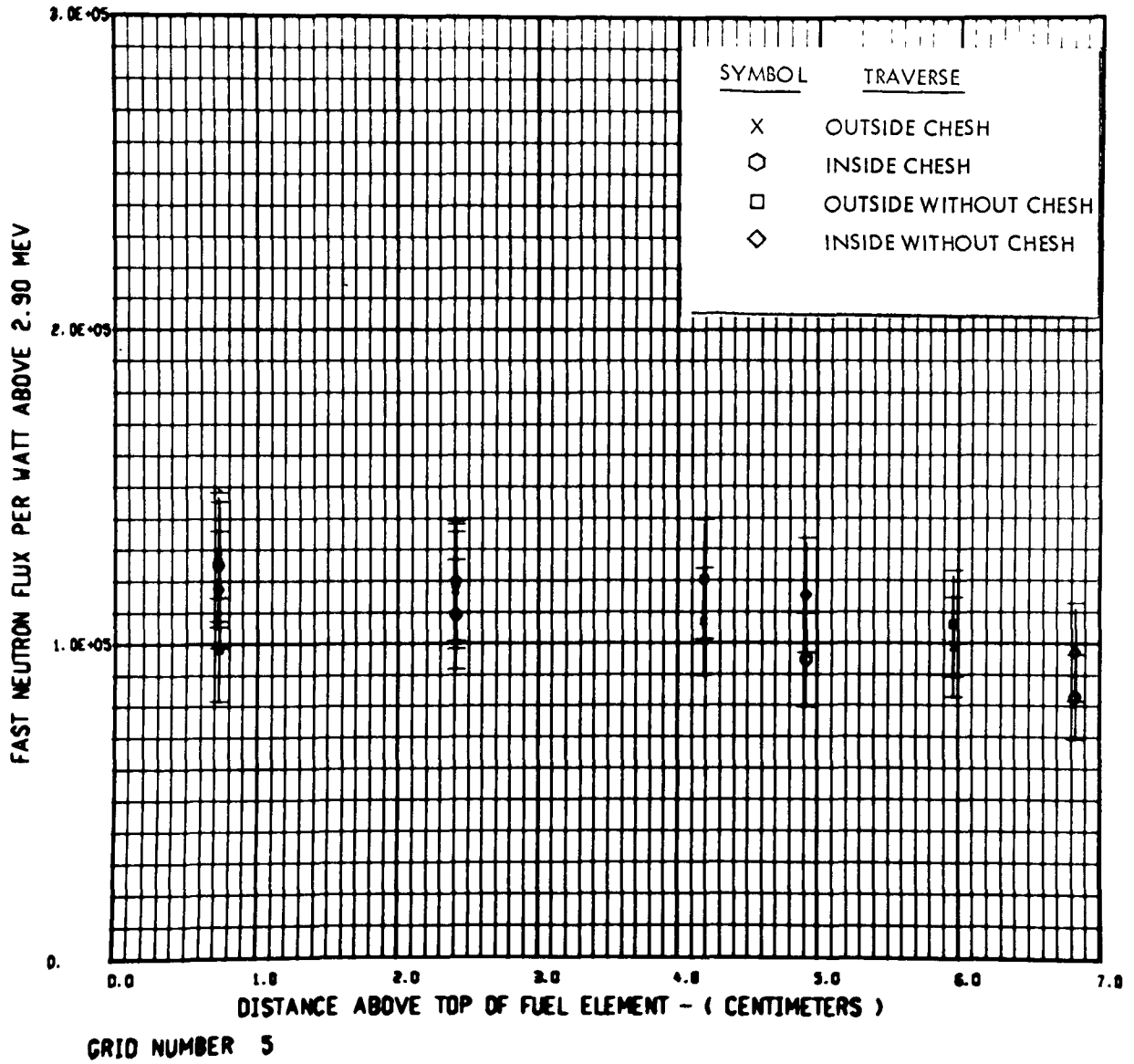
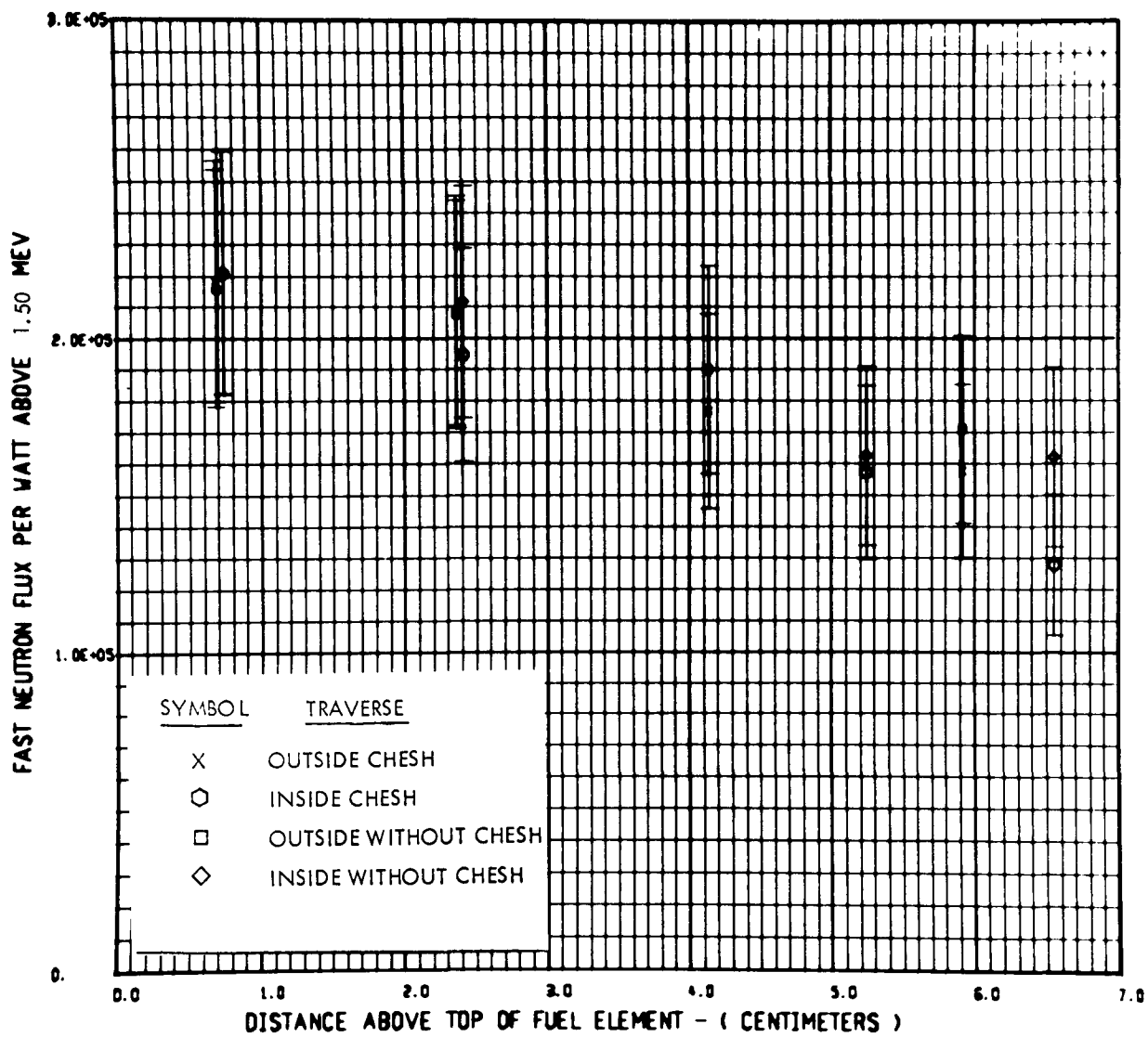


Figure 4-17. CHESH Experiment - Fast Flux From Sulfur



GRID NUMBER 6

Figure 4-18. CESH Experiment - Fast Flux From U-238

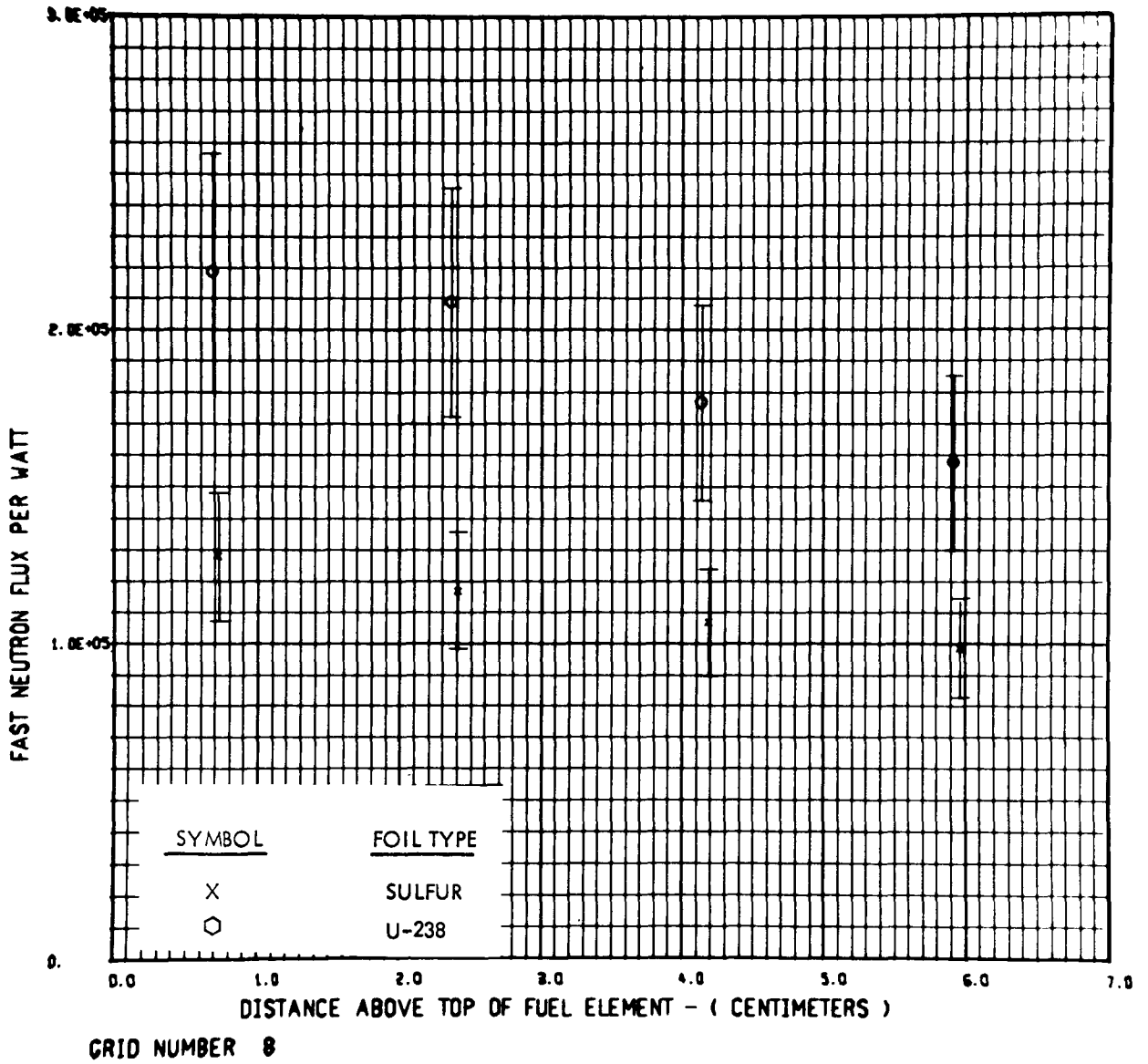


Figure 4-19. CHESH Experiment - Fast Flux Exterior to CHESH

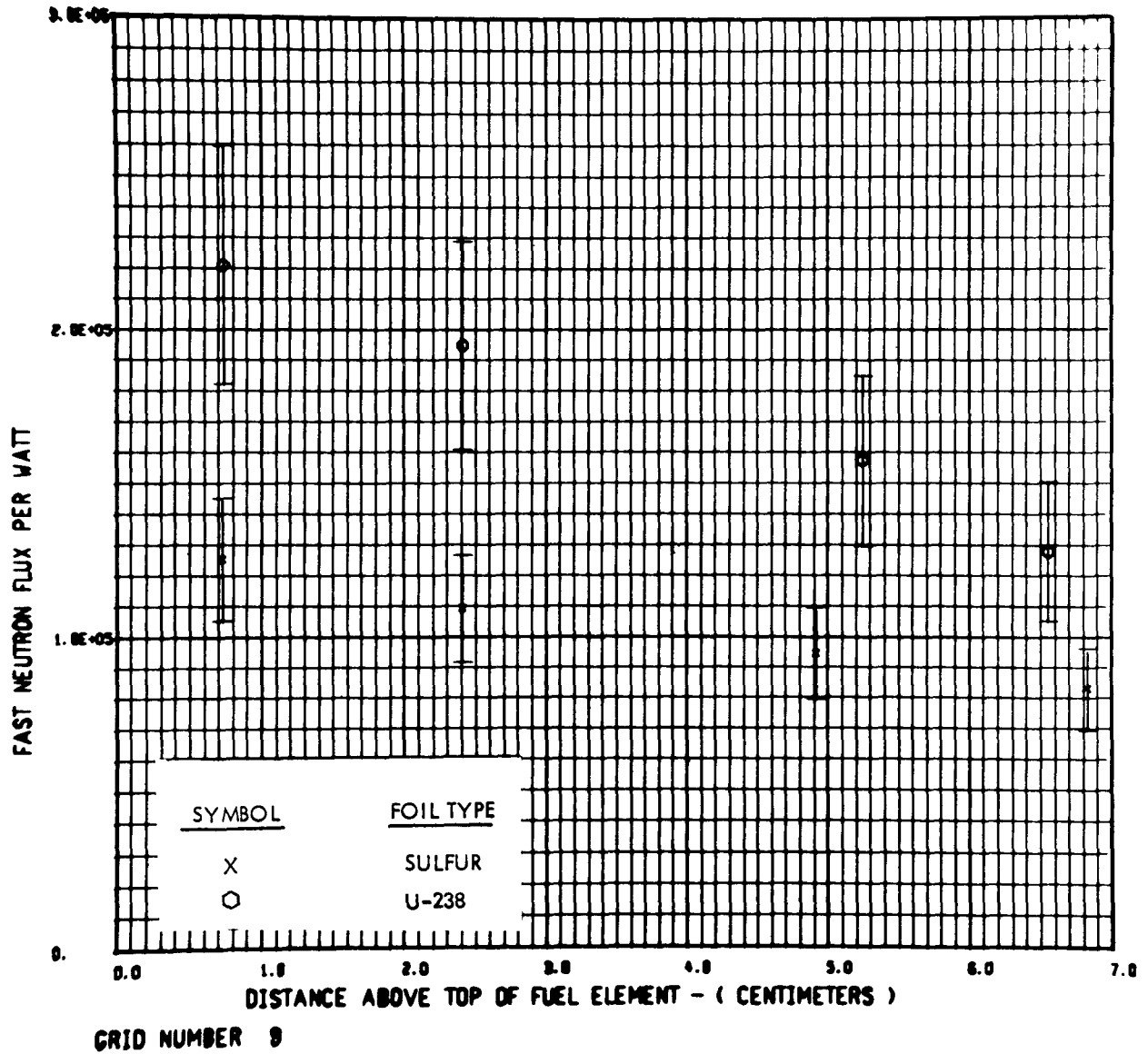


Figure 4-20. CHESH Experiment - Fast Flux Interior to CHESH



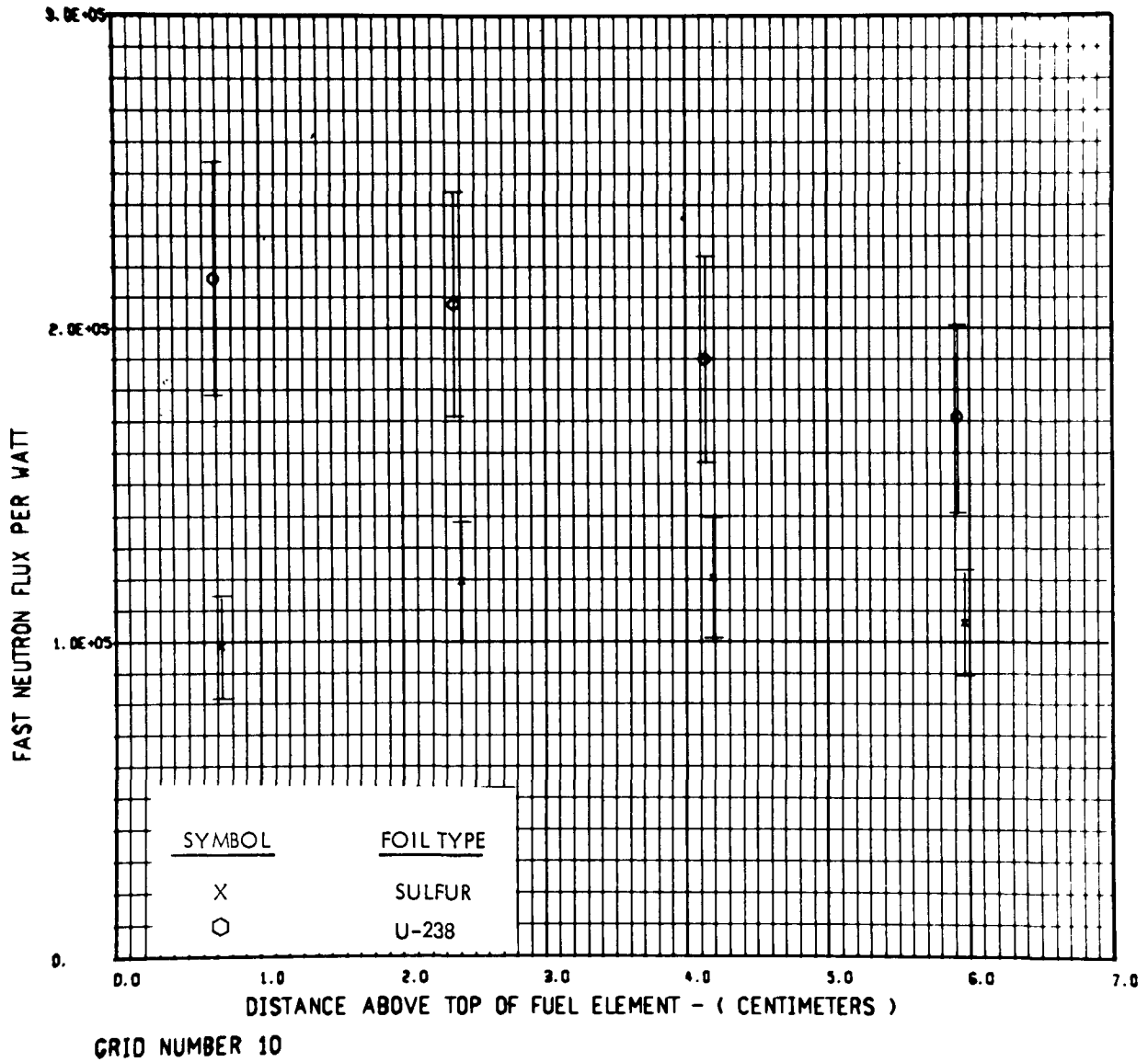


Figure 4-21. CHESH Experiment - Fast Flux Exterior W/O CHESH

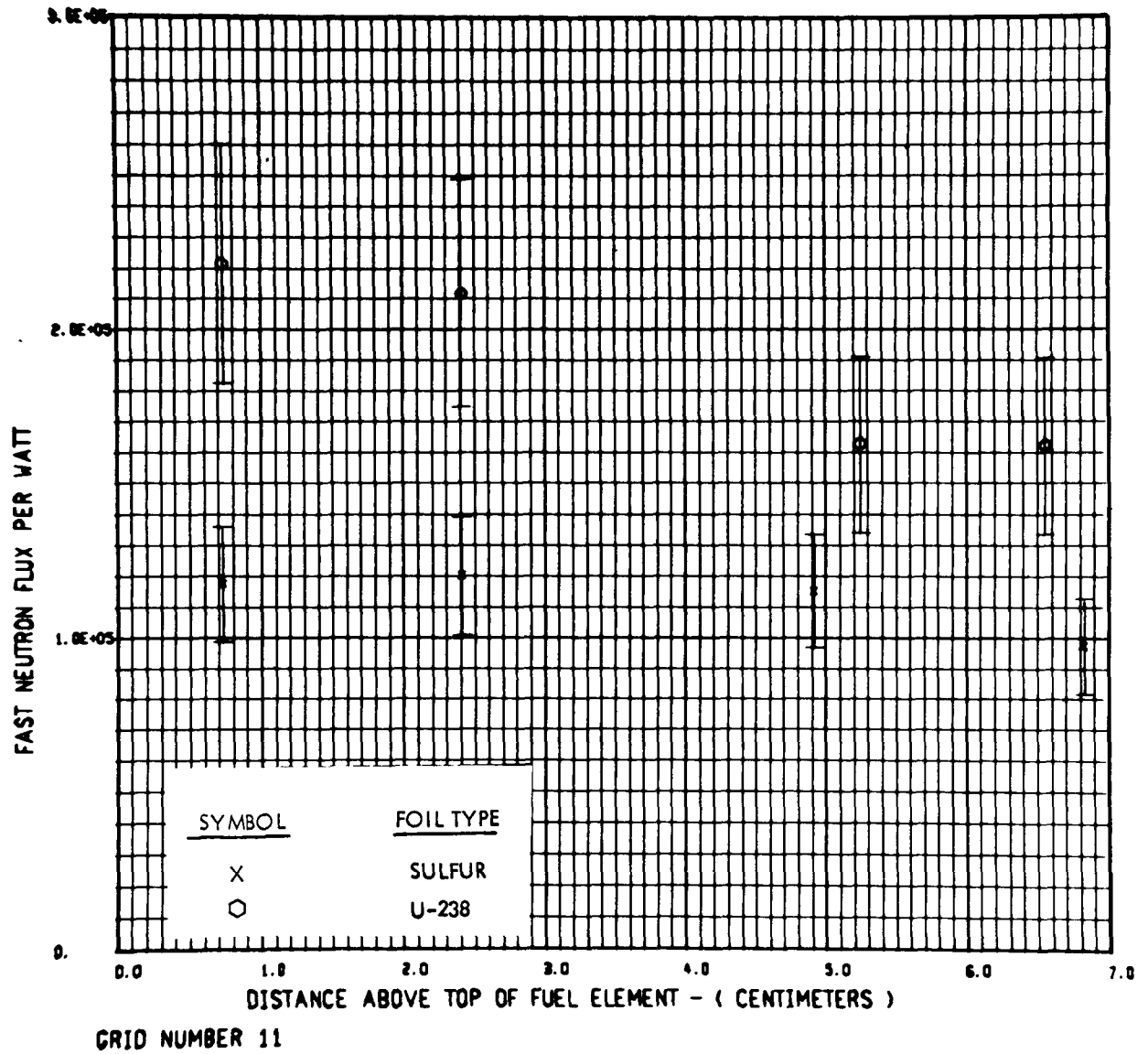


Figure 4-22. CHESH Experiment - Fast Flux Interior W/O CHESH

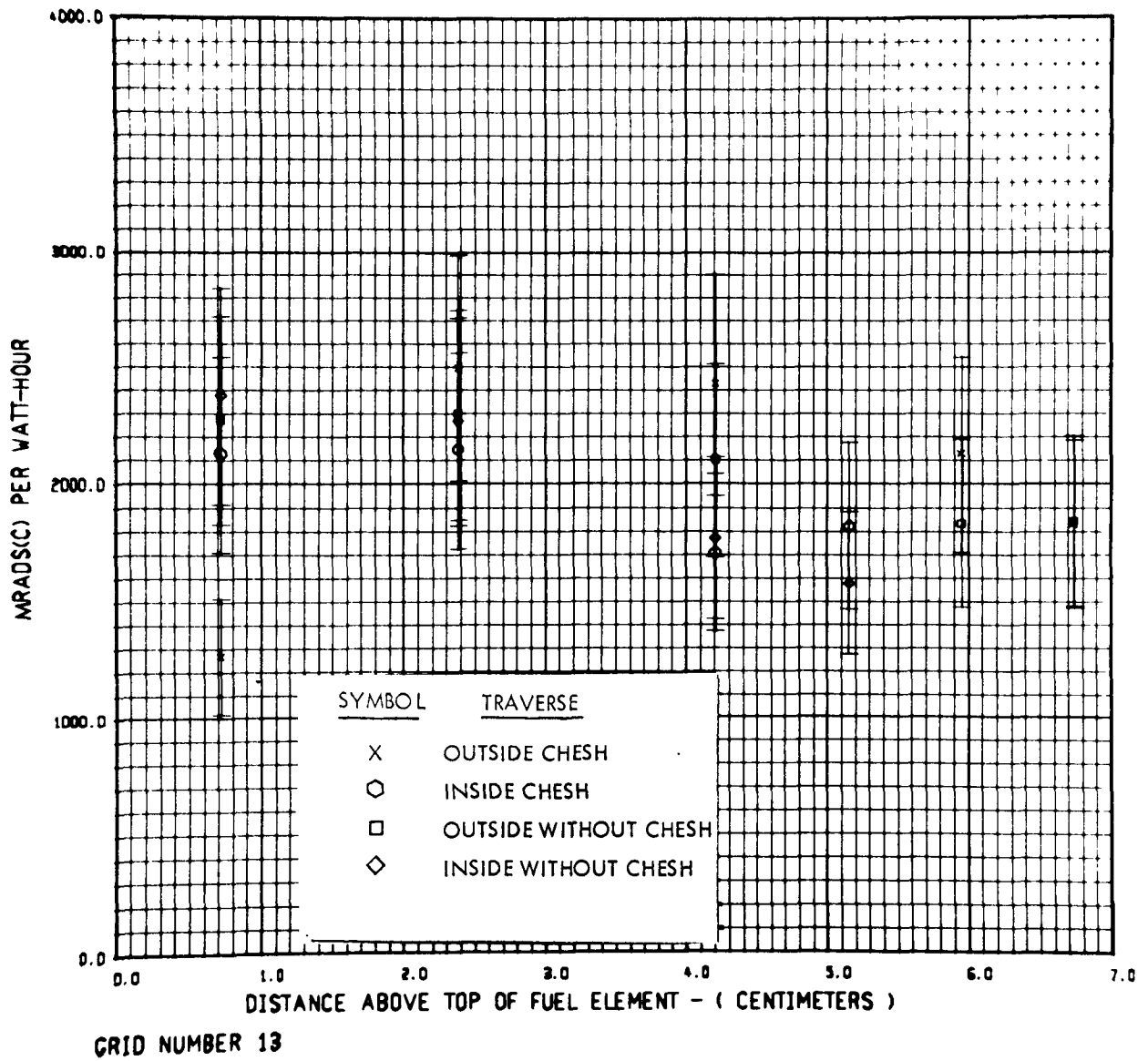


Figure 4-23. CHESH Experiment - Gamma Dose Rate From  $\text{CaF}_2$

#### 4.2.8 Phylatrons

Table 4-11 and Figures 4-24 and 4-25 present the fast neutron dose rate obtained from Phylatrons in units of rads (tissue) per watt-hour.

#### 4.2.9 Bragg-Gray Chambers

The heating rates obtained from the Bragg-Gray chambers are presented in Table 4-12 in units of watts per gram per megawatt.

TABLE 4-11

FAST NEUTRON DOSE RATES FROM PHYLATRONS

<u>Location</u>	<u>Radius (cm)</u>	<u>Height (cm)</u>	<u>Dose Rate Rads(tissue)/W-Hr</u>
EXT-W∅ ↓	1.55 ↓	0.72	4.79
		2.41	5.10
		4.19	3.50
		5.97	3.97
EXT-W ↓	↓	0.72	3.79
		2.41	4.63
		4.19	3.99
INT-W∅ ↓	0.0 ↓	5.97	3.22
		0.72	4.79
		2.41	6.11
INT-W ↓	↓	0.72	4.92
		2.41	5.84
INT-W∅ ↓	↓	5.13	3.70
INT-W	↓	5.13	3.70
EXT-W∅	↓	6.65	3.47
EXT-W	↓	6.65	3.31

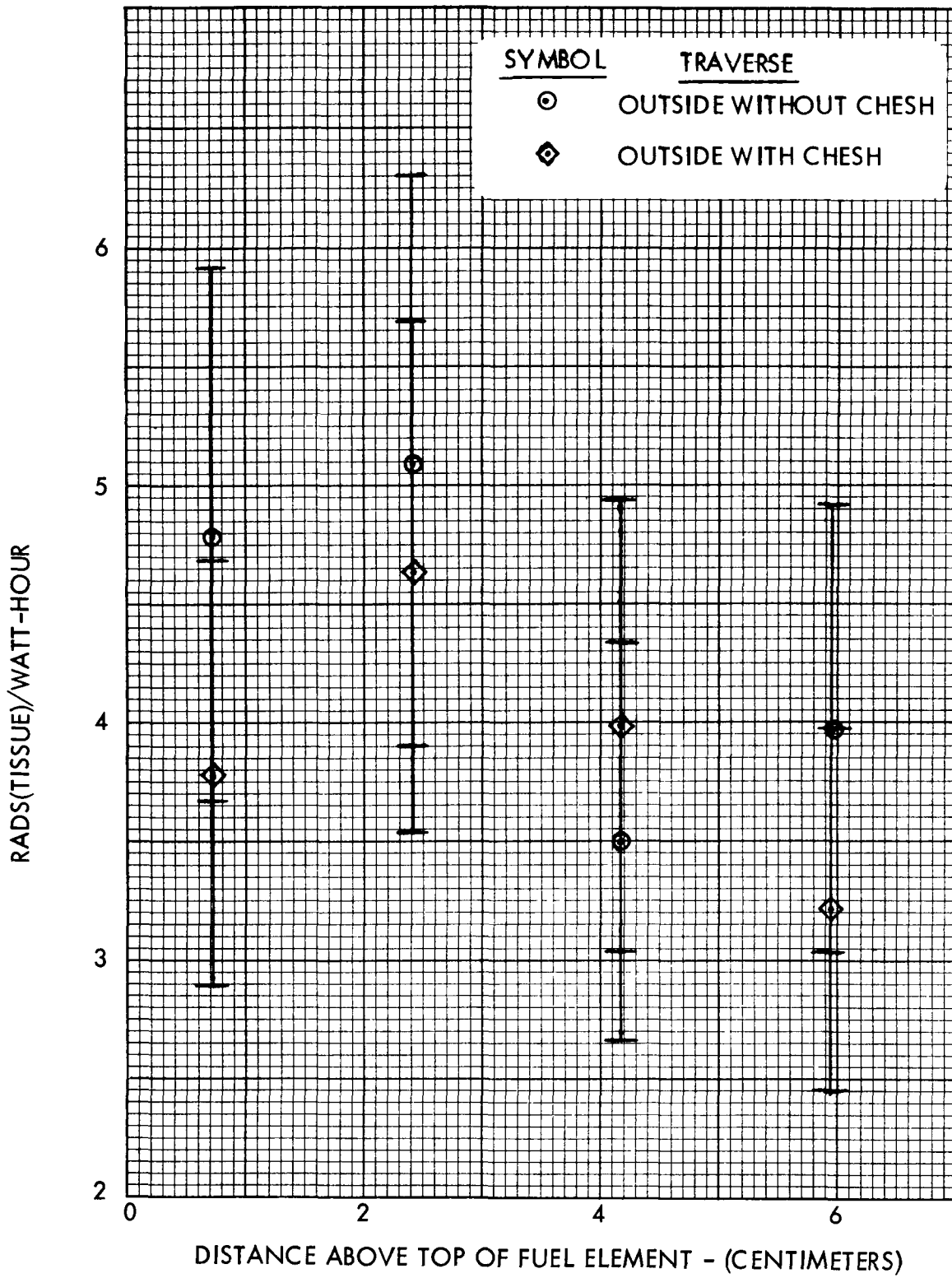


Figure 4-24. Fast Neutron Dose Rate From Phylatrons (Outside)

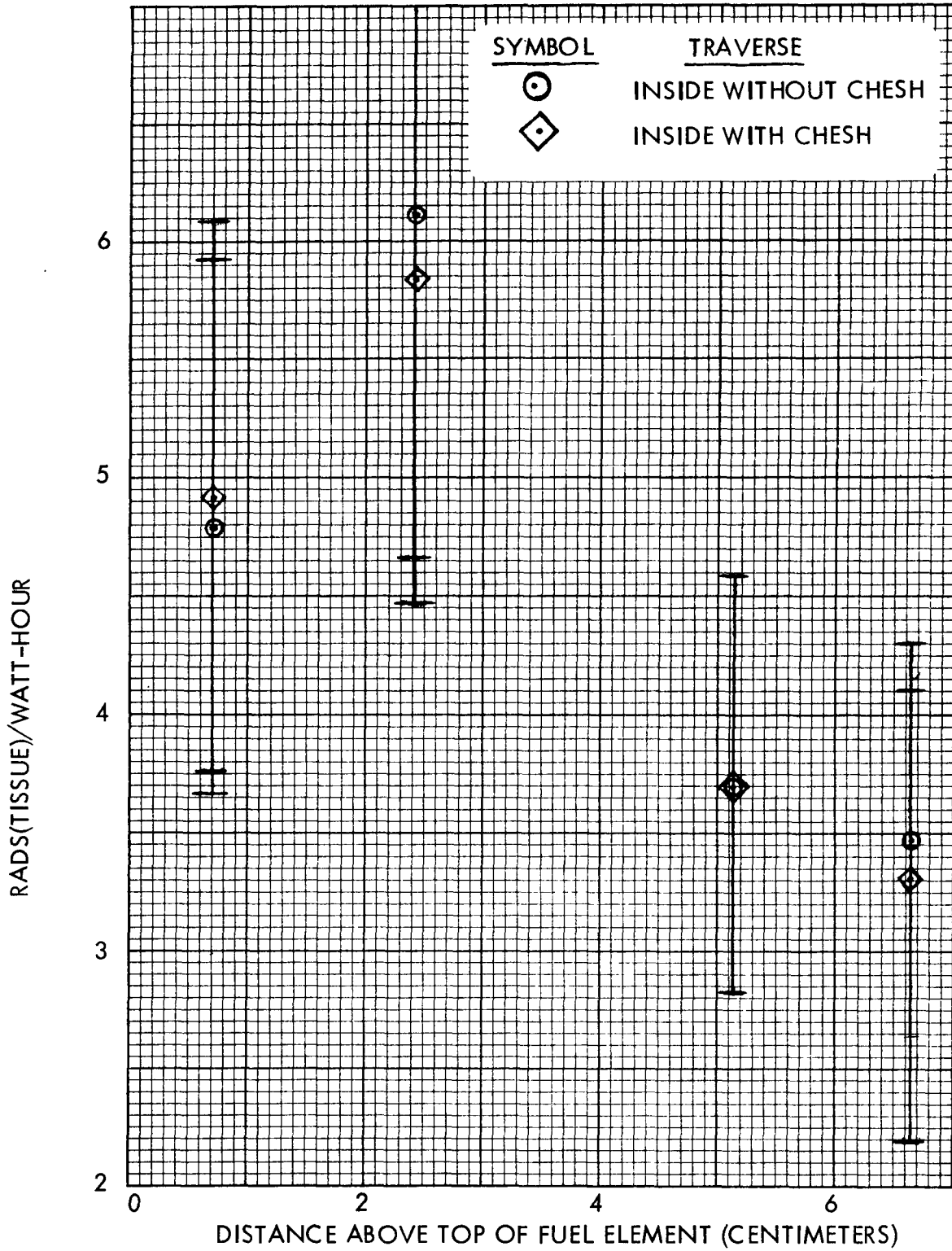


Figure 4-25. Fast Neutron Dose Rate From Phylatrons (Inside)

**TABLE 4-12**
**DOSE RATES AND HEATING RATES FROM BRAGG-GRAY DETECTORS**

Type of Detector	Graphite	Stainless Steel
Location	4C2 (radius = 13.3 cm)	5C2 (radius = 13.3 cm)
Calibration Constant	$9.76 \times 10^{12}$ rads/hr-w $\pm$ 3.9%	$7.36 \times 10^{12}$ rads/hr-w $\pm$ 4.9%
Observed Current	$1.508 \times 10^{-10}$ amperes	$1.72 \times 10^{-10}$ amperes
Background Current	$0.0004 \times 10^{-10}$ amperes	$0.00045 \times 10^{-10}$ amperes
Ion Current (Observed-Bkg)	$1.507 \times 10^{-10}$ amperes	$1.72 \times 10^{-10}$ amperes
Reactor Power	540 Watts	540 Watts
Dose Rate (rads/hr-w)	$2.79 \pm 8.5\%$	$3.19 \pm 8.5\%$
Gamma Heating Rate (w/g-Mw)	$0.00775 \pm 8.5\%$	$0.00886 \pm 8.5\%$



## 5.0 ANALYSIS OF TESTS

### 5.1 INTRODUCTION

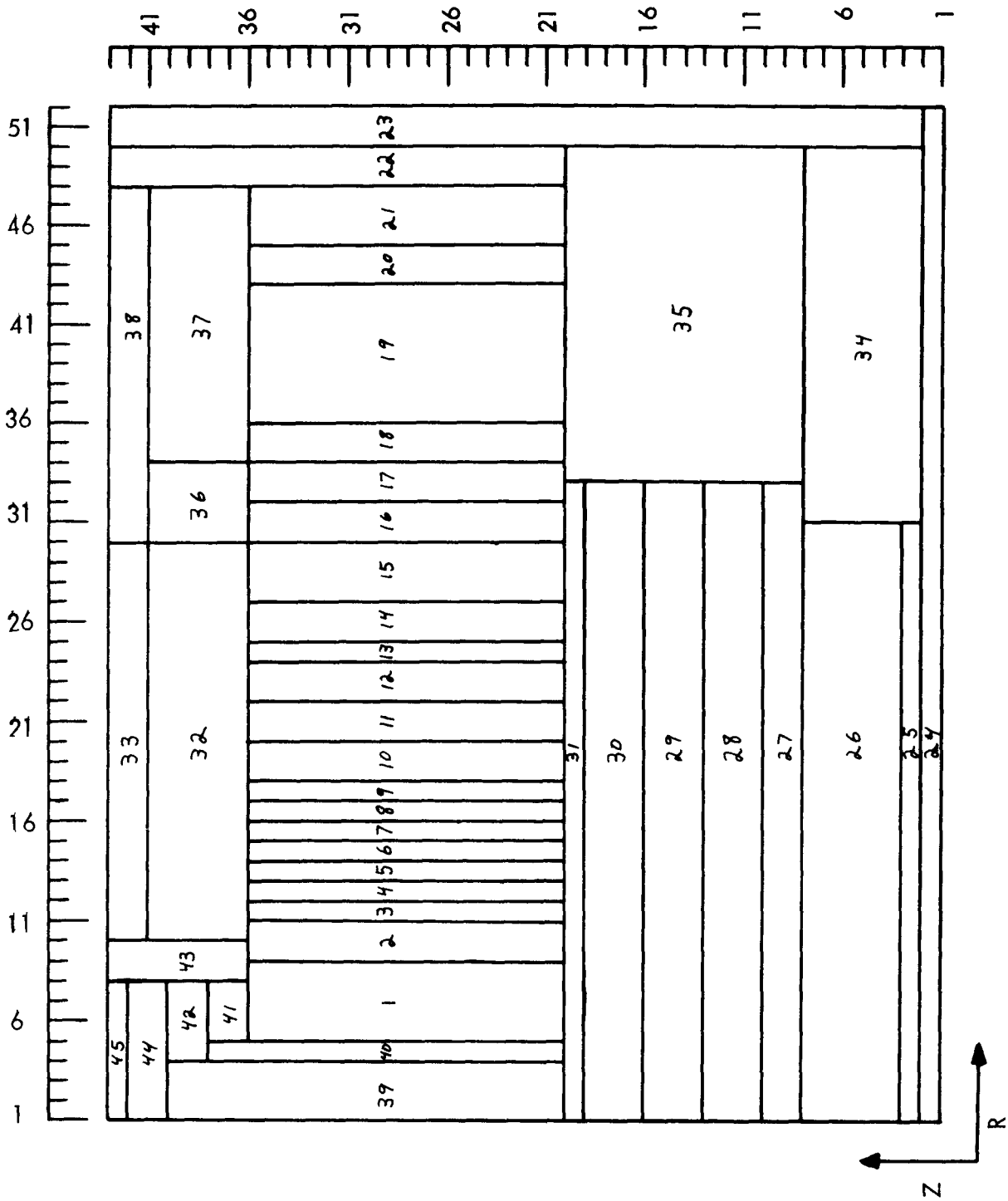
This section presents a comparison of the experimentally measured and analytically calculated radiation environment internal to and on the surface of a Cluster Hot End Support Hardware (CHESH) assembly which was placed on the aft end of the PAX-G1A reactor. The radiation environment compared consists of fast neutron fluxes (Sulfur and U-238 activation data), thermal neutron fluxes (Dysprosium activation data), fast neutron absorbed dose rates (p-i-n Si diode data), heating rates (Bragg-Gray ion chamber data), and photon absorbed dose rates (CaF<sub>2</sub> thermoluminescent detector data). All data are plotted as a function of axial distance from the aft end of the fuel.

The geometrical model and atomic number densities employed in the calculations are also presented along with the method of analysis used in obtaining the calculated results. Finally, a statistical analysis of the difference between calculated and experimental data was performed to establish uncertainty factors to be applied to calculated radiation data to obtain possible variation in the data.

### 5.2 ANALYTICAL MODEL

Figure 5-1 displays the analytical model employed in the DOT code, including region number and spatial mesh intervals. The axial reference plane ( $Z=0$ ) employed in this figure is located at the dome end of the pressure vessel with the positive portion of the Z-axis orientated towards the aft end of the reactor. However, the coordinate system employed in comparing calculated and experimental data has the axial reference plane ( $Z=0$ ) located at the outlet end of the fuel with the same orientation of the positive portion of the Z-axis. Table 5-1 presents the radial and axial mesh lines employed in the DOT code.

Table 5-2 provides the following information for the analytical model presented in Figure 5-1: 1. Region number, 2. Region description, and 3. Atomic number densities for each element in each region. Calculations were performed at ambient conditions with no hydrogen to conform to the PAX-G1 operation.



NOTE: Refer to Table 5-1 for Description of Regions and Compositions. Refer to Table 5-2 for the Radial (R) and Axial (Z) Position of all Mesh Lines.

Figure 5-1. CHESH Experiment Dot Geometry Mockup

TABLE 5-1

RADIAL (R) AND AXIAL (Z) DOT MESH

<u>Mesh Line Numbers</u>	<u>R(cm)</u>	<u>Z(cm)</u>
1	0.0	0.0
2	0.128	0.848
3	0.256	5.239
4	0.384	11.200
5	0.527	18.700
6	0.834	27.300
7	1.141	34.800
8	1.448	40.385
9	8.033	48.000
10	11.596	55.349
11	14.058	60.000
12	17.850	65.000
13	20.084	70.589
14	22.633	71.500
15	25.344	72.400
16	27.519	73.129
17	29.431	73.230
18	32.368	73.330
19	34.400	73.446
20	36.400	73.921
21	37.900	78.000
22	39.903	84.000
23	40.600	92.000
24	41.318	101.000
25	42.757	110.000
26	43.900	120.000
27	45.032	130.000
28	45.800	140.000
29	46.600	150.000
30	47.388	160.000
31	47.427	170.000
32	49.122	179.000
33	51.054	188.000
34	51.816	196.000
35	52.600	202.000
36	53.338	206.001
37	54.200	207.203
38	55.000	208.406
39	55.900	209.880

TABLE 5-1  
(Continued)

RADIAL (R) AND AXIAL (Z) DOT MESH

<u>Mesh Line Numbers</u>	<u>R(cm)</u>	<u>Z(cm)</u>
40	56.700	211.353
41	57.600	211.716
42	58.400	212.483
43	59.0738	213.984
44	59.1979	
45	59.322	
46	60.500	
47	61.700	
48	62.840	
49	63.000	
50	63.185	
51	63.600	
52	64.033	

TABLE 5-2

CHESH EXPERIMENT ATOM DENSITIES (ATOMS/BN-CM)

ELEMENT	Be	C	Fe	Ni	Cr	Mn	Nb	Ti	Mo	Al	Cu	Gd	W	Th	O	U-235	U-238	Ta
REGION																		
1 Core - 1		6 788 (-2)	1 754 (-4)	1 760 (-4)	8 790 (-5)		1 063 (-3)		1 685 (-4)							5 044 (-4)	3 750 (-5)	1 910 (-5)
2 Core - 2		6 740 (-2)	1 529 (-4)	1 534 (-4)	7 650 (-5)		1 005 (-3)		1 685 (-4)							5 406 (-4)	4 020 (-5)	1 910 (-5)
3 Core - 3		6 735 (-2)	1 681 (-4)	1 687 (-4)	8 420 (-5)		1 009 (-3)		1 685 (-4)							5 617 (-4)	4 180 (-5)	1 910 (-5)
4 Core - 4		6 667 (-2)	1 601 (-4)	1 607 (-4)	8 020 (-5)		1 035 (-3)		1 685 (-4)							5 878 (-4)	4 370 (-5)	1 910 (-5)
5 Core - 5		6 613 (-2)	1 245 (-4)	1 250 (-4)	6 230 (-5)		9 761 (-4)		1 685 (-4)							6 326 (-4)	4 700 (-5)	1 910 (-5)
6 Core - 6		6 412 (-2)	2 610 (-5)	2 620 (-5)	1 300 (-5)		1 111 (-3)		1 685 (-4)							6 610 (-4)	4 910 (-5)	1 910 (-5)
7 Core - 7		6 352 (-2)					1 077 (-3)		1 685 (-4)							7 237 (-4)	5 380 (-5)	1 910 (-5)
8 Core - 8		6 357 (-2)					1 106 (-3)		1 685 (-4)							7 251 (-4)	5 390 (-5)	1 910 (-5)
9 Core - 9		6 333 (-2)					1 128 (-3)		1 685 (-4)							7 714 (-4)	5 740 (-5)	1 910 (-5)
10 Core - 10		6 315 (-2)					1 164 (-3)		1 685 (-4)							8 129 (-4)	6 040 (-5)	1 910 (-5)
11 Core - 11		6 315 (-2)					1 164 (-3)		1 685 (-4)							8 219 (-4)	6 040 (-5)	1 910 (-5)
12 Core - 12		6 336 (-2)					1 102 (-3)		1 685 (-4)							7 142 (-4)	5 310 (-5)	1 910 (-5)
13 Core - 13		6 688 (-2)	1 681 (-4)	1 687 (-4)	8 420 (-5)		1 016 (-3)		1 685 (-4)							6 089 (-4)	4 530 (-5)	1 910 (-5)
14 Core - 14		6 807 (-2)	2 038 (-4)	2 045 (-4)	1 020 (-4)		1 005 (-3)		1 685 (-4)							4 877 (-4)	3 630 (-5)	1 910 (-5)
15 Core - 15		6 940 (-2)	2 491 (-4)	2 499 (-4)	1 247 (-4)		9 319 (-4)		1 685 (-4)							2 872 (-4)	2 130 (-5)	1 910 (-5)
16 Filler Strip		9 300 (-2)																
17 Lateral Support		4 672 (-2)																
18 Inner Reflector	8 382 (-2)	4 272 (-3)																
19 Outer Reflector I	1 003 (-1)		4 270 (-4)	5 020 (-4)	2 350 (-4)					2 450 (-3)								
20 Vane	Ring Prescription (See WANL-TME-1914)																	
21 Outer Reflector II	1 003 (-1)		4 270 (-4)	5 020 (-4)	2 350 (-4)					2 450 (-3)								
22 Void																		
23 Pressure Vessel										5 998 (-2)								
24 Pressure Vessel										5 998 (-2)								
25 Void																		
26 Simulated Shield										5 507 (-2)	1 491 (-3)							
27 Void																		
28 Support Plate			2 894 (-3)	3 708 (-4)	8 371 (-5)	8 347 (-5)				2 998 (-2)	8 559 (-4)							
29 Cluster Plate Hardware			6 846 (-3)	8 773 (-4)	1 980 (-3)	1 975 (-4)				1 945 (-3)								
30 Cluster Plate			3 714 (-2)	4 757 (-3)	1 074 (-2)	1 071 (-3)				1 945 (-3)								
31 Cluster Plate Hardware			6 846 (-3)	8 773 (-4)	1 980 (-3)	1 975 (-4)				1 945 (-3)		1 540 (-4)						
32 Support Blocks		5 722 (-2)	1 093 (-3)	1 400 (-4)	3 161 (-4)	3 152 (-5)												
33 Tie Rod Ends			1 016 (-3)	1 302 (-4)	2 940 (-4)	2 932 (-5)												
34 Drum Drive			7 906 (-4)	2 320 (-4)	2 319 (-4)	2 300 (-5)												
35 Drum Drive			8 637 (-4)	1 786 (-4)	2 533 (-4)	2 538 (-5)												
36 Lateral Support/Aft Reflector/Aft	9 609 (-2)	4 394 (-4)	5 494 (-5)	1 249 (-4)				4 143 (-3)		4 493 (-4)								
37 Reflector/Aft		1 584 (-3)	1 285 (-4)	4 782 (-4)	4 595 (-5)	5 719 (-5)	8 862 (-3)			9 255 (-4)								
38 39 Void										2 242 (-2)								
40 Support Stem & Liner			1 123 (-2)	1 026 (-2)	7 142 (-3)	1 620 (-4)	4 434 (-4)		2 498 (-4)									
41 Pedestal	4 109 (-2)																	
42 CHESH Side	1 877 (-2)	1 723 (-2)	3 264 (-3)	4 824 (-3)	5 229 (-4)	2 044 (-5)		3 857 (-4)				1 478 (-2)	2 104 (-4)	4 157 (-4)				
43 Void																		
44 CHESH Top	7 049 (-3)	1 085 (-2)	1 162 (-3)	3 023 (-3)	3 287 (-4)				1 845 (-4)				1 793 (-2)	2 551 (-4)	5 045 (-4)			
45 Void																		

NOTE Numbers in parenthesis refer to powers of ten

5-5

CONFIDENTIAL

CONFIDENTIAL

~~CONFIDENTIAL~~

THIS PAGE UNCLASSIFIED.

It should be noted that this analytical model explicitly represents: 1) the CHESH on the aft end of the reactor, 2) the tie tube void through the core and into the CHESH, and 3) the void around the CHESH created by removing PAX support blocks. This representation of the CHESH exists on the reactor centerline which is the axis of symmetry for the calculation. The experimental data were obtained at a radial distance of 13.3 cm from the core center. However, the explicit representation of the CHESH in the calculations can only be made about the axis of symmetry. Therefore, the positioning of the CHESH on the reactor centerline for the calculations introduces some uncertainty in the calculated data. Based on the calculated and experimental information at the aft end of the fuel in WANL-TME-1914, "Radiation Environment in Various NERVA Components", the change in the U-238, sulfur, fast neutron dose rate, photon dose rate and Bragg-Gray data from the reactor centerline to 13.3 cm is less than two percent. This change in the dysprosium data (thermal neutron flux) is 17 percent. Therefore, the representation of the CHESH on the reactor centerline in the calculations essentially introduces uncertainties only in the thermal neutron data.

The analytical model for the reactor utilized the PAX-G1A as-built material inventory for the 60 degree R-1 mockup sector. In effect, the analytical model described the reactor with 360 degree azimuthal symmetry; whereas, the PAX-G1A was not symmetrical. The PAX-G1A reactor employed ten 30 degree KIWI reflector sectors containing 10 NRX-type control drum configurations in the 300 degree sector of the reflector. Also, asymmetry occurs in the core region near the reflector where the 60 degree R-1 fuel loading is greater than the remaining 300 degree portion of the core. The central region is symmetrical. Since the measurements on the CHESH were performed in the 60 degree test sector at a radius of approximately 13 cm, these asymmetries will not adversely affect the analytical and experimental comparisons.

### 5.3 METHOD OF ANALYSIS

Figure 5-2 is a schematic diagram of the computational procedure employed to obtain the analytical results presented in this report. This procedure is basically the

~~CONFIDENTIAL~~  
THIS PAGE UNCLASSIFIED.

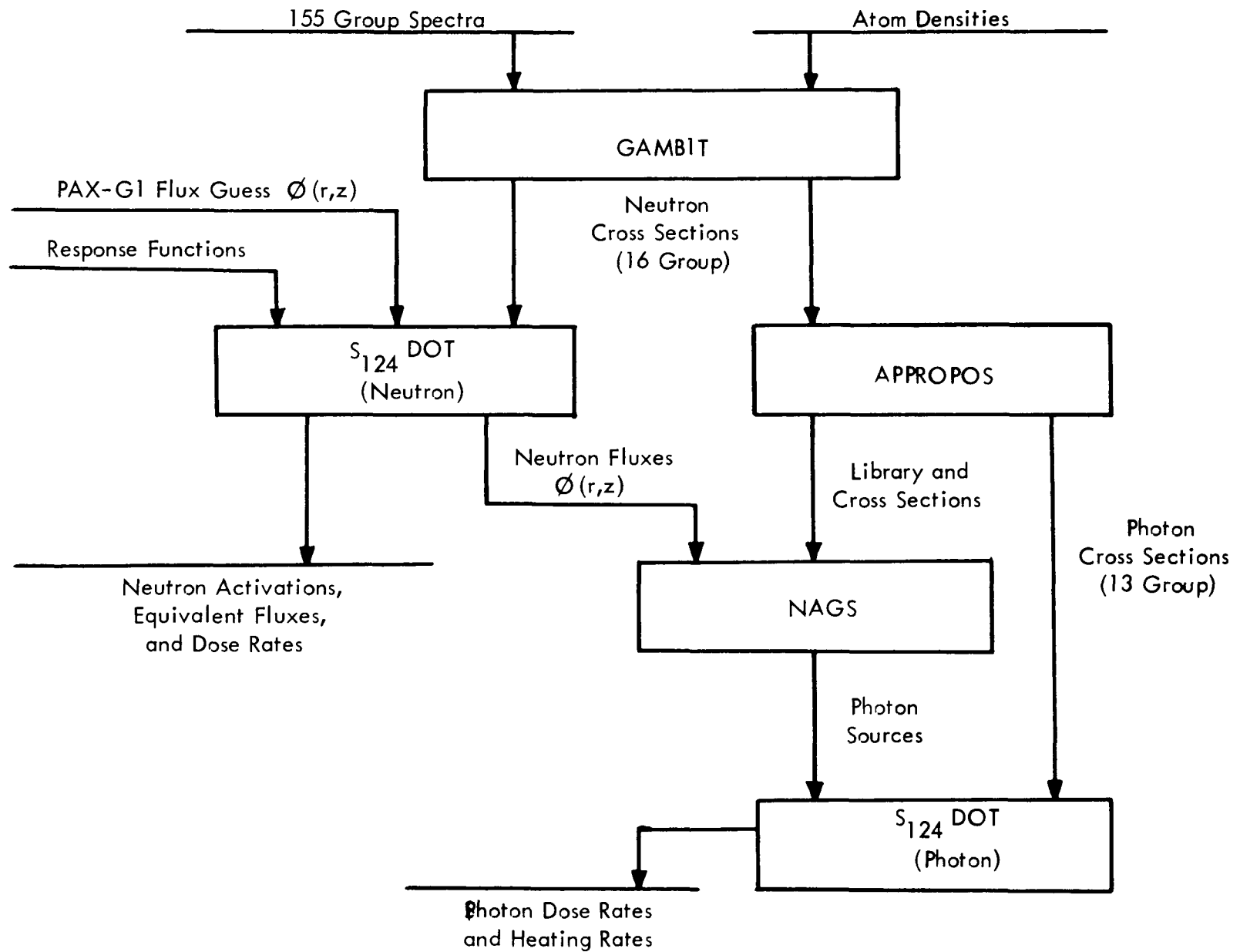


Figure 5-2. CHESH Experiment Computational Flow Chart

WISDM (WANL Integrated Nuclear, Radiation and Shielding Standard Design Method) technique<sup>(1)</sup>.

A converged, region dependent, 155 fine energy group neutron spectrum was calculated for the PAX-G1 reactor via an iterative loop employing the GAMBIT<sup>(2)</sup>-ANISN<sup>(3)</sup>-ANISIG codes. On the first iteration, GAMBIT utilizes the  $P_1$  equations to generate 52 group,  $P_0$  transport corrected, neutron cross sections for an infinite media spectrum. These cross sections are employed in the one-dimensional, discrete ordinates transport code ANISN, to obtain 52 neutron energy group average fluxes and currents for each reactor region. These data are interpolated by the ANISIG code to 155 neutron energy groups which then becomes the region-dependent fine energy group spectrum employed in GAMBIT to generate new spectrum averaged cross sections. This process is repeated until a converged spectrum (change in spectrum between two iterations is small) is obtained. This converged spectrum is then employed in the GAMBIT code to generate region dependent 16 energy group  $P_0$ , transport corrected macroscopic neutron transport and microscopic photon production cross sections. These cross sections plus a tape containing microscopic photon cross sections are input to the APPROPOS code which generates  $P_0$  and  $P_1$  13 group photon transport cross sections for use in the DOT<sup>(4)</sup> photon code, and microscopic and macroscopic cross section libraries to be employed in the NAGS<sup>(5)</sup> data processing code.

The 16 energy group neutron transport cross sections were employed in a two-dimensional, discrete ordinates transport calculation with the DOT code which employed an S-124 angular quadrature scheme. The angular quadrature scheme had a higher degree of resolution in the axial direction so that streaming effects through the tie tube void could be detected. The DOT calculation also employed a scalar flux guess from a previous DOT calculation for the PAX-G1 reactor. The computation from which the flux guess was obtained is described in detail in WANL-TME-1914.

The DOT neutron fluxes and the library data from the APPROPOS code were employed in the NAGS code to generate photon sources. These sources were then used in a fixed source, 13 energy group, full  $P_1$ , photon DOT computation with an S-124 angular



quadrature scheme.

The calculated neutron activation, neutron equivalent flux, neutron dose rate, photon dose rate, and heating rate data were obtained directly from the DOT code via response functions. Section 5.3.2 of WANL-TME-1914 contains a discussion of: 1) the relationship between activation and equivalent flux, 2) the relationship between the calculated and experimental data, and 3) the response functions employed to obtain the calculated data from DOT.

#### 5.4 COMPARISON OF EXPERIMENTAL AND ANALYTICAL RESULTS

The following sections compare the experimental and calculated fast neutron flux ( $E > 2.9$  Mev and  $E > 1.5$  Mev), thermal neutron ( $E < 0.4$  ev), fast neutron absorbed dose rate, and gamma absorbed dose rate as a function of axial position above the top of the fuel. Bragg-Gray data in the vicinity of the CHESH are also compared. The neutron foil data are presented in units of neutron flux rather than saturated activity since this unit is normally used in reporting data. This does not detract from the comparisons, because the experimental and analytical saturated activities were reduced to neutron fluxes using a common denominator. (Detailed discussions are documented in WANL-TME-1914). Thus, in reality, detector saturated activities rather than fluxes are being compared with one-to-one correspondence between experiments and calculations.

It should be noted that this set of computations is consistent with the computations performed for the in-core measurements reported in WANL-TME-1914. However, in these computations, the support blocks for the eighteen clusters adjacent to the CHESH analytical model were removed. This results in a decreased return of thermal neutrons to the core which causes a reduction in the fission rate in the fuel adjacent to the void created by the removal of the support blocks. The reduced fission rate decreases the source term for neutrons of all energies. Therefore, a comparison of these calculated results at the outlet end of the fuel with similar data from WANL-TME-1914 will show that these calculated results are lower due to the removal of the support blocks. A comparison of the DOT data for the two sets of computations at a radial position for which

both computations had support blocks displayed no essential difference between the two sets of calculated data.

#### 5.4.1 Sulfur (E>2.9 Mev) Fast Neutron Flux Data

Figure 5-3 compares the calculated and experimentally measured neutron flux data obtained with sulfur pellets. Because the  $S^{32}$  (n,p) reaction data are a threshold reaction, these data correspond approximately to the integrated fast neutron flux with an energy greater than 2.9 Mev.

This figure compares the calculated and measured neutron flux as a function of axial position above the top of the fuel. The experimental data were obtained on the outside surface of the CHESH model and on the inside of the support stem assembly (referred to as the inside of the CHESH model).

From this figure, it can be seen that the calculated shape of the sulfur data agrees well with the measured data. On an average pointwise basis (average derived in Section 5.5), the calculations are 60 percent lower than the measurements internal to the CHESH and 64 percent lower than the measurements on the surface of the CHESH. It should be noted that comparisons of calculated and experimental sulfur data in the core of the PAX-G1 reactor result in the calculated data being 32 percent lower than the experimental data on an average basis. Therefore, the difference between the calculated and experimental sulfur data in the CHESH is, in part, symptomatic of the differences that have been observed previously.

The difference in absolute magnitude between the calculated and measured data may be due to: 1) the use of only one energy group above 2.9 Mev in the calculations, 2) the use of  $P_0$  transport corrected cross sections, 3) the use of the Cranberg fission spectrum, and/or 4) a possible contribution to the sulfur counting rate due to neutron reactions that are not of the (n,p) type. Each of these reasons postulated for differences between experimental and calculated data must be further systematically evaluated to isolate the cause of the difference.

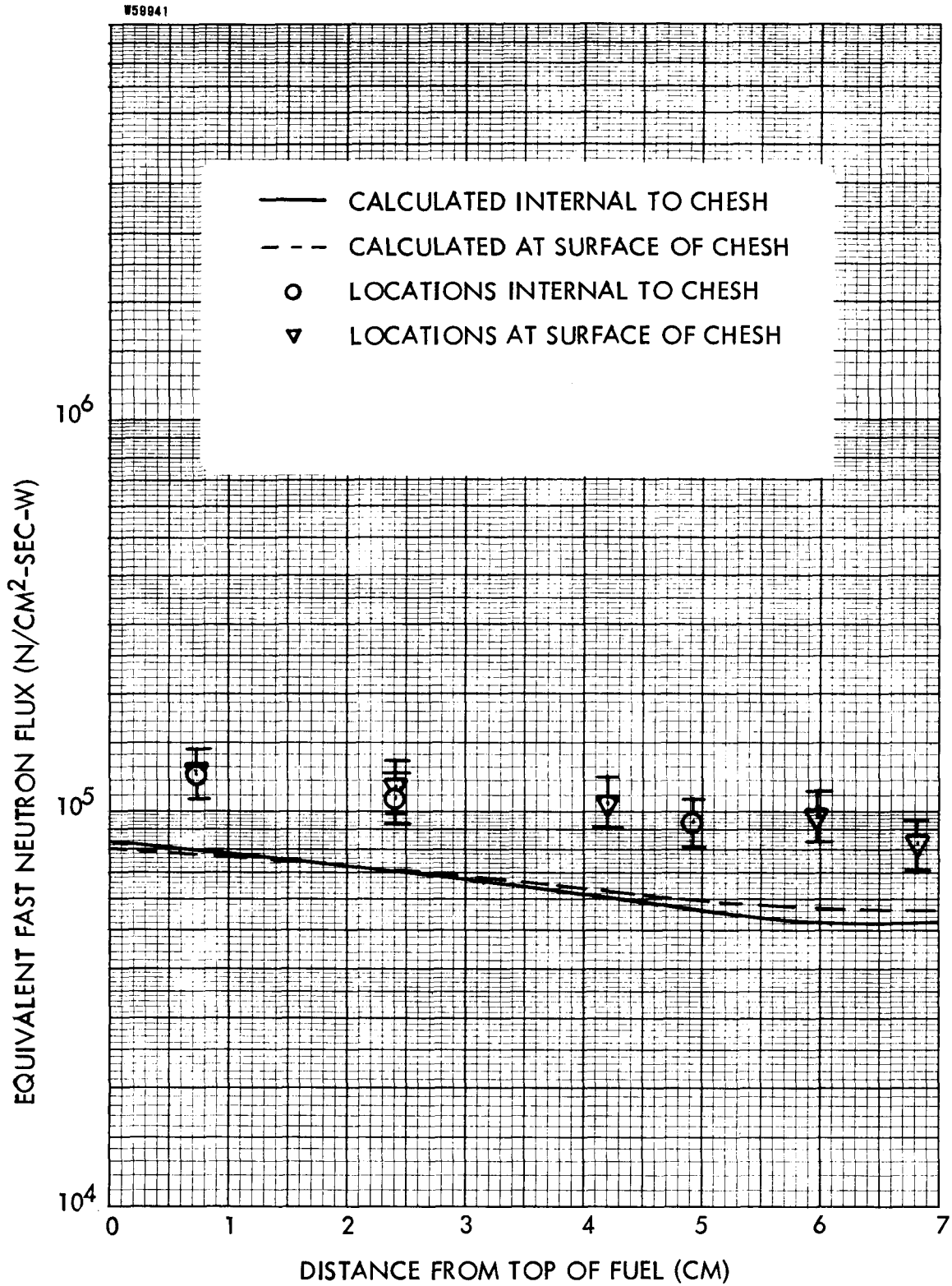


Figure 5-3. Comparison of the Calculated and Experimental Sulfur Fast Neutron Flux ( $E > 2.9$  MeV) As a Function of Axial Position Above the Top of the Fuel

#### 5.4.2 U-238 (E>1.5 MeV) Fast Neutron Flux Data

Figure 5-4 compares the calculated and experimentally measured neutron flux data obtained with U-238 foils. These foils contained 190 ppm of U-235. Cadmium covers were employed with the foils to partially suppress the fissioning in U-235 so that the primary activation measured was that due to fast fission in U-238. Calculated data indicate that 1.4 percent of the activation is due to U-235 fissions. Therefore, the U-238 foil data correspond approximately to the integrated fast neutron flux with an energy greater than 1.5 MeV.

This figure compares the calculated and measured neutron flux as a function of axial position above the top of the fuel. The experimental data were obtained on the outside surface of the CHESH model and on the inside of the support stem assembly (referred to as the inside of the CHESH model).

Figure 5-4 indicates that the shape of the calculated data agrees quite well with the shape of the experimentally measured data. On an average pointwise basis, the calculations are 19% higher than the measurements internal to the CHESH and 17 percent higher than the measurements on the surface of the CHESH. These differences between the calculated and experimentally measured data are very nearly within the limits of experimental uncertainty. Therefore, there is fairly good agreement between the calculated and experimental data.

In the preceding section, it was noted that the calculated sulfur data, which represent the fast neutron flux ( $E > 2.9$  MeV) were low by approximately 60 percent while the calculated U-238 data, which represents the fast neutron flux ( $E > 1.5$  MeV) were high by approximately 18 percent; thus, clearly indicating that the calculated neutron spectrum is too "soft" relative to the experimental results for energies greater than 2.9 MeV. It is expected that investigation of the possible reasons for the sulfur differences given in Section 5.4.1 might also explain the differences observed in the comparison of the U-238 data.

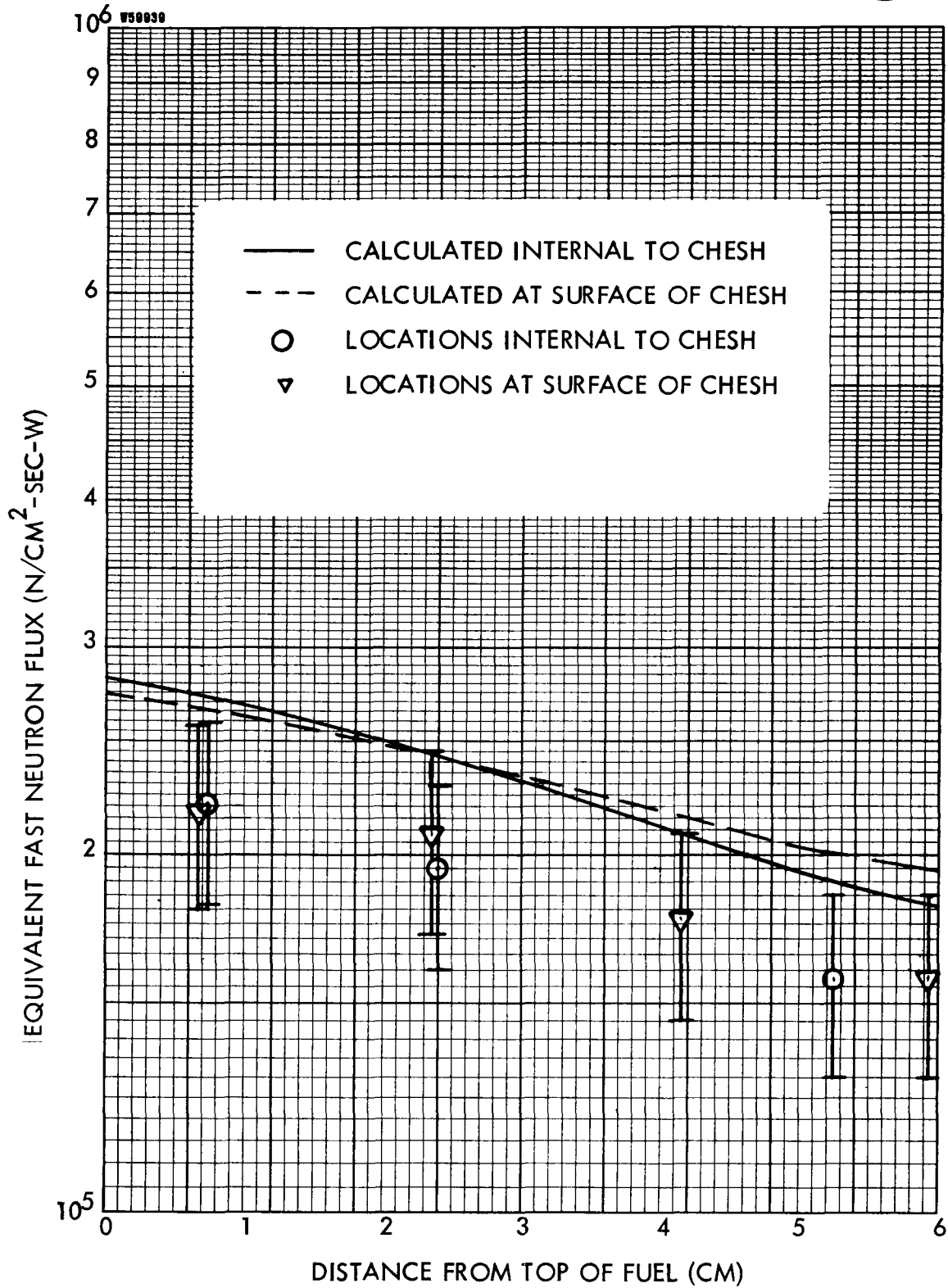


Figure 5-4. Comparison of the Calculated and Experimental U-238 Fast Neutron Flux ( $E = 1.5$  MeV) as a Function of Axial Position Above the Top of the Fuel

### 5.4.3 Dysprosium ( $E < 0.4$ eV) Thermal Neutron Flux Data

The comparisons in this section are the calculations of the thermal neutron flux ( $E < 0.4$  eV) and experimental data obtained with bare and cadmium-covered Dy foils. The data presented are the difference between the bare and cadmium-covered activities converted to flux using a common denominator for experiment and calculations (a detailed discussion is given in WANL-TME-1914).

Figure 5-5 compares the calculated and measured thermal neutron flux as a function of position above the top of the fuel. The experimental data were obtained on the inside and outside surface of the CHESH.

Figure 5-5 indicates that the shape of the calculated data agrees with the shape of the experimentally measured data. On an average pointwise basis (see Section 5.5), the calculations are a factor of four higher than the experimental results for the data internal and external to the CHESH.

It should be observed that the experimental uncertainties are large. This is due to a combination of the low cadmium ratio obtained with Dy and the relative uncertainties associated with the individual bare and cadmium-covered measurements. This could contribute, in part, to the large difference between the calculated and experimental results. Another factor which could contribute to the difference between the calculated and experimental data is that the correction to the Dy cross section for cadmium shielding was based on semi-empirical results for Au foils in the center of the core (see Reference 6). Further investigation into this area plus an examination of the Dy cross section should be performed to resolve the difference between calculated and experimental Dy data.

### 5.4.4 Fast Neutron Absorbed Dose Rate Data

The comparisons presented in this section are the calculations of the fast neutron absorbed dose rate and the experimental data obtained with p-i-n junction silicon diodes.

Figure 5-6 compares the calculated and measured fast neutron absorbed dose

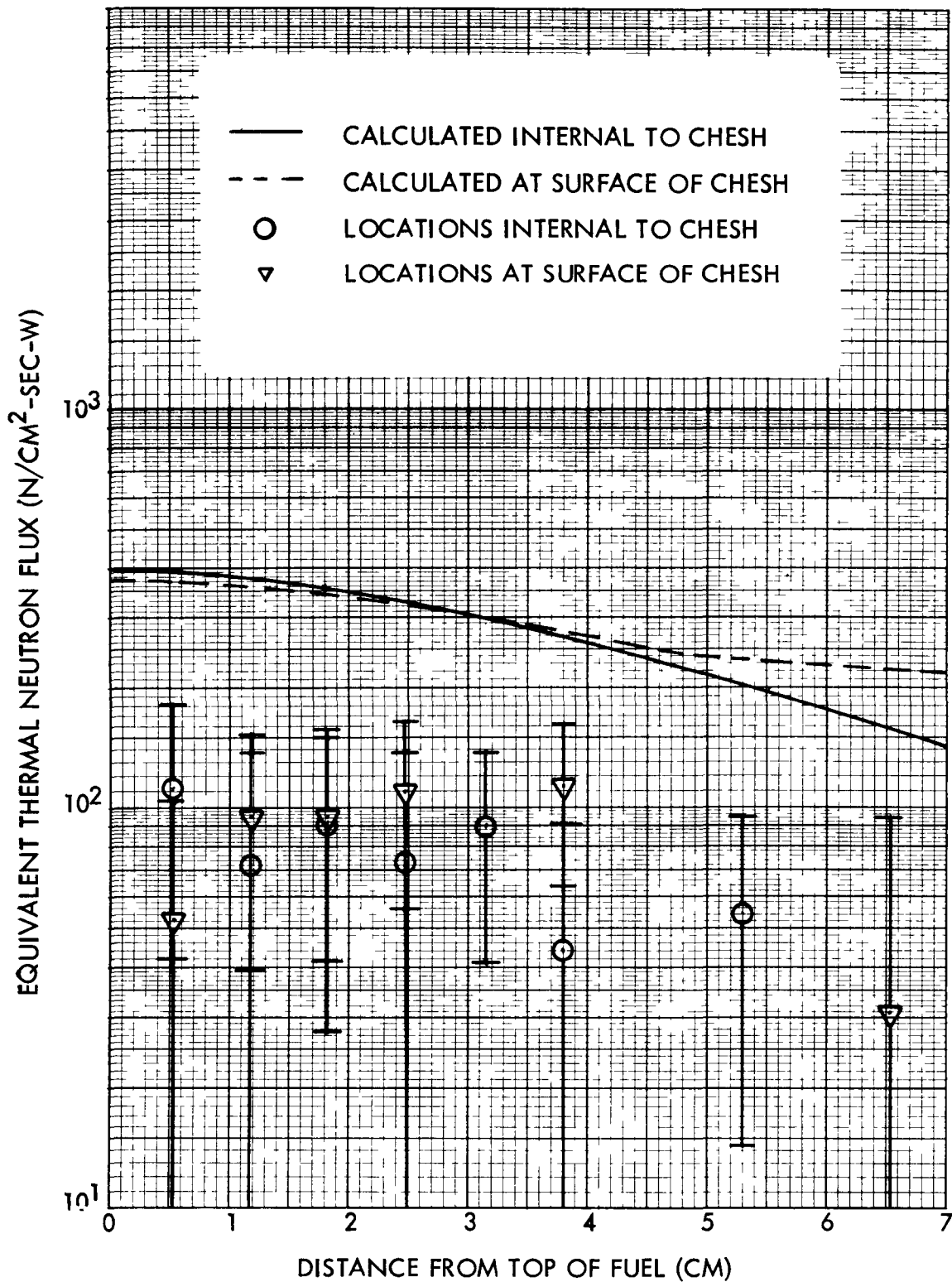


Figure 5-5. Comparison of the Calculated and Experimental Dysprosium Thermal Neutron Flux ( $E < 0.4$  eV) as a Function of Axial Position Above the Top of the Fuel

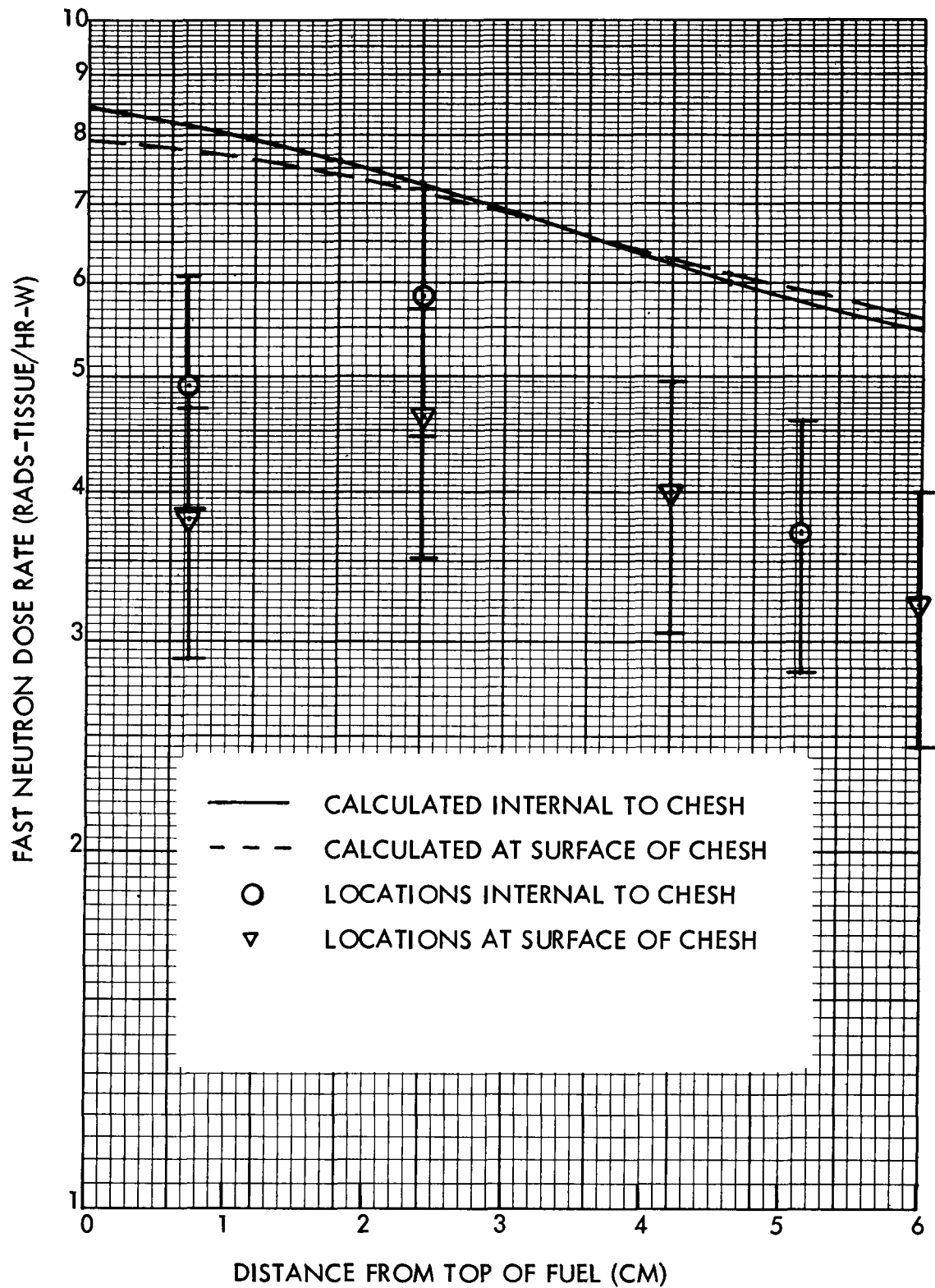


Figure 5-6. Comparison of the Calculated and Experimental Phylatron Fast Neutron Absorbed Dose Rate as a Function of Axial Position Above the Top of the Fuel



rate as a function of axial position above the top of the fuel. The experimental data were obtained on the outside surface of the CHESH and on the inside of the CHESH model.

On an average pointwise basis (see Section 5.5), the calculations are 32 percent higher than the experimental results internal to the CHESH while the calculations on the surface of the CHESH are 42 percent higher than the experimental results. Figure 5-6 indicates that there is relatively good agreement between the shape of calculated and experimental results beyond 2.4 cm from the top of the fuel. At this location, the experimental data display a peak. This could be due to streaming in the relatively large hole created by the support stem or self-shielding by the pedestal. However, this effect is not observed in the sulfur and U-238 data for  $E > 2.9$  MeV and  $E > 1.5$  MeV, but streaming and pedestal shielding become more evident for a medium with a large attenuation when compared to a medium with a small radiation attenuation. Since the core material has a higher removal cross section for neutron dose than for neutrons with energy greater than 1.5 MeV, neutron dose streaming could be possible. However, the DOT calculation employed an S-124 angular quadrature with one degree of resolution in the axial (Z) direction which should resolve a streaming effect.

Spectral corrections of the p-i-n junction Si diode measurements of the fast neutron absorbed doses were not made. The diodes were calibrated by the vendor in a bare graphite moderated reactor, but adjustments of the detector response due to neutron spectral differences between those of the PAX reactor and the calibration reactor were not made which may contribute to the difference between the calculated and experimental data.

#### 5.4.5 Photon Absorbed Dose Rate Data

The comparisons presented in this section are the calculations of the gamma absorbed dose rate and the experimental data obtained with  $\text{CaF}_2$  thermoluminescent dosimeters (TLD).

Figure 5-7 compares the calculated and measured TLD gamma absorbed dose rate as a function of axial position above the top of the fuel. The experimental data were

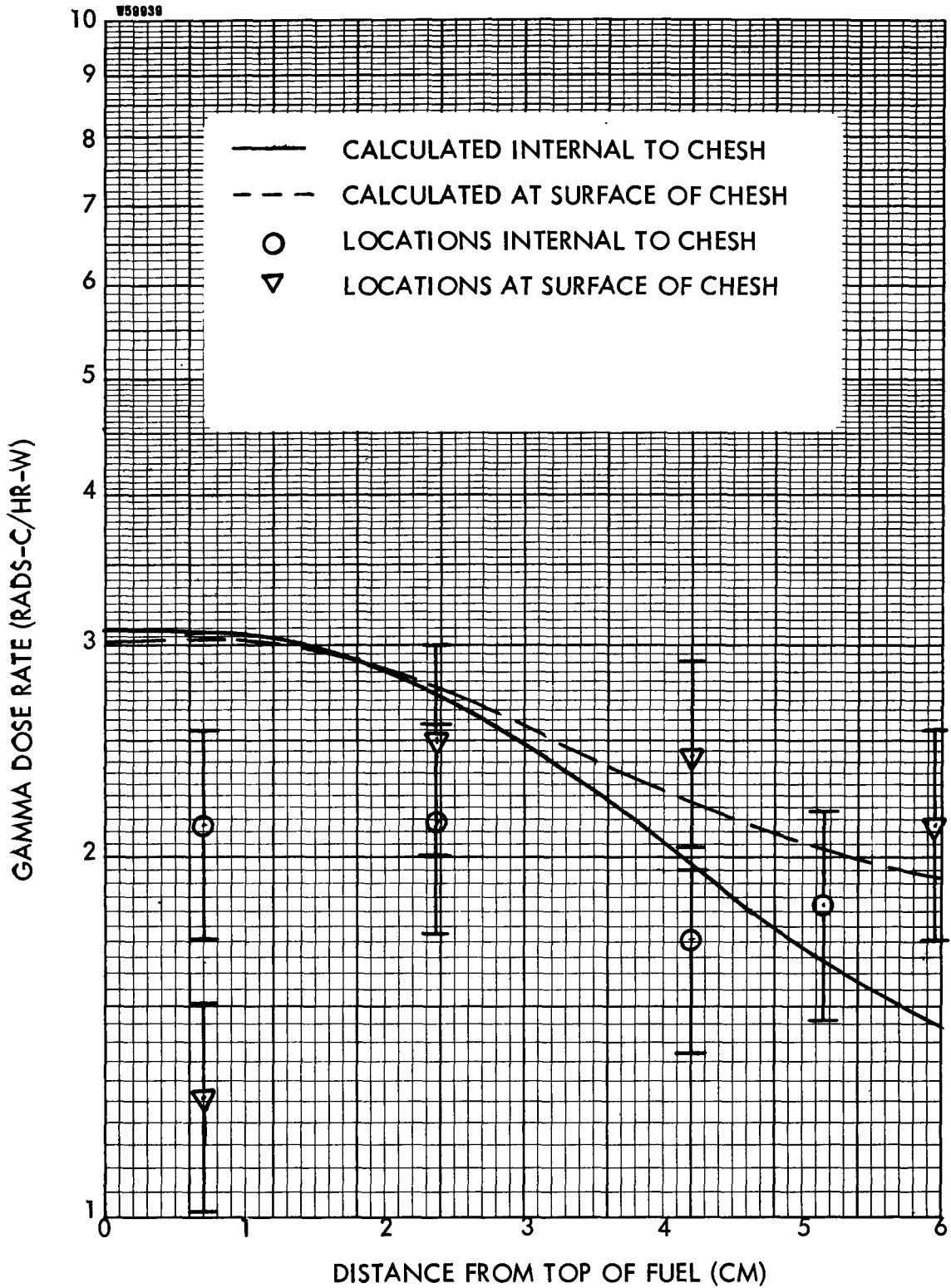


Figure 5-7. Comparison of Calculated and Experimental  $\text{CaF}_2$  TLD Gamma Ray Absorbed Dose Rate as a Function of Axial Position Above the Top of the Fuel

obtained on the outside surface of the CHESH and on the inside of the CHESH model.

On an average pointwise basis, the calculations are 15 percent higher than the experimental results internal to the CHESH while the calculations on the surface of the CHESH are 18 percent higher than the experimental results. Again, the shape of the calculated results agree relatively well with the experimental results beyond 2.4 cm from the top of the fuel. As in the case of the fast neutron absorbed dose rate, the cause for this phenomenon is not known.

Spectral difference effects were not considered in the comparison of the thermoluminescent photon dose measurements made with  $\text{CaF}_2$  dosimeters. The calibration was made in terms of light output units in a known Co-60 field.  $\text{CaF}_2$  does not have an energy independent photon absorption coefficient and does not exactly parallel that of carbon, but comparisons of calculated energy absorption in terms of energy absorption of carbon is made with the  $\text{CaF}_2$  measurements.

#### 5.4.6 Bragg-Gray Ion Chamber Heating Rate Data

The comparisons presented in this section are for the calculated photon heating rate in carbon and stainless steel and the experimental data obtained with Bragg-Gray detectors for these materials. The experimental data were obtained at a distance of 3.8 cm above the fuel next to a support stem without the CHESH model in place. The calculated data were obtained on the outside surface of the CHESH model and at a point in the void region midway between the CHESH model and PAX support blocks. Both sets of calculated data were obtained at the same axial position; however, it was not possible to obtain calculated results at the same location (i.e., next to a support stem without the CHESH model in place) as the experimental results.

Table 5-3 compares the calculated and experimental data. The calculated data on the outside surface of the CHESH are, respectively, for carbon and stainless steel 17 and 35 percent below the experimental data. The calculated data in the void region midway between the CHESH and support blocks are, respectively, for carbon and stainless

TABLE 5-3

COMPARISON OF CALCULATED AND EXPERIMENTAL PHOTON HEATING RATES  
FROM BRAGG-GRAY DETECTORS

Data Type	Calculated Data		Experimental Data
	Outer Surface of CHESH	Void Region between CHESH and Support Blocks	
1) Carbon Heating Rate (w/gm-c-Mw)	0.00645	0.00723	0.00775
2) Stainless Steel Heating Rate (w/gm-SS-Mw)	0.00662	0.00740	0.00886

steel 7 and 16 percent below the experimental data. Because of the attenuation due the CHESH model, it is believed that the calculated data in the void region are more representative of the experimental measurements.

These calculated results could be further increased by a maximum of 7 percent to account for the effect of streaming through the support stem void. This would improve the agreement with experimental results; however, the exact magnitude of the correction cannot be determined because the Bragg-Gray detector does not measure the heating rate at a point. In other words, the radiation striking the Bragg-Gray detector comes not only from the support stem but also directly from the end of the core. While 7 percent would account for the difference due to streaming through the support stem void, the portion of the radiation reaching the Bragg-Gray detector from the end of the core and through the support stems is not known.

It should be noted from Section 5.4.5 that the calculated results were higher than the experimental data obtained with  $\text{CaF}_2$  TLD s. The opposite trend occurs in the comparison of calculated and experimental Bragg-Gray data. This could be due in part to a combination of: 1) a neutron response of the Bragg-Gray chamber that is greater than the TLD neutron response, and 2) experimental uncertainties.

## 5.5 STATISTICAL ANALYSIS OF THE DATA

### 5.5.1 Introduction

This section provides the statistical analysis of the difference between the calculated and experimental data. This section contains the derivation of the average difference between calculations and experiments and the one standard deviation limits on the average difference. Section 5.5 of WANL-TME-1914, "Radiation Environment in Various NERVA Components," contains a detailed discussion of the manner in which the statistical analysis was performed.

### 5.5.2 Statistical Results

Table 5-4 provides the average ratio of experimental data to calculated data

TABLE 5-4

## STATISTICAL ANALYSIS OF THE DIFFERENCE BETWEEN CALCULATED AND EXPERIMENTAL DATA

Data Type and Location	Average Ratio of Experimental to Calculated Data	One Standard Deviation in the Ratio Between Calculated and Experimental Data	
		Upper Limit	Lower Limit
U-238 Data <sup>(1)</sup> - Internal to CHESH	0.81	0.83	0.80
U-238 Data <sup>(1)</sup> - At CHESH Surface	0.83	0.84	0.81
Sulfur Data <sup>(2)</sup> - Internal to CHESH	1.60	1.66	1.54
Sulfur Data <sup>(2)</sup> - at CHESH Surface	1.64	1.73	1.55
Dy Thermal Flux Data <sup>(4)</sup> - Internal to CHESH	0.24	0.29	0.19
Dy Thermal Flux Data <sup>(4)</sup> - at CHESH Surface	0.24	0.37	0.16
Phylatron Data <sup>(5)</sup> - Internal to CHESH	0.68	0.77	0.60
Phylatron Data <sup>(5)</sup> - at CHESH Surface	0.58	0.65	0.52
CaF <sub>2</sub> TLD Data <sup>(6)</sup> - Internal to CHESH	0.85	1.01	0.71
CaF <sub>2</sub> TLD Data <sup>(6)</sup> - at CHESH Surface	0.82	1.22	0.55

(1) Neutron Flux ( $E > 1.5$  MeV)(2) Neutron Flux ( $E > 2.9$  MeV)(4) Neutron Flux ( $E < 0.4$  eV)

(5) Neutron Dose Rate

(6) Photon Dose Rate

and the one sigma limits on this ratio. As an example of the use of this data, Table 5-4 indicates that, on the average for the internal CHESH data, the calculated U-238 data were 9 percent higher than the experimental data. Further, the experimental data lay between the product of 0.80 and 0.83 times the calculated data for 68% of the observations.

A statistical analysis to determine whether the shape of the calculated and experimental data were the same was not performed because for most of the CHESH radiation measurements only four or five experimental data points (the data internal to the CHESH must be separated from the data on the surface of the CHESH due to a possible difference in the shape of the two sets of data) were available for analysis. Therefore, while the analysis could be performed, the results would be statistically inconclusive because of the limited amount of data available.

## 5.6 APPLICABILITY OF COMPARISONS TO DESIGN CALCULATIONS

This section discusses the applicability of the uncertainty factors (Section 5.5) obtained from these comparisons of calculated and experimental results to design computations. The reason that this question arises is that the calculations for these comparisons employed an explicit representation of the CHESH; whereas, design calculations employ a "smeared" (homogeneous) representation of the CHESH.

Figure 5-8 presents a comparison of the gamma ray dose rate as a function of axial position. The calculated data presented are for a smeared representation of the CHESH and the average dose rate in the explicit representation of the CHESH. The smeared data were obtained directly from Reference 7 merely by adjusting the data to one watt of reactor power. This figure typifies the differences between the data obtained with a smeared representation of the CHESH and the data obtained with the explicit representation of the CHESH employed in this analysis.

Figure 5-8 indicates that the calculated and smeared data have the same initial value at the surface of the fuel; however, the two sets of data have different shapes and the data obtained from the smeared computation fall off much more rapidly than the data

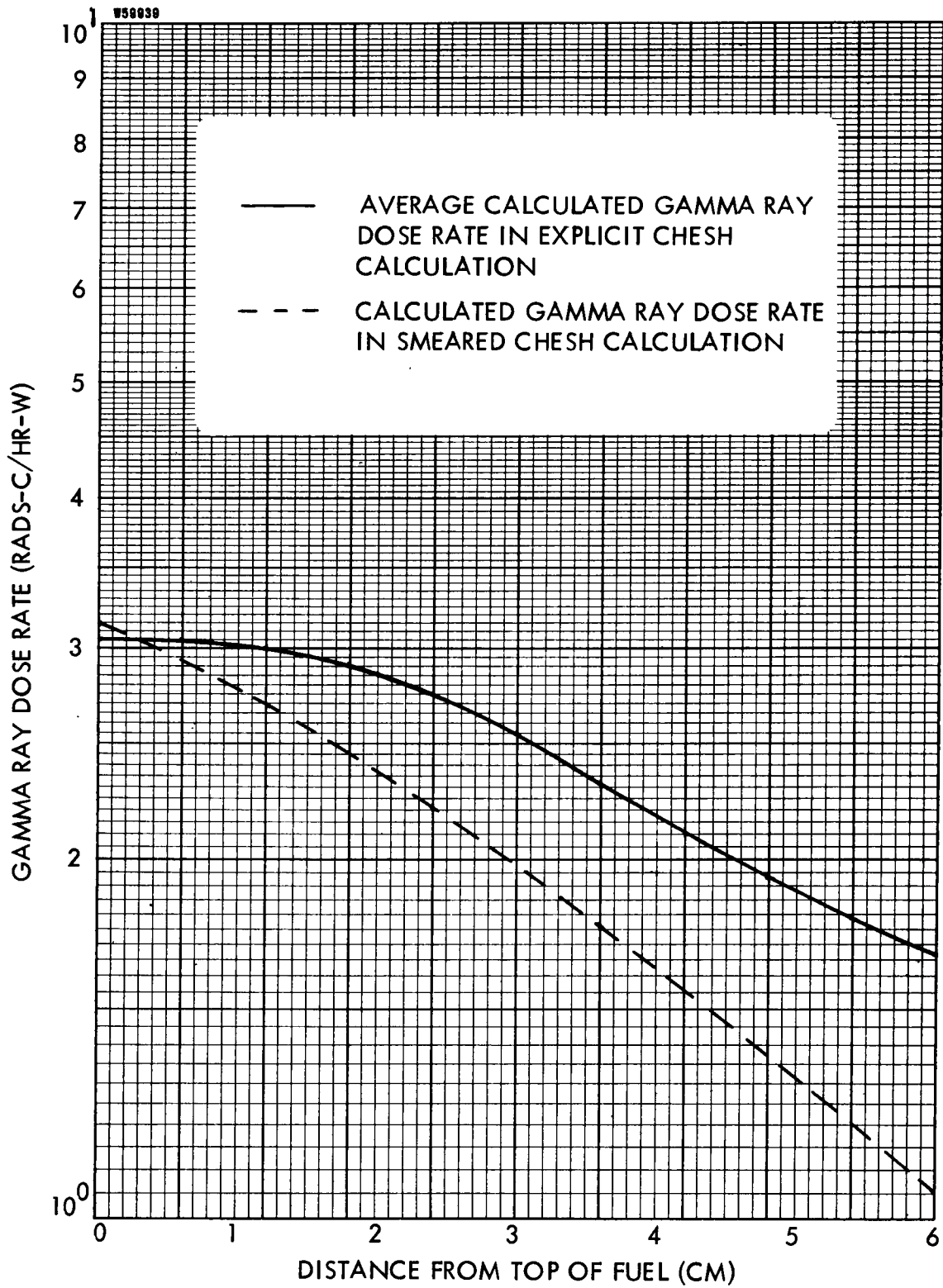


Figure 5-8. Comparison of the Gamma Ray Dose Rate Obtained By an Explicit And a Smeared Representation of the CHESH as a Function Of Axial Position Above the Fuel



obtained from the explicit computation. The smeared data fall off by a factor of 2.9 from the top of the fuel to six centimeters above the top of the fuel while the explicit data fall off only a factor of 1.8 over this distance. To understand this difference, one must examine the two sets of computations more closely. The smeared computation, in essence, has a CHESH in each cluster; however, the explicit computation has a CHESH in only one cluster and the eighteen surrounding clusters have no CHESH at all. Thus, in the explicit calculation the CHESH is surrounded by a void which is approximately 10 cm thick; whereas, in the smeared computation, the effective void distance between CHESH is only 2.5 cm. Therefore, the effective region density due to the CHESH for the smeared computation is higher than the effective region density for the explicit computation. This, then, is the reason that the smeared results fall off more rapidly with distance than the explicit results.

The results obtained with the smeared computation are more representative of the actual reactor because a CHESH exists for each cluster. The comparison of the explicit and smeared results do indicate a difference in shape which indicates that there are small variations\* in the radiation data across the CHESH which would not be seen by the smeared representation of the CHESH; however, it is concluded that the smeared computations represent the average radiation environment in the CHESH. It is further concluded that the uncertainty factors obtained from this comparison of analytical and experimental results are representative of the cross sections and codes employed in the analysis. Therefore, the uncertainty factors obtained in this analysis can be applied to design computations.

---

\* Corrections to the average radiation data obtained from smeared computations could be made through the use of explicit computations to account for the variations due to the explicit nature of the CHESH. The computations in this analysis indicate that these variations would be less than 10 percent for both photon and neutron data.

## 5.7 REFERENCES

1. WANL-TME- to be published, "The Evaluation of the WANL Integrated Nuclear, Radiation and Shielding Standard Design Method (WISDM)."
2. WANL-TME-1969, "Second Version of the GAMBIT Code," G. Collier, G. Gibson, L. L. Moran, R. K. Disney, and R. S. Kaiser, November 1969.
3. K-1693, "A User's Manual for ANISN, A One-Dimensional Discrete Ordinates Transport Code with Anisotropic Scattering," W. W. Engle, Jr., March 1967.
4. WANL-TME-1982, "User's Manual for the DOT-IIW Discrete Ordinates Transport Computer Code," R. G. Soltesz, R. K. Disney, and G. Collier, 1969.
5. WANL-PR(LL)-010, "Synthesis of Calculational Methods for the Design and Analysis of Radiation Shields for Nuclear Rocket Systems," - Volume 7, R. K. Disney, R. G. Soltesz, and S. L. Ziegler, June, 1967.
6. American Nuclear Society Paper Presented at the 1969 Winter Meeting, "Neutron Flux Spectra Measurements with Energy Dependent Activation Foils and Comparison with Multigroup Reaction Rate Calculations," S. Salah, W. D. Rankin, and V. S. Oblock.
7. DRM 1069, "Internal Neutron and Photon Radiation Levels for the R-1 Reference Design (Dwg. 939J635)," S. L. Anderson, and R. N. Nassano, January, 1969.

## 6.0 CONCLUSIONS

Based on the preceding analysis, discussion, and the results obtained in WANL-TME-1914 the following conclusions were made:

- 1) The uncertainty factors obtained from this analysis which employs an explicit representation of the CHESH are applicable to design computations which employ a smeared representation of the CHESH:
- 2) The uncertainty in the fast neutron flux ( $E > 1.0 \text{ MeV}$ ), which is required radiation environment data, is based on the difference between the calculated and experimental U-238 data. The average uncertainty factor to be applied to the calculated fast neutron flux in the CHESH is 0.82. The one standard deviation (one sigma) variation in this factor is 0.81 to 0.84. Therefore, at ambient conditions, it is concluded that the actual fast neutron flux lies between the product of 0.81 and the calculated data and the product of 0.84 and the calculated data approximately 68 percent of the time.
- 3) The uncertainty in the thermal neutron flux ( $E < 0.4 \text{ eV}$ ), which is required radiation environment data, is based on the difference between the calculated and experimental subcadmium dysprosium data. The average uncertainty factor at ambient conditions, to be applied to the calculated thermal neutron flux in the CHESH is 0.24. The one sigma variation in this factor is 0.17 to 0.33. The possible one sigma variations in the calculated data are obtained in a manner similar to that in item two.
- 4) The uncertainty in neutron heating and neutron dose rate is based on the difference between the calculated and experimental fast neutron absorbed dose rate obtained with Si diodes. The average uncertainty factor, at ambient conditions, to be applied to the calculated data in the CHESH is 0.62. The one sigma variation in this factor is 0.56 to 0.71. The possible one sigma variations in the calculated data are obtained in a manner similar to that in Item 2).
- 5) The uncertainty in photon heating and photon dose rate is based on the difference between the calculated and experimental photon absorbed dose rate obtained with  $\text{CaF}_2$  TLDs. This uncertainty was not based on the Bragg-Gray data because only two

experimental points were available and a completely analogous comparison of calculated and experimental Bragg-Gray data was not possible. The average uncertainty factor, at ambient conditions, to be applied to the calculated data in the CHESH is 0.83. The one sigma variations in this factor are 0.63 to 1.10. The possible one sigma variations in the calculated data are obtained in a manner similar to that in item two.

6) Because of the limited amount of experimental data for any one detector, and large uncertainties in portions of the data it was not possible to statistically analyze the shapes of the calculated and experimental results to determine whether the two sets of data had the same shape to a reasonable level of confidence. An examination of the calculated and experimental data revealed that the sulfur, U-238, and dysprosium results appeared to have the same shape. The Si diode and  $\text{CaF}_2$  TLD data had the same shape beyond 2.3 cm above the top of the fuel; however, at 2.3 cm the experimental data reached a local maximum while the calculated results monotonically decreased. At this time, an explanation for this difference does not exist.

As a result of this analysis, it was determined that the following areas merit further investigation which may lead to the elimination of some of the difference between calculated and experimental data:

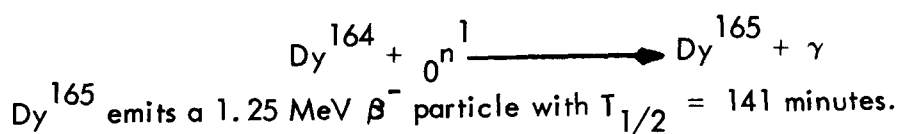
- 1) The effect of thermal activation in sulfur should be evaluated analytically in order to resolve the discrepancy between the calculated and experimental sulfur data.
- 2) The effect of fission spectrum, anisotropic cross sections, and group structure on the calculated sulfur data should also be evaluated.
- 3) The effect of a neutron response in the  $\text{CaF}_2$  TLD and Bragg-Gray detectors should be examined.
- 4) The effect of spectral differences on the calibration of the  $\text{CaF}_2$  TLD and Si diode detectors should be examined.
- 5) The calculated cadmium shielding factors for dysprosium should be evaluated, and the dysprosium cross section examined.

## APPENDIX A

### PASSIVE DOSIMETERS

#### A.1 TYPES OF DETECTORS

Dysprosium-Aluminum Wires - Dy-Al wires with 10.86 w/o Dy in Al were used to obtain thermal neutron flux information. They were irradiated both bare and with cadmium covers. The nuclear reaction used to monitor the neutron flux is:



The  $\text{Dy}^{165}$  isotope was counted for  $\beta^-$  activity using a three-channel,  $2\pi$  flow proportional counting system described in Section 3.1.4 of WANL-TME-1911. The isomeric state of  $\text{Dy}^{165}$  with the half-life of 1.3 minutes was permitted to decay for a sufficient time before counting. There are no effects from the irradiation of the additional stable isotopes of dysprosium or aluminum present in the foil.

The cadmium covering for the Dy-Al wires consisted of cadmium tubing with an outside diameter of 0.090 inches and a wall thickness of 0.020 inches.

The weight percent content of the Dy dispersed in the aluminum matrix was determined from a sample of the dosimeter material by means of X-ray fluorescence techniques in which the wire was compared with a sample of known dysprosium content. The accuracy of the determination was to within  $\pm 7.0$  percent on a one-sigma basis. The analysis was carried out by the Westinghouse Advanced Reactor Division at Waltz Mill, Pa. Figure A-1 shows the documentation supplied by them for this calibration.

Sulfur Pellets - The sulfur pellets were used to obtain fast neutron flux information above a neutron energy of 2.9 MeV. The nuclear reaction used to monitor the fast neutron flux is:



The  $\text{P}^{32}$  emits a 1.71 MeV  $\beta^-$  particle with  $T_{1/2} = 14.3$  days. The  $\text{P}^{32}$  disintegration rate was measured with the low background gas-flow proportional counter system described in Section 4.4.11 of WANL-TME-1852, Volume 1.

**ANALYTICAL REQUEST**  
WAPD FORM 24

**WESTINGHOUSE ATOMIC POWER DIVISION**

DESCRIPTION OF SAMPLE	REQUEST NO.
4 Dysprosium - Aluminum Samples	DATE SUBMITTED 10-16-67
OBJECT OF ANALYSIS	SUBMITTED BY G. E. Kubansek
Determination of Dysprosium	SECTION WANEP
	RM. NO. EXT. 226
	CHARGE NO. 59-81700

ANALYTICAL DATA: CHEMICAL  SPECTROGRAPHIC  RADIOCHEMICAL

TSL NO.	SAMPLE DESIGNATION	DETERMINATION	CONC. RANGE	1	2	3	AVERAGE
10-67-30	0.005" foil	1/8 dia Dy	Wt. %	4.02	4.13	3.88	4.01
10-67-31	0.010" foil	1/4 dia Dy	Wt. %	5.88	5.86	5.86	5.87
10-67-32	0.030" wire #5	Dy	Wt. %	10.91	10.74	10.94	10.86
10-67-33	0.030" wire #6	Dy	Wt. %	11.19	11.08	10.27	10.85
4-67-30							
→ 4-67-49	5.8 ± 0.2 mil foil P.S. 4222	Dy	Wt. %	3.61	3.57	3.77	3.65

REMARKS  
Results in weight percent Dy ± 1% relative

Sample size - 150 mg for 5% and 75 mg for 10%

NOTEBOOK REFERENCE	DATA REPORT# 10-30-67	APPROVED BY J. L. Johnson <i>J. L. Johnson</i>
PLATE NO. <i>N</i> 4539	TOTAL NO. OF SAMPLES 5	TOTAL NO. OF DETERMINATIONS 15

Figure A-1. Dy-Al Alloy Content Report

U-238 Foils - The U-238 foils were used in order to obtain fast neutron flux information above a neutron energy of 1.4 MeV. They were reported to contain 190 ppm of U-235 (see WANL-TME-1852, Volume 1). The foils were irradiated under cadmium covers in order to minimize the neutron fission of U-235. The nuclear reaction used to monitor neutron flux is:

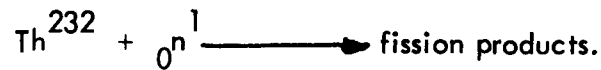


The gamma rays emitted by the fission products were counted with the NaI gamma counting system described in Section 4.4.10 of WANL-TME-1852, Volume 1, with the gamma energy discriminator set at 0.66 MeV to help eliminate the natural activity background and other unwanted activities such as from the (n,γ) reaction.

The cadmium covers consisted of a two-piece box formed of overlapping cups pressed from 0.020 inch thick cadmium sheet. The boxes were typically 3/8 inch in diameter and 3/32 inch thick. The side walls were twice the cadmium thickness due to the overlap. For those measurements within the support stem or CHESH assemblies, somewhat smaller cadmium boxes were used because of space limitations. The smaller boxes consisted of a cup and a flat cadmium disc which fit into the cup. The diameter of the disc and of the foils as well as the inside diameter of the cup were all approximately 1/4 inch. This left some possibility of thermal neutron leakage to the foils but this effect was negligible due to the relative magnitudes of the fluxes involved and the amount of leakage which was possible.

The U-238 and the thorium foils were irradiated simultaneously in the same cadmium covers and were separated from each other by a layer of thin cardboard.

Thorium Foils - The thorium foils containing Th-232 were used in order to obtain fast neutron flux information above a neutron energy of 1.35 MeV. The foils were irradiated under cadmium covers (along with the U-238 foils, see above) in order to minimize the thermal neutron reactions in the foils. The nuclear reaction used to monitor fast neutron flux is:



The gamma rays emitted by the fission products were counted with the NaI gamma counting system described in Section 4.4.10 of WANL-TME-1852, Volume 1, with a gamma energy discrimination of 1.0 MeV to help eliminate the natural activity background and other unwanted activities such as from the (n,γ) reaction.

Thermoluminescent Dosimeters (TLD) - The TLD hot pressed chips were used to monitor gamma dose. The mechanism of gamma detection is that ionizing radiation incident upon the material produces metastable energy states in the chip. When the material is heated, the release of the stored energy produces detectable photons. The quantity of photons released during heating, as a function of time, can be related to the amount of energy deposited in the chip by appropriate calibration methods. The TLD chips were annealed prior to irradiation in order to remove any residual metastable states present in the dosimeter. After irradiation, the accumulated energy deposition was obtained by readout with an Edgerton, Germeshausen and Grier (EG&G) Model TL-3 reader unit as described in Section 4.4.13 of WANL-TME-1852, Volume 1, "R-1 Parametric Shield Measurements Conducted on the NERVA Permanent Assembly Experiment (PAX) Reactor".

During the irradiation, the chips which were placed on the outside of the CHESH assembly and the reference assembly, were mounted inside packets formed from 0.020-inch thick Tygon tubing, (see Figure A-2).

Two types of TLD chips were used, CaF<sub>2</sub> and Li<sup>7</sup>F.



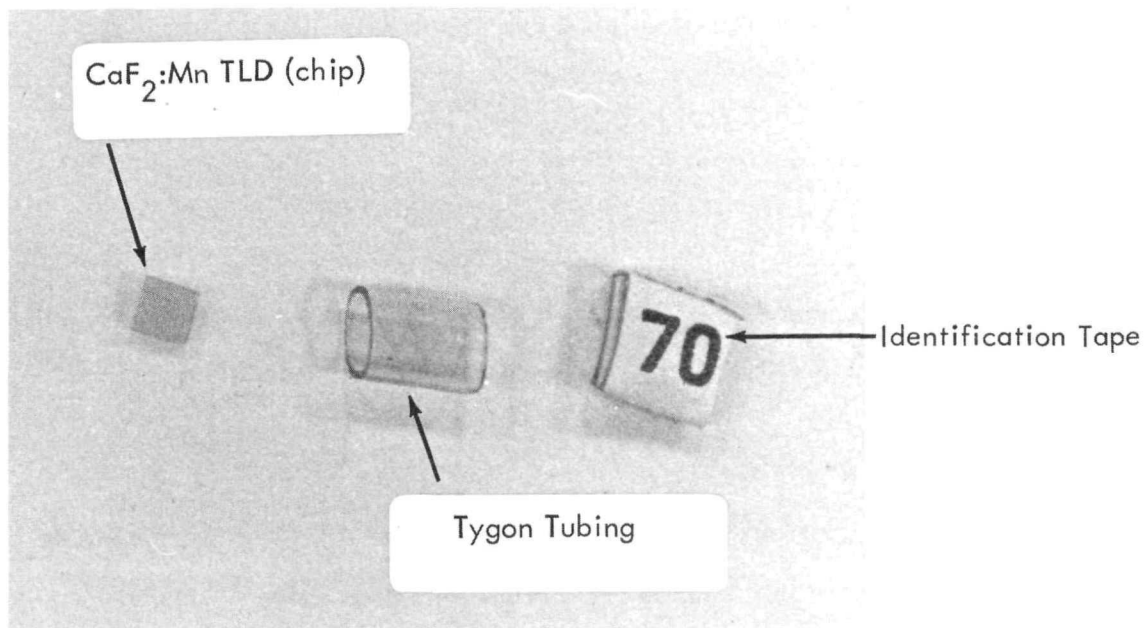


Figure A-2. Thermoluminescent Dosimeters With Tygon Covers

Phylatrons - Phylatron dosimeters (p-i-n silicon diodes) were used to measure fast neutron dose. They are essentially a wide-based p-i-n silicon diode approximately 7-mm long by 3-mm in diameter. Figure A-3 shows a schematic description of the diode structure. The dosimeters are manufactured by the Precision Instruments Corporation, Columbus, Ohio. The dosimeter's principle of operation is that the fast neutron dose to which the device is exposed changes the minority carrier lifetime of the base region. When the device is operated with a forward bias current sufficient to modulate the conductivity of the base, the voltage drop across the diode is very sensitive to the minority carrier lifetime.

The SNDR-2 Phylatron dosimeter reader, described in Section 4.4.12 of WANL-TME-1852, Volume 1, supplies the constant current and measures the forward voltage drop by a null method. The manufacturer supplies calibration curves for the dosimeters which relate forward voltage change to the neutron dose. The range of the dosimeters that can be purchased spans the region of 5-15,000 rads (tissue). The specific diodes used for this experiment had total dosage ranges of 700 rads and 3000 rads.

## A.2 DOSIMETER CALIBRATIONS

General - The passive dosimeters (Dy, S, U-238 and Th) which were counted on the beta or gamma detector instrumentation required calibration factors to enable count rates to be converted to activities. In each case, this was accomplished by counting one or more irradiated dosimeters on the WANEF instrumentation and then sending them out of the facility for chemical or activation analysis to have their absolute activity determined.

Dysprosium-Aluminum - The Dy-Al wires were sent to Westinghouse Advanced Reactor Division, Waltz Mill, Pa. for determination of absolute activity. The foils were gamma counted and these results were converted to activity through application of the known counter efficiency. This calibration was reported with an accuracy, on a one-sigma basis, of  $\pm 5$  percent as shown in Figure A-4.

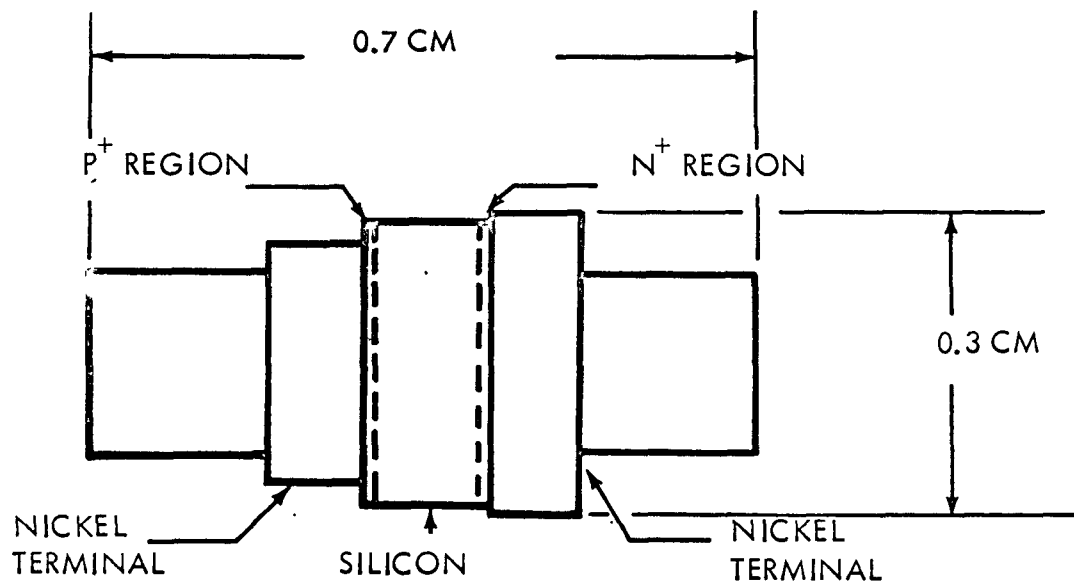


Figure A-3. View of Silicon Diode Phylatron Dosimeters

CHEMICAL ANALYSIS REPORT  
FORM 54741

WESTINGHOUSE ATOMIC POWER DIVISIONS  
ANALYTICAL SERVICE LABORATORIES  
WALTZ MILL SITE

ANAL. SERV. REQUEST NO.  
1373

ORIGINATOR <b>R. BRAWDY</b>	DEPT. & GRP. <b>WANEF</b>	EXT. <b>5226</b>	ROOM NO.	FACILITY <b>W.M.</b>
APPROVAL SIGNATURE <b>C. Blackburn</b>		DATE RECEIVED <b>6-23-69.</b>	DATE REPORTED <b>6-27-69</b>	

METHOD	ANALYST	REFERENCE	METHOD	ANALYST	REFERENCE
<b>γ spectrometry</b>	<b>CAB.</b>	<b>FILE - WANEF</b>			
		<b>JUNE 1969.</b>			

RESULTS OF ANALYSIS

ORIGINATOR'S SAMPLE NO.	ANAL. SERV. LAB. NO.	ACTIVITY	REMARKS
		<b>165 Dy</b>	
		<b>dpm/--- ± 5%</b>	<b>Corrected for decay to reactor shut down 15:41 hrs 6-23-69</b>
<b>Dy WIRE #48</b>	<b>8295</b>	<b>5.64 × 10<sup>5</sup></b>	
<b>Dy WIRE #49</b>	<b>8296</b>	<b>5.72 × 10<sup>5</sup></b>	
<b>Dy WIRE #50</b>	<b>8297</b>	<b>5.56 × 10<sup>5</sup></b>	

REMARKS:

.030 x .260 Dy-Al WIRE, CHEM REP.

Figure A-4. Dy-Al Wire Activity Calibration Report

Sulfur - The sulfur pellets were sent to the Physical Science Laboratory (PSL) of the Westinghouse Astronuclear Laboratory to determine the amount of P-32 formed in the sample. The sulfur pellets were dissolved in an Erlenmeyer flask with the addition of a phosphorous carrier. The sulfur in the flask was heated to the melting point. The vapors were burned at the lip of the flask until all of the sulfur was gone. The residue in the flask was dissolved with  $\text{HNO}_3$  and analyzed for P-32 content using a standard phosphorous determination procedure. The final precipitate was mounted on an aluminum disc and counted in an end window beta proportional counter. The counts per minute were converted to disintegrations per minute by using an efficiency factor that was established by  $4\pi$  counting a P-32 isotope standard obtained from ORNL. Using this procedure, the disintegrations per minute of the P-32 were determined to within  $\pm 5$  percent on a one-sigma basis. (Figure A-5)

U-238 and Th-232 - The U-238 (190 ppm U-235) and the Th-232 fission foils were sent to the PSL to determine the total number of fissions that occurred in the sample during a particular reactor operation. The total fissions were determined by analysis for Mo-99 content.

At the PSL, the sample was burned by ignition in a quartz combustion tube with flowing oxygen. The residue was dissolved in  $\text{HNO}_3$  and diluted to 100 ml in a volumetric flask. Aliquots were taken and analyzed for Mo-99 using a standard radiochemical separation procedure. The purified Mo-99 samples were mounted on aluminum discs and gamma counted. Counting rates were corrected for chemical yield, aliquot, and decay. A factor was applied to convert counts per minute of Mo-99 to fissions. The conversion factor was established by intercalibration with LASL, and the reported number of fissions was good to within  $\pm 2$  percent provided the sample had undergone a sufficient amount of fissions. No effect due to changes in the change of mass yield of Mo-99 with neutron fissioning energy was considered. If count rates were low, larger error limits would result due to counting statistics. The high pressure ionization chamber, with error limits of  $\pm 5$  percent was used as a check for fission determination.

The accuracies of the calibration obtained were limited by low count rates to  $\pm 10$  percent for the U-238 and  $\pm 25$  percent for the Th-232, on a one-sigma basis as shown in Figure A-5.



PSL:455

*From* : Physical Sciences Laboratory  
*WIN* :  
*Date* : July 1, 1969  
*Subject* : Analysis of WANLF Sulfur  
Pellets and Fission Foils

ASTRONUCLEAR LABORATORY

To: R. W. Brawdy, WANLF

cc: F. S. Frantz, WANLF

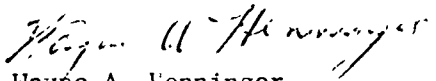
T. O. Harves

V. S. Oblock, WANLF

W. D. Rankin, WANLF ←

J. Roesmer

Three sulfur samples dated June 17, 1969 and two fission foils dated June 20, 1969 have been analyzed in the Physical Sciences Laboratory as requested. The sulfur samples were dissolved and analyzed for P-32 which was corrected for decay to 11:54, June 17, 1969 using a half-life value of 14.3 days. The U-238 and Th-232 samples were dissolved and analyzed for Mo-99 to determine the number of fissions. Large error limits had to be applied, especially for the Th-232 foil, because of low count rates. The results are given in the attached table.

  
Wayne A. Henninger  
Physical Sciences Laboratory

Approved by



G. T. Rymer, Supervisor  
Physical Sciences Laboratory

/lfd

Attachment

Figure A-5. U-238, Th, and S Calibration Report (2 Sheets)

RESULTS OF THE ANALYSIS OF WANEF SAMPLES  
DATED JUNE 17, AND JUNE 20, 1969

Sample Designation	Sample Type	Weight (Grams)	Activity Determined	Total DPM*	Total Fissions**
1	Sulfur Pellet	12.248	P-32	$8.45 \times 10^4 \pm 5\%$	
2	Sulfur Pellet	12.274	P-32	$7.74 \times 10^4 \pm 5\%$	
17	Sulfur Pellet	0.3298	P-32	$1.43 \times 10^3 \pm 5\%$	
U-238	Fission Foil	0.0734	Mo-99		$2.88 \times 10^8 \pm 10\%$
Th-232	Fission Foil	0.0438	Mo-99		$4.8 \times 10^7 \pm 25\%$

\*P-32 corrected to 11:54, June 17, 1969.

\*\*Zero time for fission foils = 16:25, June 20, 1969.

Figure A-5. U-238, Th, and S Calibration Report (Continued)

TLD - The thermoluminescent dosimeters were calibrated with a 30 Ci Co-60 source located at WANEF. The source was calibrated by using a carbon wall CO<sub>2</sub>-filled gas ion chamber. This chamber was calibrated at NBS. The TLDs were exposed to the Co-60 source and read on the EG&G readout device. The peak of the glow curve was calibrated by knowledge of the integrated dose received by the dosimeters. The accuracy of the calibration was  $\pm 6.4\%$  standard deviation on a one-sigma basis. The calibration is described in more detail in DRM 51176 and DRM 51176A.

Phylatron - A calibration curve supplied by the manufacturer was used to determine the dose measurement. These curves were generated by exposure in known dose levels at the Sandia Pulsed Reactor Facility and the Health Physics Research Reactor at Oak Ridge. Spectral differences between those at the above facilities and the PAX could contribute additional uncertainties. The accuracy of the calibration was  $\pm 20\%$  standard deviation on a one-sigma basis.



## APPENDIX B

### REACTOR POWER LEVELS

The determination of reactor power levels involves both the inter-calibration of excessive reactor runs during an experiment to establish relative power levels and the absolute calibration of one run to establish absolute power levels. These two subjects are discussed below.

#### B. 1 INTER-RUN POWER CALIBRATION

##### B. 1. 1 Passive Dosimetry

For those reactor runs in which passive dosimeters are exposed, it is important to know a time-averaged power level. The activation of gold wires, one inch long and 0.30 inch diameter, is used for this purpose. The wires are placed at the midplane of the core in elements of the center cluster and also on the surface of the PAX pressure vessel and dome. The activation is measured on the gamma counting system (see Section 4.4.10 of WANL-TME-1852, Volume 1) and the resulting data are reduced on a programmable desk calculator. By use of calibration factors established from the absolute calibration of reactor power, (see Section B.2), the reactor power for each run is established.

##### B. 1. 2 Active Dosimetry

The reactor console instrumentation is used to determine the reactor power levels for active dosimetry measurements, (i. e., Bragg-Gray chamber measurements). This instrumentation is calibrated in terms of absolute reactor power as a result of the power calibration described in Section B.2.

## B.2 ABSOLUTE REACTOR POWER CALIBRATION

### B.2.1 Basis

The absolute calibration of the reactor power depends on two types of measurements in the reactor. The first is a high power run with radiochemistry performed on sections of a fuel element irradiated in the center cluster of the core in order to establish an axial profile of the absolute number of fissions per gram of uranium in that element and, hence, the average fissions per gram of uranium in that element.

At the same time, gold inter-run calibration wires are irradiated as described in Section 4.1.4.1 to establish the basis for power level determinations of future runs.

The second type of measurement is a map of fission distribution throughout the midplane of the core in order to establish the ratio of the fissions per gram of uranium in the central element to the average fissions per gram of uranium in the core. The fission distribution data, upon which this power calibration is based, are given in WANL-TME-1917.

From these two types of measurements, the reactor power can be calculated using the formula:

$$P = \frac{F_g W}{A T_e F_w}$$

where

- P = reactor power in watts
- $F_g$  = fissions per gram of uranium in the calibration element
- W = total number of grams of uranium in the core
- A = ratio of fission density in the calibration element to average fission density in the core
- $T_e$  = reactor run time in seconds
- $F_w$  = total number of fissions per watt-second

From this power calculation result, the reactor console instrumentation was calibrated and the calibration factors for the gold wires were established. Further details of the power calibration procedure are given in the following sections.

### B.2.2 Center-to-Average Fissions Per Gram of Uranium

The ratio of fissions per gram of uranium in the central element to the fissions per gram of uranium averaged over the core was assumed to be equal to the ratio of the fissions per gram at the midplane of the central element to the average fissions per gram over the midplane of the 90 degree test sector of the core. In order to determine this value, the data of WANL-TME-1917 were used. These data consisted of a measurement in one or two channels of each fueled non-central element in the center 60 degrees of the test sector. The measurements were accomplished by irradiation of one inch long U-Al wires and the data were reported in the form of fissions/gram in a fuel element channel relative to fissions/gram in the center cluster.

These data points were averaged for each element, multiplied by the uranium loading, and summed over the 60 degree sector of the core. Corrections were made for any fueled elements not measured and then the sum was divided into the sum of the uranium loadings. The result was the desired ratio of center-to-average fissions per gram of uranium.

### B.2.3 Fissions/Gram Determination in Central Cluster (U)

The fissions per gram of uranium in the central cluster were determined by irradiation of fuel in the central cluster. The fuel was then analyzed by radiochemistry techniques for absolute fissions.

For the irradiation, thirteen 1/4 inch thick slices of virgin fuel were spaced equally over the length of a fuel element between spacers of 1-7/8 and 3-3/4-inch long fuel element sections. Figure B.1 shows a sketch of this sectioned fuel element.

Following the irradiation, the thirteen 1/4-inch slices were sent to the Physical Science Laboratory of the Westinghouse Astronuclear Laboratory to be analyzed for total fissions in each slice. The procedure used was identical to that reported in Appendix A for calibration of U-238 foils.

The results, see Figure B-2, were plotted, graphically integrated, and corrected for element loading in order to obtain the desired average fissions per gram of uranium in the center element.

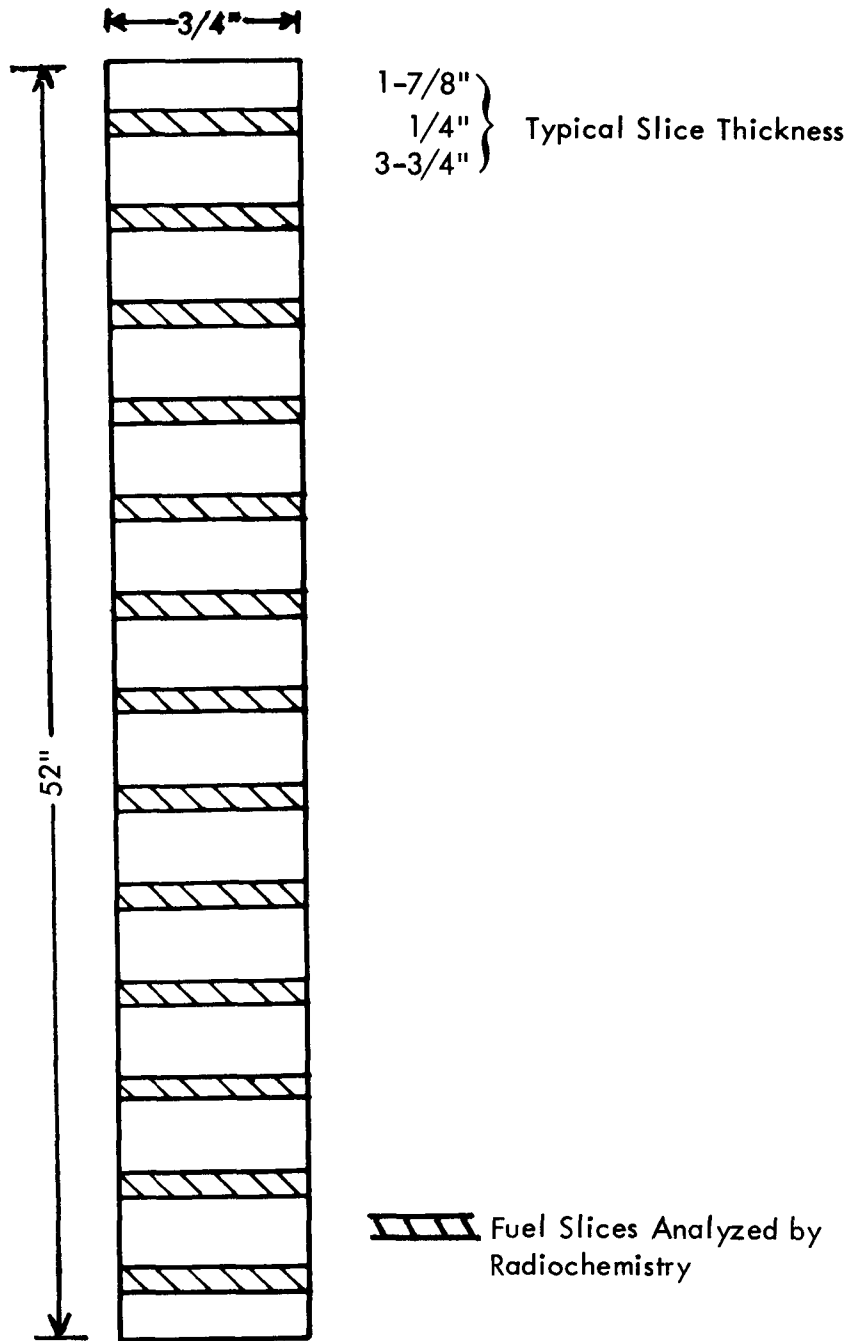


Figure B-1. Sectioned Fuel Element

PSL:470

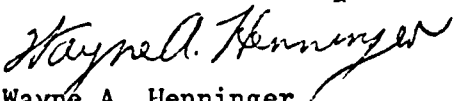
*From* : Physical Sciences Laboratory  
*WIN* :  
*Date* : August 15, 1969  
*Subject* : Analysis of WANEF Fuel Wafers  
Dated August 5, 1969

ASTRONUCLEAR LABORATORY

To: R. W. Brawdy, WANEF

cc: L. F. Becker  
F. S. Frantz, WANEF  
T. O. Harves  
V. S. Oblock, WANEF  
W. D. Rankin, WANEF ←  
J. Roesmer  
H. C. Woodsum, WANEF

The thirteen fuel wafers received from WANEF on August 6, 1969 have been analyzed in the Physical Sciences Laboratory for fission concentration. This was accomplished by dissolving the samples and analyzing radiochemically for 66.5 hour Mo<sup>99</sup>. The zero time used for decay correction was the irradiation midpoint, 1200 August 5, 1969. The results obtained are given in the attached table. These results do not differ from those reported by phone on August 14, 1969. A recount of the Mo<sup>99</sup> samples on August 15, 1969 confirmed their validity.

  
Wayne A. Henninger  
Physical Sciences Laboratory

Approved by:



G. T. Rymer, Supervisor  
Physical Sciences Laboratory

/lfd


Attachment

Figure B-2. Fission Analysis of Fuel Wafers (2 Sheets)

WANEF FUEL WAFERS DATED AUGUST 5, 1969

Sample Number	Total Weight Grams	Total Fissions ± 2%
1	3.29	1.94 x 10 <sup>11</sup>
2	3.35	3.18 x 10 <sup>11</sup>
3	3.35	4.14 x 10 <sup>11</sup>
4	3.32	4.92 x 10 <sup>11</sup>
5	3.29	5.48 x 10 <sup>11</sup>
6	3.27	5.79 x 10 <sup>11</sup>
7	3.27	5.77 x 10 <sup>11</sup>
8	3.28	5.59 x 10 <sup>11</sup>
9	3.28	5.15 x 10 <sup>11</sup>
10	3.29	4.45 x 10 <sup>11</sup>
11	3.29	3.59 x 10 <sup>11</sup>
12	3.29	2.60 x 10 <sup>11</sup>
13	3.29	1.51 x 10 <sup>11</sup>

Figure B-2. Fission Analysis of Fuel Wafers (Continued)

	TITLE <b>Radiation Environment on CHESH Components</b>	
	DOCUMENT NO. <b>WANL-TME-1915</b>	DATE <b>July 1970</b>
ABSTRACT <p>The radiation environment at mockups of the R-1 Cluster Hot End Support Hardware (CHESH) was measured in the PAX-G1 reactor. Results obtained include neutron flux densities from sulfur, U-238, and Dy-Al dosimeters, fast neutron dose rates from Phylatrons, and gamma dose rates from TLD's and Bragg-Gray chambers.</p> <p>Results are compared with analytical calculations based on the DOT two-dimensional transport code. Reasonable agreement was generally observed.</p>		
Fold ----- or Cut	DATA ITEM NO. <b>T-119</b>	SECURITY CLASSIFICATION OF DOCUMENT <b>[REDACTED]</b>
	CDRL LINE NO.	TOTAL NO. OF PAGES <b>112</b>
KEY WORDS	<b>Radiation Environment      Cluster Hot End Support Hardware</b> <b>CHESH</b> <b>R-1 Reactor</b> <b>PAX</b> <b>Neutron Flux Density</b> <b>Neutron Dose Rate</b> <b>Gamma Dose Rate</b> <b>DOT</b>	
AUTHOR/EDITOR <b>W. D. Rankin/D. J. Hill</b>		PREPARING DEPT. <b>WANEF</b>
W Form 59943		DOCUMENT INFORMATION SUMMARY

 Fold  
-----  
or Cut

CLEVELAND  
OHIO

RECEIVED

MAY 25 PM 2 24

STATION-C  
CLEVELAND, OHIO



~~CONFIDENTIAL~~

100

